BEAM DYNAMICS STUDIES OF FOUR-GAP LOW-BETA SUPERCONDUCTING RESONATORS

By

Kihun Joh

A DISSERTATION

Submitted to
Michigan State University
in partial fulfillment of the requirements
for the Degree of

DOCTOR OF PHILOSOPHY

Department of Physics and Astronomy

1993

ABSTRACT

BEAM DYNAMICS STUDIES OF FOUR-GAP LOW-BETA SUPERCONDUCTING RESONATORS

BY

Kihun Joh

Four-gap superconducting resonators have been developed at Argonne for use in the low-beta positive ion injector for ATLAS. These structures have been used successfully for ion velocities as low as 0.007c with q/m=0.1. It was previously observed that at low velocities these structures can be focusing in both longitudinal and transverse phase spaces due to an inherent alternating-phase-focusing property. Calculations indicate that a series of three such resonators have large transverse and longitudinal acceptances even when operated without the transverse focusing elements.

Detailed studies of the beam dynamics of these types of resonators are presented. For this the first-order transverse and longitudinal matrices are evaluated analytically point-by-point through the system. The phase space transformations are generalized to accelerating systems to study acceptances in such systems. Also a new method is presented to establish criteria for defining in a quantitative way the size and orientations of the linear acceptances in any accelerator or beam transport system.

These studies also include the effects of higher order distortions in the longitudinal and transverse phase spaces since minimizing such aberrations is very important for most nuclear physics applications of such accelerators.

To my mother and to the memory of my father

ACKNOWLEDGEMENTS

I would like to thank the professors who instructed me at the Department of Physics and Astronomy. I also would like to thank my colleagues, the staff, and the faculty of the National Superconducting Cyclotron Laboratory for their support of my education. I especially thank Dr. Al Zeller and professor Brad Sherrill for their guidance in learning and understanding various computer codes and beam transport systems. I thank Dr. Felix Marti for his guidance in using the code Cyclone to study central region of the K1200 Cyclotron. I also thank the operators of the NSCL for their help in measuring the beam emittances of the K1200 Cyclotron.

My thanks go to professor Edwin Kashy, professor Martin Berz, professor Norman Birge, and professor J. S. Kovacs for their efforts and advice in evaluating my Ph. D. program. I wish to give special thanks to professor Martin Berz for the useful discussions about beam optics and for his enthusiastic instruction of his own computer code COSY INFINITY.

I thank Dr. Richard Pardo and Dr. Kenneth Shepard at Argonne National Laboratory for their help in understanding basic accelerating structures of the ATLAS Linac. I also thank Kevin Beyer for his proofreading of this dissertation.

I want to deeply thank my thesis adviser Dr. Jerry Nolen. He was always generous in giving his busiest time for useful discussions. His creative suggestions, teaching, and encouragements were greatly appreciated. I also thank him for considering me for work at Argonne National Laboratory in order to write my Ph. D. dissertation.

I want to share my delight with my mother, late father, two brothers, sister-in-law, Min Kuk, Min Cho, brother-in-law, and sister. I recognize that without their love and support a page of this thesis would not exist.

Finally I thank GOD in my heart for giving me my wife, Ki-Ok, and two children, Minji and Minsol in the USA. They were the source of my strength and hope in continuing my study even through the hardest times.

I am also grateful to Michigan State University and Argonne National Laboratory for financial support during my graduate study.

Contents

List of Tables

List of Figures

Chapter 1

Introduction and Motivation

1.1 The Positive Ion Injector of ATLAS

The positive ion injector (PII) for the ATLAS heavy ion accelerator was designed to inject ions as heavy as uranium into the existing ATLAS heavy ion linac [Pardo 87b], [Bollinger 93]. The basic components of PII consist of an electron cyclotron resonance (ECR) ion source and superconducting linac as shown in Figure 1.1.

The beam from the ECR positive ion source is magnetically analyzed (analyzer 1), bunched (buncher 1), and accelerated by the 350kV accelerator tube. The beam is passed through object slits and then further analyzed at analyzer 2. After the next 90° bend the beam is chopped to remove the tails of unbunched beam, and finally the beam is rebunched at buncher 2 and injected into the linac.

The linac is able to accelerate ions from a velocity of 0.008c to 0.04c. The configuration of the PII linac as shown in Figure 1.2 is an array of four types of superconducting resonators and superconducting focusing solenoids.

1.1.1 The Beam Optics of the PII Linac

The basic concept of the PII linac beam optics is to use an alternating array of various types of superconducting resonators and superconducting focusing solenoids as shown

in Figure 1.2. Longitudinal focusing of the beam is done by the independently-phased superconducting resonators (which are generally transverse defocusing). Transverse focusing of the beam is done by superconducting solenoids located between the resonators. Also, the field strengths of the focusing solenoids are adjusted to make beam waists at the center of each resonator in order to minimize beam envelopes at the resonators. This reduces nonlinear distortions of transverse phase space due to radial defocusing forces in the resonators and the coupling of radial and longitudinal phase spaces. Therefore, the frequent alternation of longitudinal and transverse focusings would maintain a beam stable through the linac without serious degrading of the beam quality. As a consequence of having minimum beam envelopes at the resonators the beam envelopes at the focusing solenoids are maximized. Possible nonlinear effects from the solenoids in the PII linac were not investigated before this work.

1.1.2 The Resonators of the PII Linac

The resonators of the PII linac [Shepard 87], [Shepard 89] consist of four different types of accelerating structures (type I1-I4) to span a wide range of velocities from 0.008c to 0.04c. To accept very low velocity heavy ions the resonators have short accelerating gaps with a four-gap interdigital structure and very low rf frequencies of 48.5 MHz (I1-I3) and 72.75 MHz (I4).

1.2 The Beam Dynamics of Type I1 Resonators

The most interesting aspects of beam dynamics are in the type I1 resonator mainly because of its rapid velocity change starting from very low velocities. In usual operating cases the beam energy is more than doubled in the first resonator. Figure 4.3 in Chapter 4 shows a very rapid velocity change of an $^{40}Ar^{12+}$ beam through the

four-gaps of I1 under the given axial electric field profiles. One aspect of this low velocity effect in type I1 is its unusual pattern of energy gain vs initial rf phase angles [Bollinger 92]. Unlike usual cosine like patterns of high velocity accelerating structures it shows its own energy gain curve as shown in Figure 1.4.

Another aspect of the low velocity effect in type I1 is its very strong transverse focusing properties even for heavy ion beams like uranium which have low incident energies. This strong transverse focusing of type I1 was realized from raytracing studies [Pardo 87a]. The focal length of type I1 for relatively light beam like $^{40}Ar^{12+}$ is short enough to form a focal point inside the resonator as shown in Figure 1.11. This means that type I1 might act as a focusing element simultaneously both for longitudinal and for transverse directions. This kind of triple focusing was studied already in a heavy ion cryogenic linac [Chambers 76]. This rather surprising result implies that type I1 resonators might have alternating-phase-focusing properties because a simple accelerating gap does not have both transverse and longitudinal focusing actions simultaneously. Also, it turned out that even type I2 resonators have nonnegligible transverse focusing strengths and alternating-phase-focusing properties similar to type I1 resonators.

A final aspect of the low velocity effect is the possibility of distortions of transverse and longitudinal phase spaces coming from higher order radial forces and coupling of longitudinal and transverse phase spaces when a beam envelope is large. Figure 1.5 provides information about the sign conventions of transverse (left) and longitudinal (right) phase spaces in the raytracing calculations. The details will be presented in Chapter 3.

Figures 1.6 - 1.10 show transformations of phase spaces with very strong focusing properties both for transverse and for longitudinal directions: The new growth of the longitudinal phase spaces from the transverse phase space due to off axial fields appear

clearly in Figure 1.8. Also, the distortions of the longitudinal phase space on axes are shown with asymmetric distributions both in time and energy structures in Figure 1.7. The effects of coupling between the transverse and longitudinal coordinates are well represented in Figure 1.9 and Figure 1.10.

1.3 Goals and Motivations

Despite the unusual behaviors of a beam in the very low velocity region of PII they were understood in rather qualitative ways. Since the beam is very slow it is not easy to find any analytical solutions in closed forms or even in Taylor series forms of its equations of motion. The brute force method of raytracing does not provide much quantitative and systematic informations about beam dynamic properties of a system.

One of the goals in this thesis is to understand the beam dynamics of PII and also each of its resonators in a more detailed and quantitative way than what was previously known. It might present new possibilities to make use of inherent alternating-phase-focusing properties of the PII resonators [Nolen 93] without using any transverse focusing elements at the beginning stage of PII. To study each resonator would be useful because of its potential applications for ions with velocities less than 0.007c and q/m less than 0.1 [Nolen 93].

The other goal of this thesis is to extend the use of matrix optics to rf resonators with very low velocity ion beams and generalize phase space transformations to systems with acceleration [Joh 93a]. There have been several ion optical matrix optics codes for rf cavities based on analytical modelling of rf fields [Ben-Zvi 79], [Lu 87] or based on thin lens approximations [Brown 79], [Servranckx 85], [Berz 93]. Also, the matrix optics formalism has been extended and developed at SLAC [Brown 67],

[Brown 81] to the linear phase space transformations of systems without acceleration.

Even though the PII linac consists of only three kinds of optical elements namely rf resonators, magnetic solenoids and drift spaces it is the most complex system in the sense that the time dependent accelerating field exists in the rf resonators. Also, due to rapid changes in velocity during the acceleration some kinds of approximations, like thin lens for a resonator, are no longer valid. So we will test another way to use matrix optics for rf cavities to see the possible use of matrix optics for studies of rf resonators and phase space matchings of a linac system etc.

We have been mainly interested in the low velocity region in PII because the nonlinearity of a beam might not be significant after gaining some energy from accelerations if the initial phase spaces are well matched. Also, because of the smaller aperture size of type I1 resonators and the reduction of transverse emittance with acceleration, we expect that the acceptances of the PII linac will be mainly determined by the first I1 resonator or the first few elements of PII. So it might be useful to study the beginning part of the system to understand the beam dynamics of the whole system. This has been one of the motivations for this thesis.

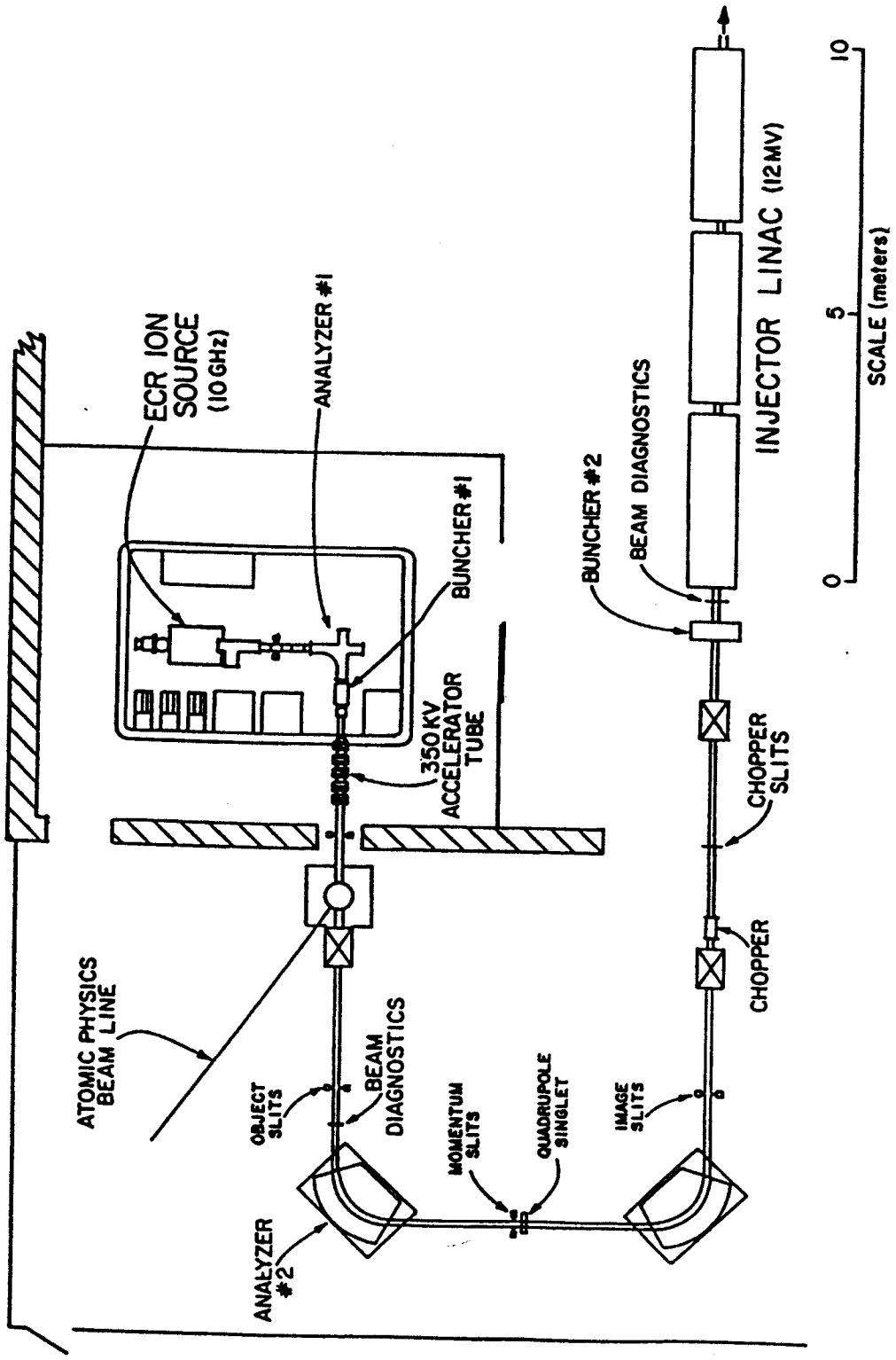

Figure 1.1: The layout and main components of the positive ion injector (PII) of ATLAS.

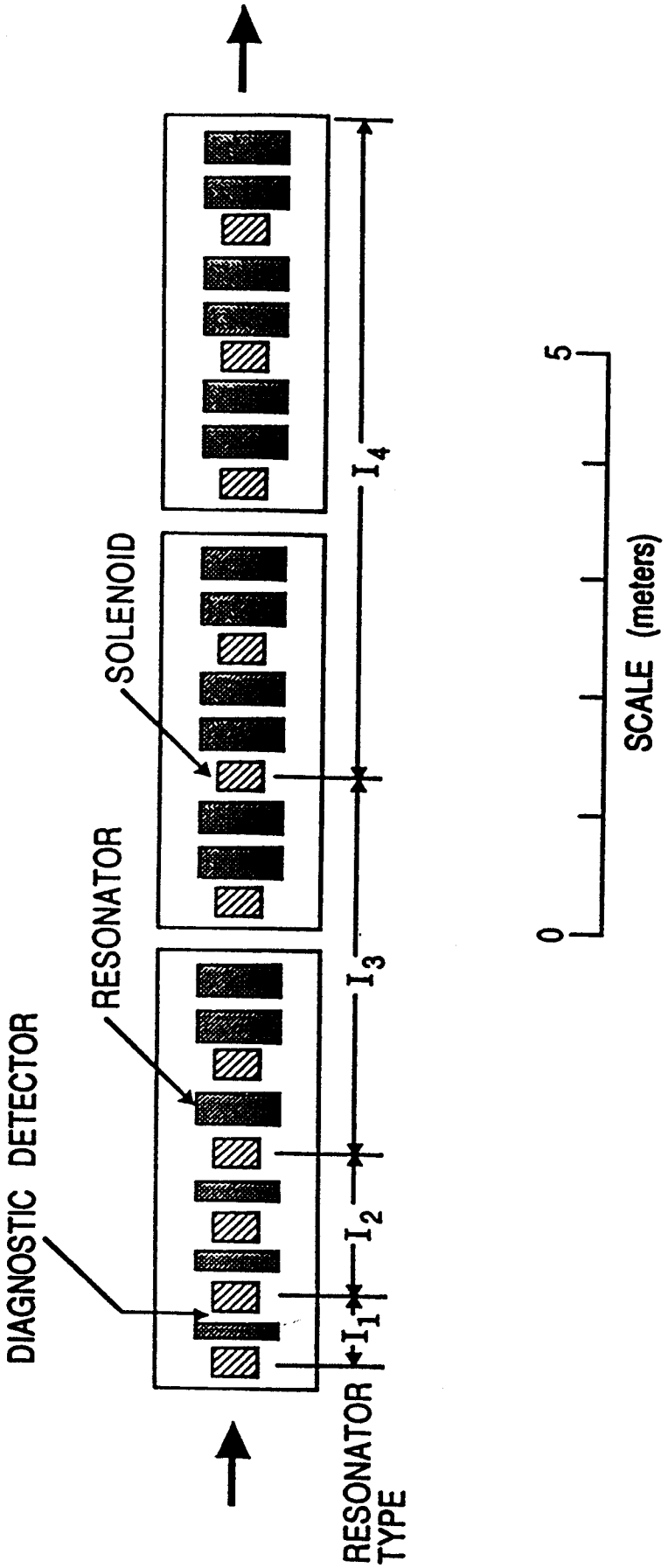

Figure 1.2: The configuration of the PII linac.

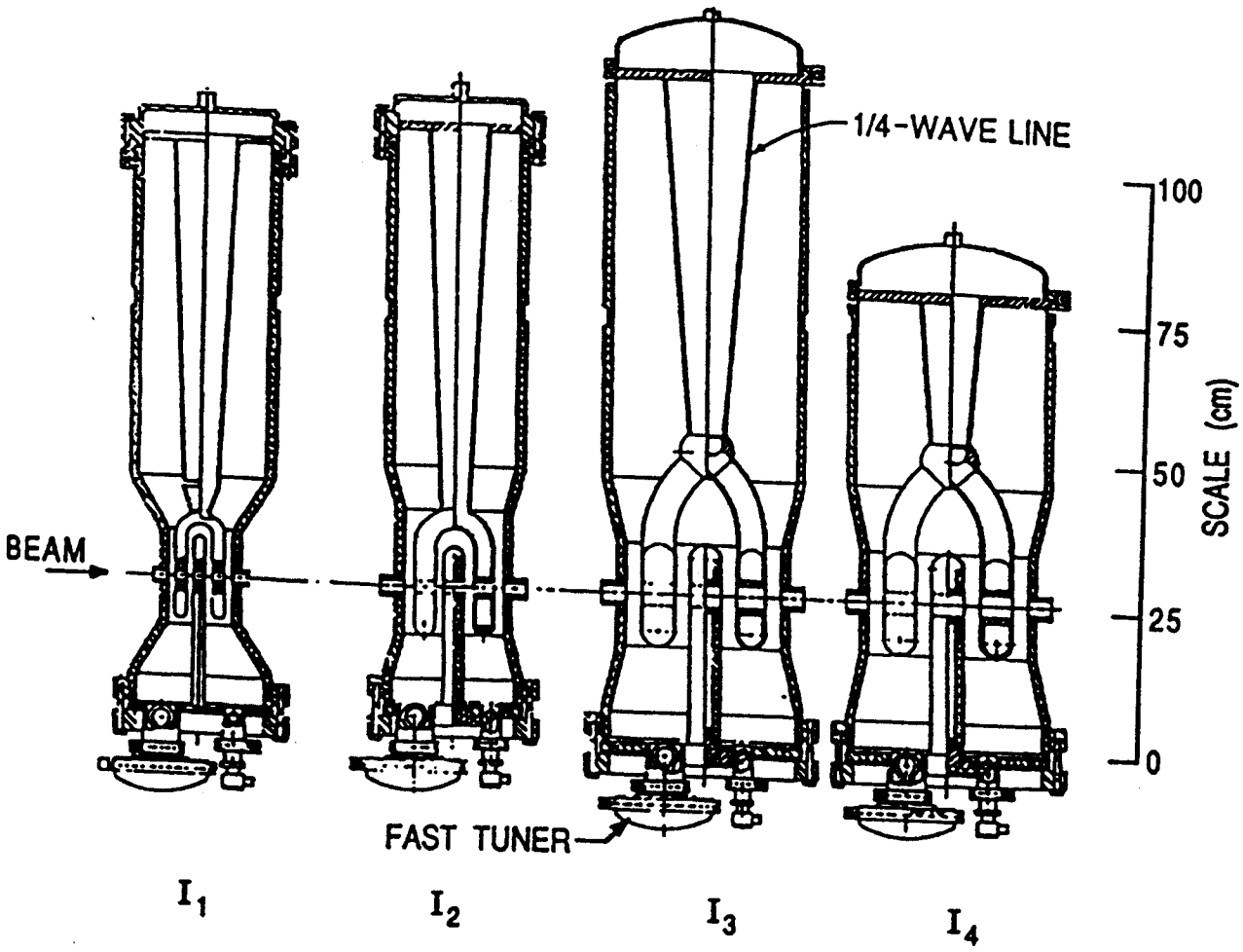

Figure 1.3: The resonators of the PII linac.

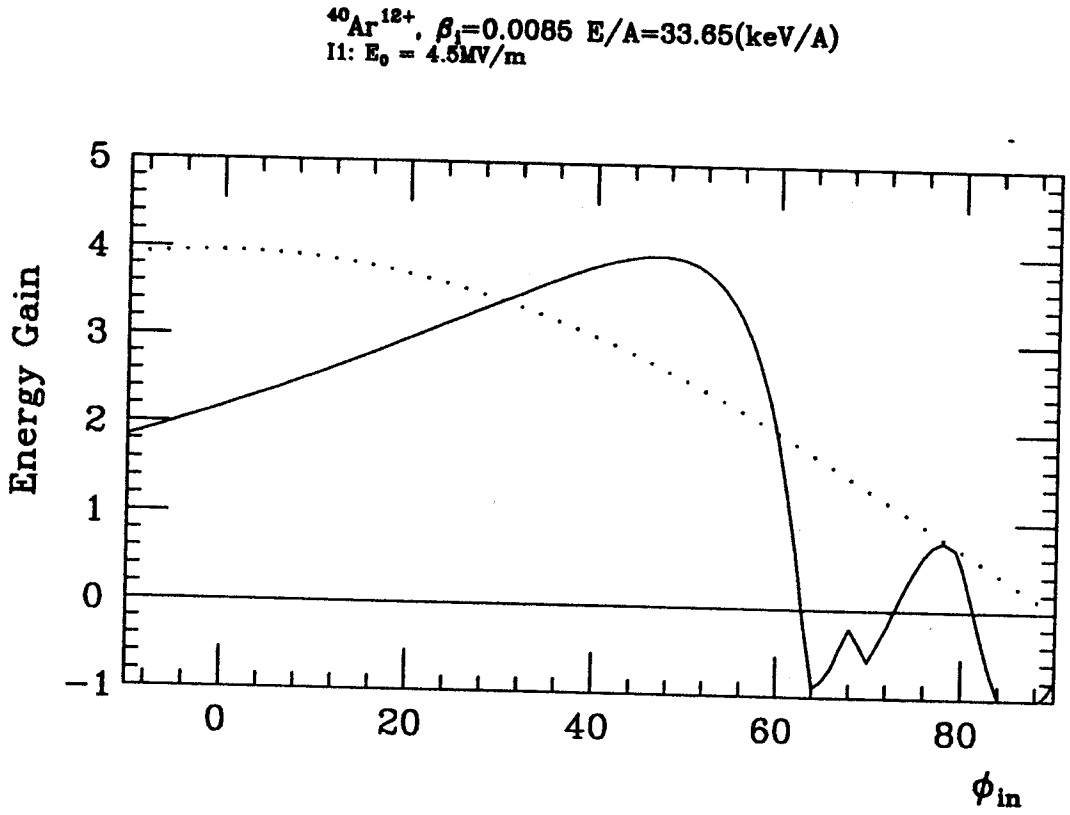

Figure 1.4: The curve of energy gain versus incident rf phase angle of type I1 resonator. The dotted line is the typical energy gain curve of a high beta resonator (not scaled).

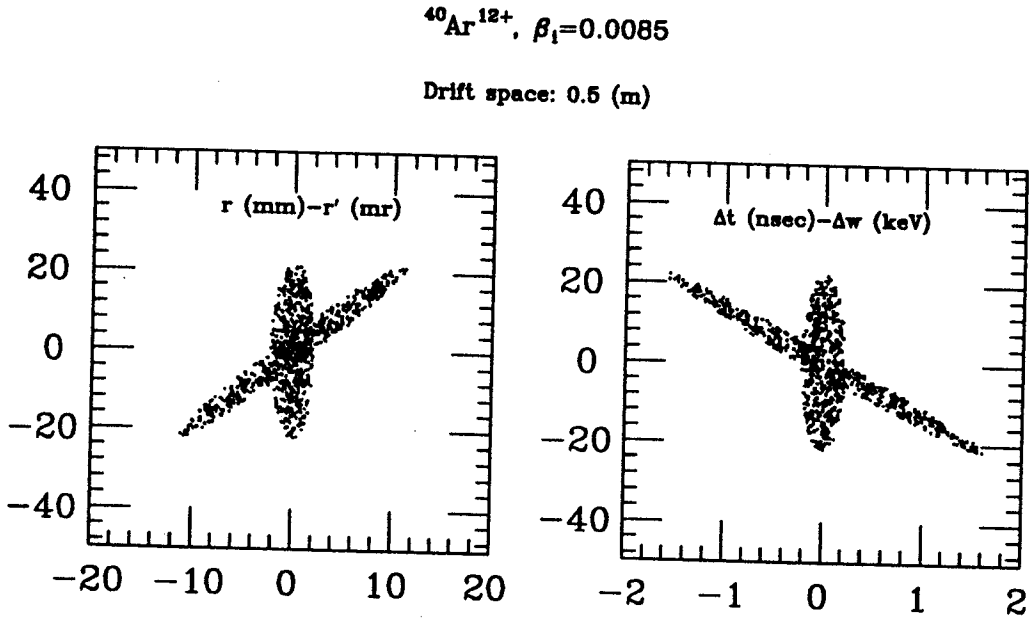

Figure 1.5: The actions of drift space on the transverse (left) and the longitudinal (right) phase spaces. The initial phase space ellipses are upright.

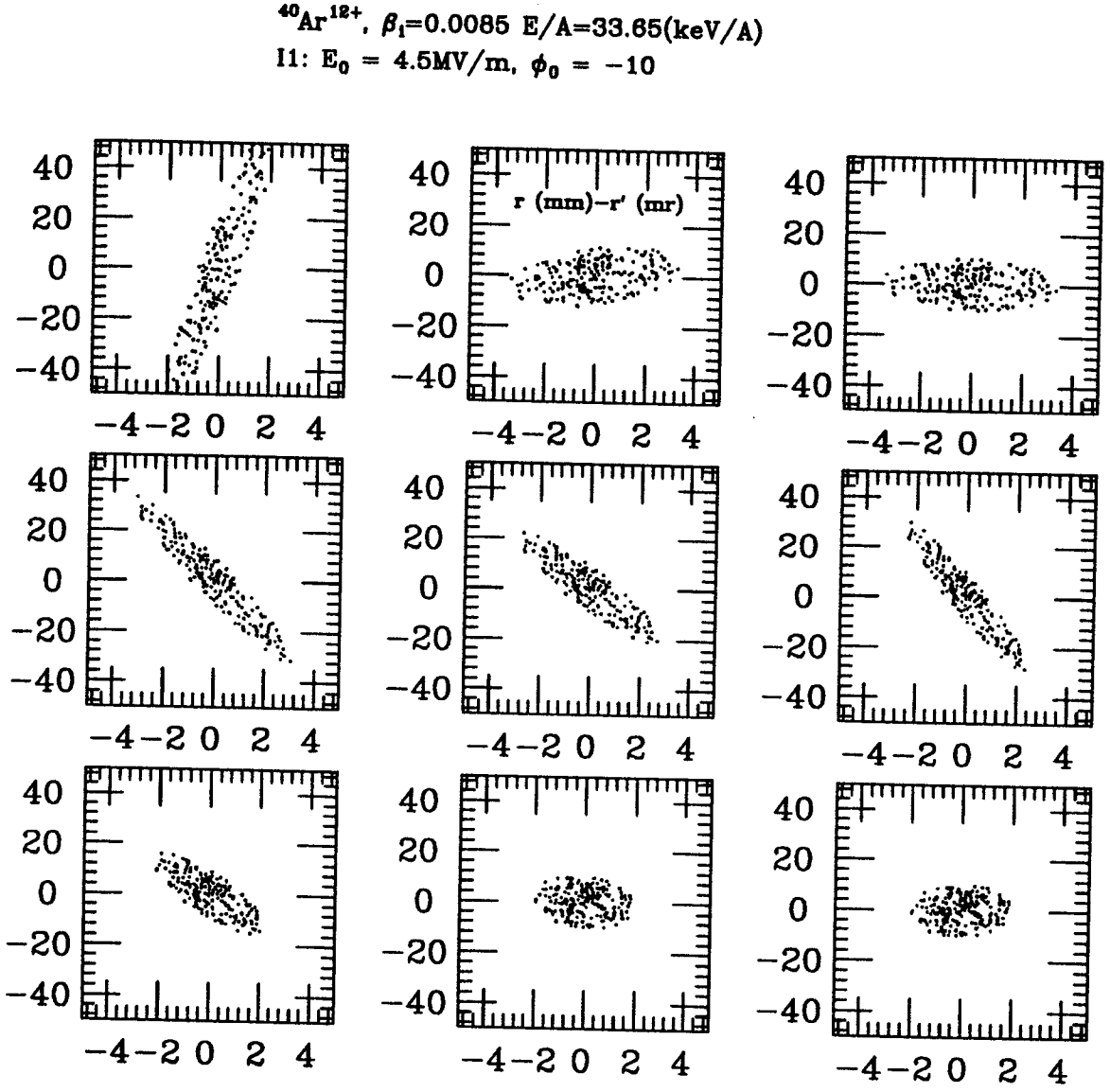

Figure 1.6: The transverse phase space transformations of $^{40}Ar^{12+}$ with incident velocity 0.0085c through type I1 resonator. Starting from the top left the positions of plots are at the entrance of gap1, at the center of gap1, and at the exit of gap1 or at the entrance of gap2 etc. The amplitude of electric field gradient and initial rf phase angle were 4.5 MV/m and −10 degrees respectively. The initial emittance of the beam was 50 mm·mr (area 50π mm·mr) without longitudinal emittance.

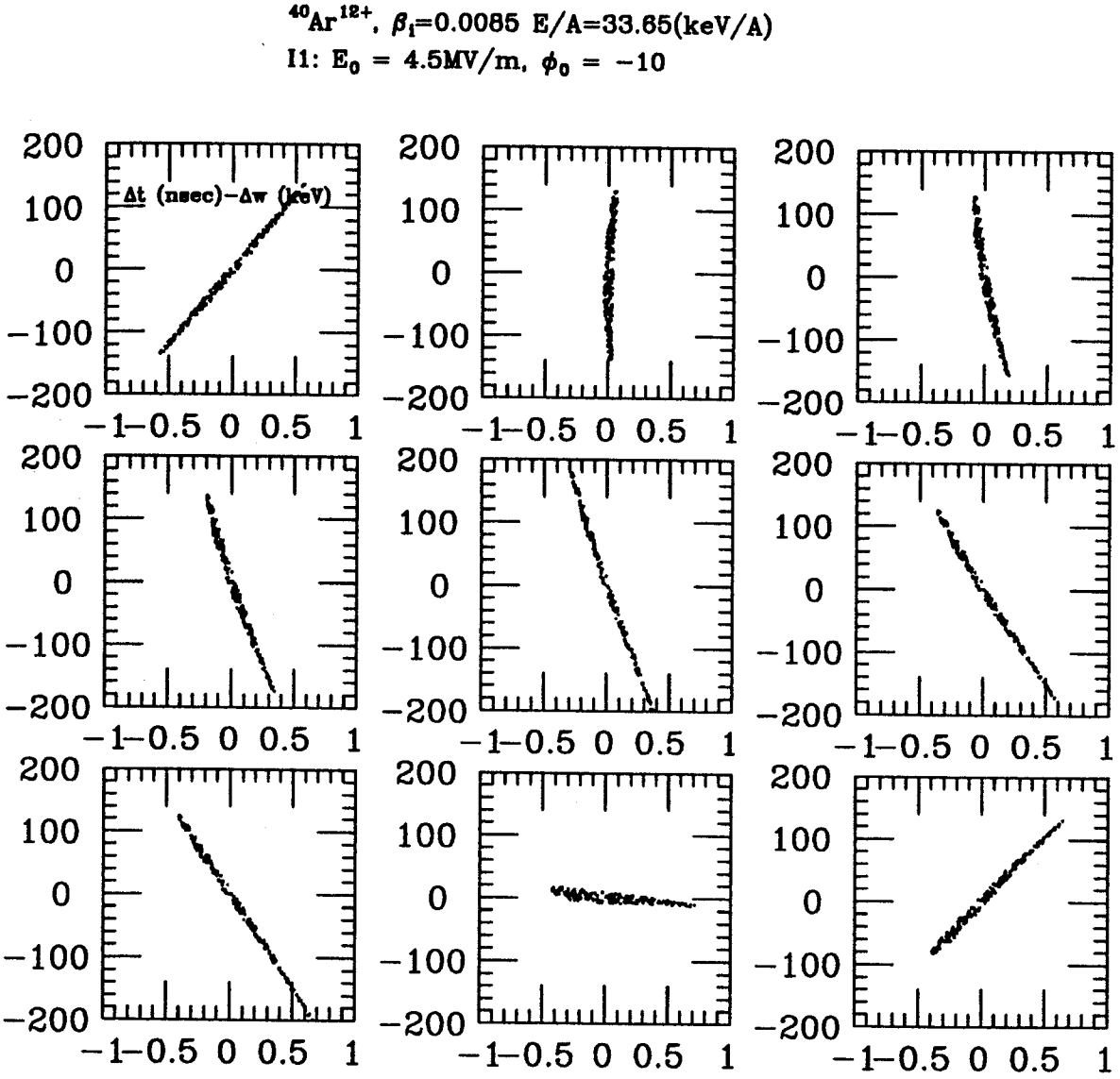

Figure 1.7: The longitudinal phase space transformations of $^{40}Ar^{12+}$ with incident velocity 0.0085c through type I1 resonator. Starting from the top left the positions of plots are at the entrance of gap1, at the center of gap1, and at the exit of gap1 or at the entrance of gap2 etc. The amplitude of electric field gradient and initial rf phase angle were 4.5 MV/m and −10 degrees respectively. The initial emittance of the beam was 5 keV ·nsec (area 5π keV·nsec) without transverse emittance.

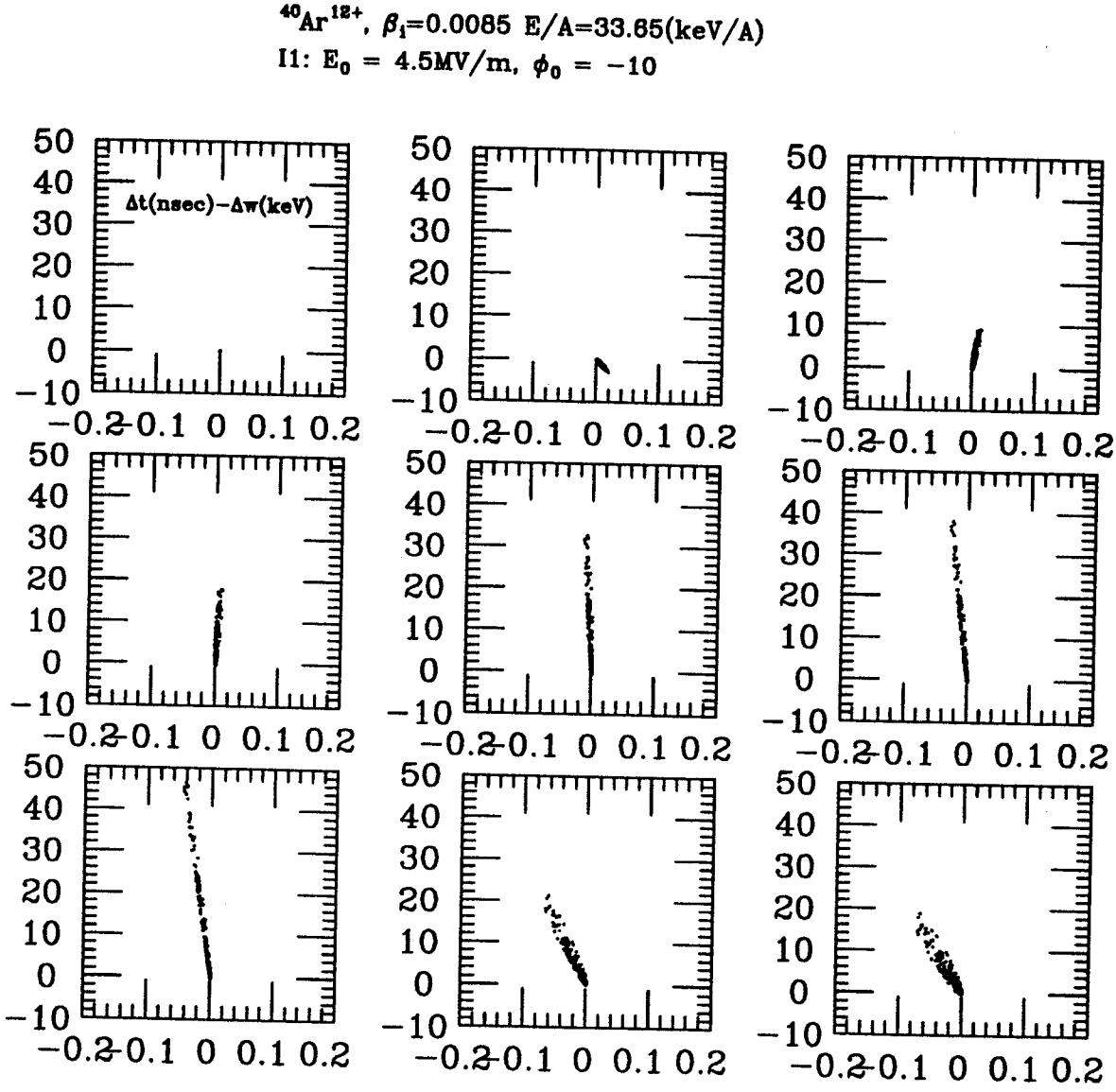

Figure 1.8: The growth of longitudinal phase space of $^{40}Ar^{12+}$ with incident velocity 0.0085c through type I1 resonator. Starting from the top left the positions of plots are at the entrance of gap1, at the center of gap1, and at the exit of gap1 or at the entrance of gap2 etc. The amplitude of electric field gradient and initial rf phase angle were 4.5 MV/m and −10 degrees respectively. The initial emittance of the beam was 50 mm·mr (area 50π mm·mr) without longitudinal emittance.

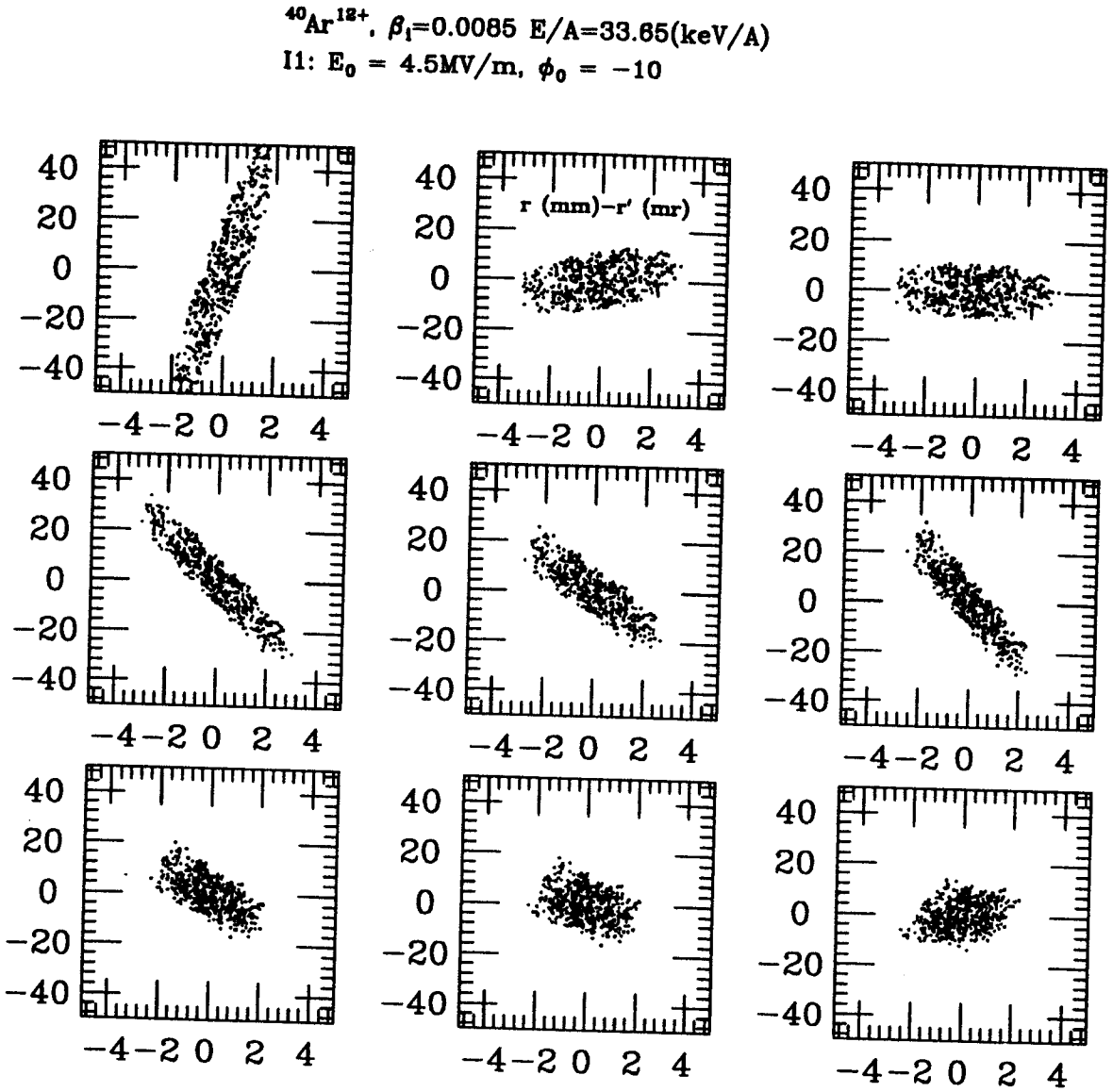

Figure 1.9: The transverse phase space transformations of $^{40}Ar^{12+}$ with incident velocity 0.0085c through type I1 resonator. Starting from the top left the positions of plots are at the entrance of gap1, at the center of gap1, and at the exit of gap1 or at the entrance of gap2 etc. The amplitude of electric field gradient and initial rf phase angle were 4.5 MV/m and −10 degrees respectively. The initial emittance of the beam was 50 mm·mr (area 50π mm·mr) with longitudinal emittance 5 keV·nsec.

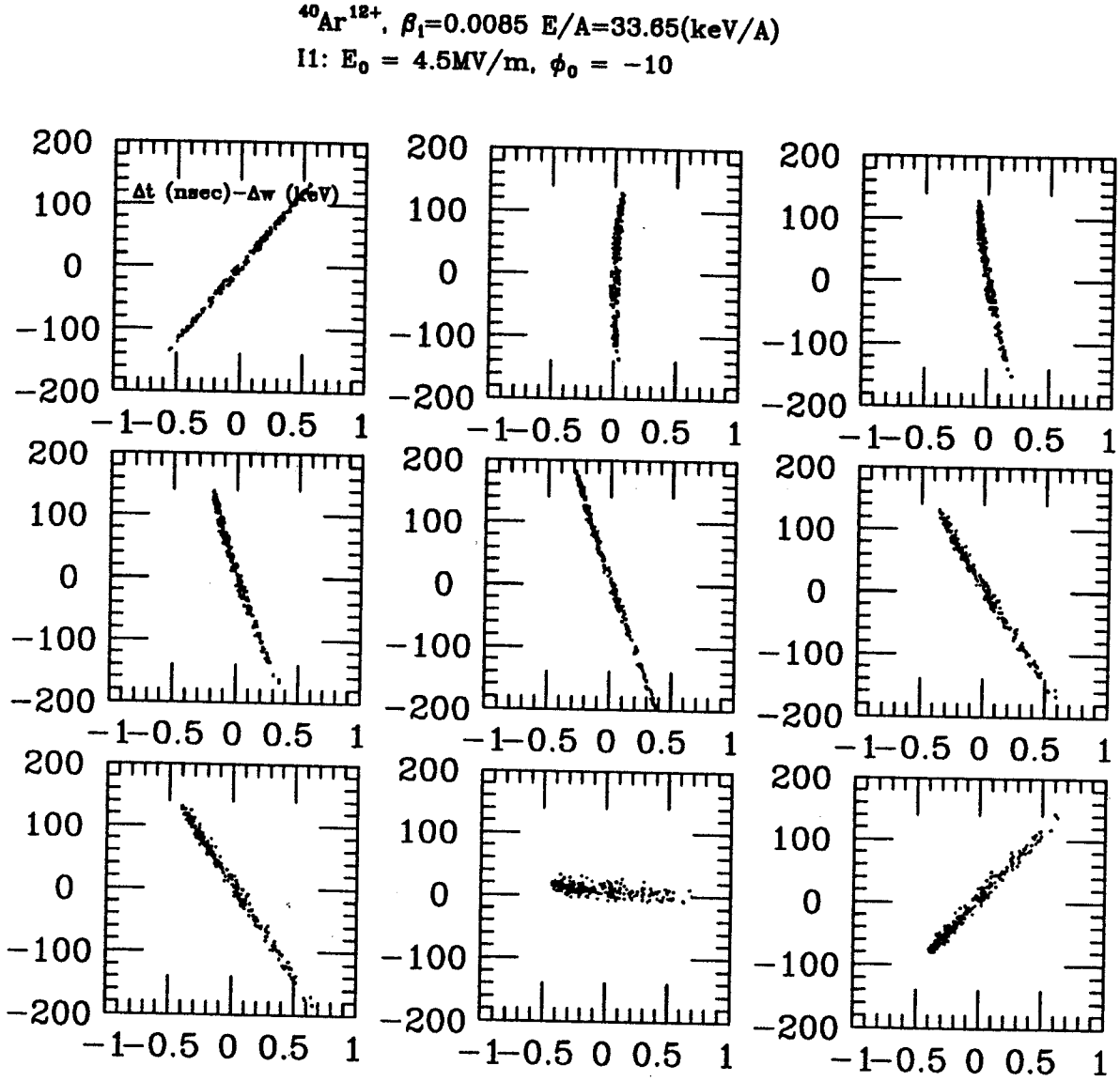

Figure 1.10: The longitudinal phase space transformations of $^{40}Ar^{12+}$ with incident velocity 0.0085c through type I1 resonator. Starting from the top left the positions of plots are at the entrance of gap1, at the center of gap1, and at the exit of gap1 or at the entrance of gap2 etc. The amplitude of electric field gradient and initial rf phase angle were 4.5 MV/m and −10 degrees respectively. The initial emittance of the beam was 50 mm·mr (area 50π mm·mr) with longitudinal emittance 5 keV·nsec.

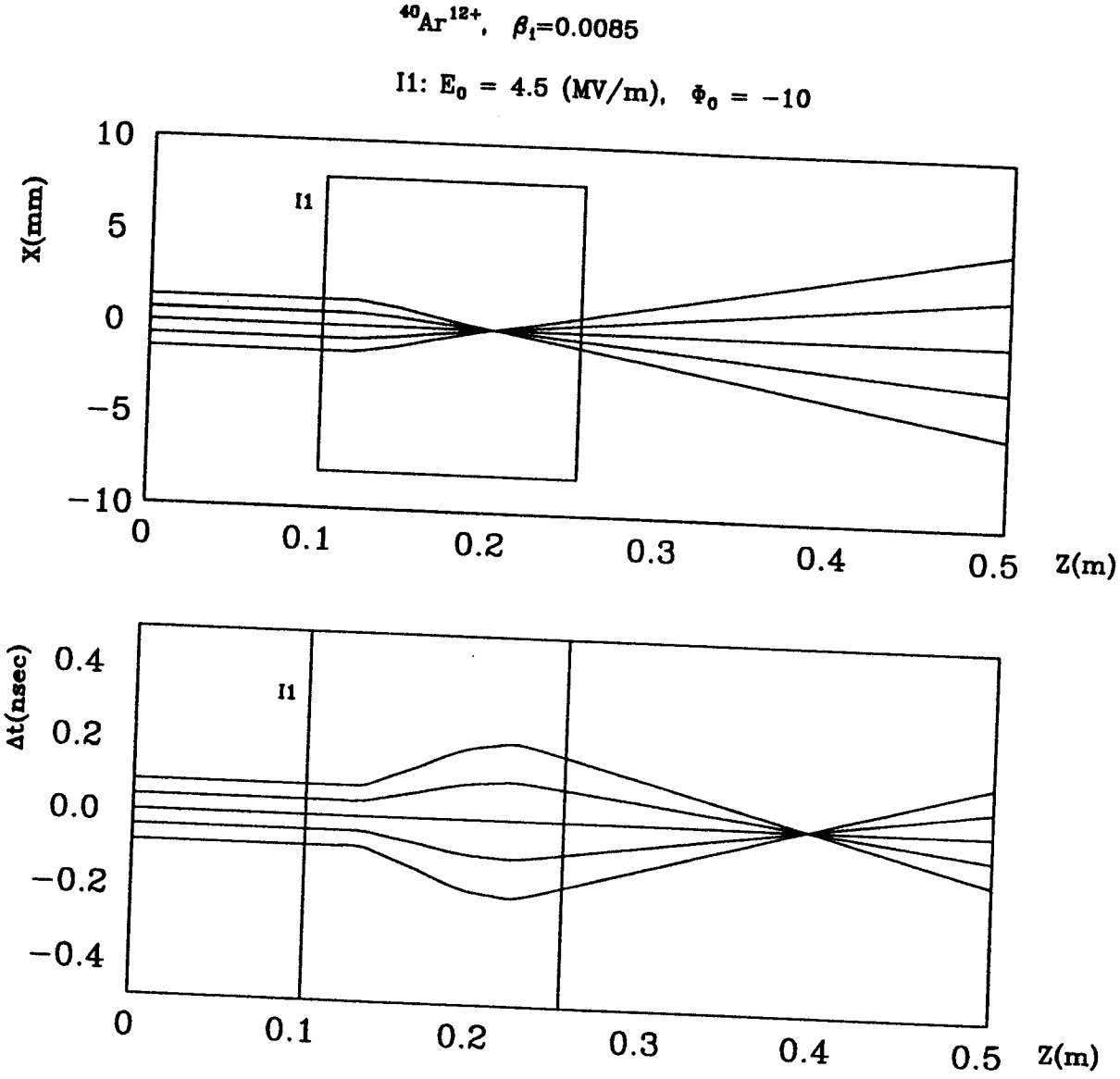

Figure 1.11: The transverse (upper) and longitudinal (lower) focusing properties of type I1 resonator for $^{40}Ar^{12+}$ beam with incident velocity 0.0085c. The amplitude of electric field gradient and initial rf phase angle were 4.5 MV/m and −10 degrees respectively.

Table 1.1: Accelerating structures of the PII resonators.

Type	No. of Gaps	RF Frequency (MHz)	β	Active Length (cm)	Nominal Field (MV/m)	Number of Units
I_1	4	48.5	0.008	10	4.5	1
I_2	4	48.5	0.015	16	3.0	2
I_3	4	48.5	0.024	25	3.0	5
I_4	4	72.75	0.036	25	3.0	10

Chapter 2

First Order Matrix Optics

2.1 Introduction

Matrix optics is a way to represent solutions of differential equations of motion of a particle or ray in a compact matrix form called a transfer matrix or transfer map. The transfer map relates initial coordinates of a particle or ray to its final coordinates. The transfer map is called 1st order if it contains 1st order solutions only and nth order if it contains solutions up to nth order. It is equivalent to a Taylor series approximation of the corresponding order.

The advantages of the matrix method compared with raytracing calculations are: First, it represents a system by the transfer map not by an individual particle as in raytracing, where it is necessary to integrate equations repeatedly for different initial conditions. Second, because of its explicit representation of a system, optimization or fitting is possible with an appropriate optimizer or even from a simple formula. For example, in a system consisting of a magnetic solenoid with two drift spaces before and after the solenoid, the magnetic field strength for an image condition can be found easily by an optimizer once the first order transfer map is known.

The other advantage of the matrix method itself is its extension to the transformation of the phase space ellipse of a bunch of particles or beam. In accelerator

physics the trace of a beam is usually more important than the trace of an individual particle, because a beam consists of numerous individual particles. The trace of a beam through a system is well described up to first order by the transformation of a phase space ellipse which can be calculated from a first order transfer map of the system.

First order matrix theory has been developed i.e. for transformation of particle coordinates and phase space ellipsoids when there is no acceleration (damping) in a system [Brown 73],[Brown 81], where the determinant of the transfer map is equal to one. It has been recently generalized to an accelerating system for betatron function parameterization in two dimensional decoupled phase space [Douglas 88].

This chapter briefly reviews the basic equations of first order matrix optics. Then we independently generalize first order phase space transformation based on the geometric characteristics of the phase ellipse for systems with acceleration, i.e. where the determinant of transfer map is not equal to one.

2.2 Transfer Map

The trajectory of an arbitrary particle in a beam is described by deviations from a reference trajectory in a given phase space. We assume that the solution of the equation of motion of these coordinate deviations of an arbitrary particle is given by a Taylor expansion. If the initial deviation is not large the first few terms in the Taylor expansion would be enough to describe the trajectory.

For a simple case we consider the two dimensional phase space of (x, x'). The final phase space coordinates, at distance z in the system, can be written by a Taylor

expansion in terms of the initial coordinates:

$$x(z) = \sum_{i,j}(x|x_0^i x_0'^j)x_0^i x_0'^j \ , \tag{2.1}$$

$$x'(z) = \sum_{i,j}(x'|x_0^i x_0'^j)x_0^i x_0'^j \ . \tag{2.2}$$

In the expansion the subscript 0 means initial deviation and the sum of $i+j$ determines the order of solution. The expansion coefficient is an abbreviation of the Taylor coefficients:

$$(x|x_0^i x_0'^j) = \frac{1}{(i+j)!}\frac{\partial^{i+j}x}{\partial^i x_0 \partial^j x_0'} \ . \tag{2.3}$$

If we consider the first order solution it can be expressed in matrix form:

$$\begin{pmatrix} x \\ x' \end{pmatrix} = \begin{pmatrix} (x|x) & (x|x') \\ (x'|x) & (x'|x') \end{pmatrix} \begin{pmatrix} x_0 \\ x_0' \end{pmatrix} \ . \tag{2.4}$$

Then the large parenthesis which contains Taylor expansion coefficients is called the transfer map or transfer matrix of the system. So if we apply the transfer map to the initial coordinates we get the final coordinates of the particle. The transfer map for higher order calculations can be derived from higher order Taylor expansion coefficients.

2.2.1 The Multiplication of Transfer Maps

Sometimes it is useful to build a whole system for several subsystems such as focusing elements, bending elements, and drifts. In this case we need multiplication of transfer maps. We consider a system consisting of two subsystems.

Let the transfer map from the point i to j be $M(i \to j)$ and $\vec{r}(k)$ be the coordinate vector at the point k. Then we get:

$$\vec{r}(2) = M(1 \to 2)\vec{r}(1) \ , \tag{2.5}$$

$$\vec{r}(3) = M(1 \rightarrow 3)\vec{r}(1) \; . \tag{2.6}$$

But $\vec{r}(3)$ can be rewritten by using equation (2.5):

$$\begin{aligned} \vec{r}(3) &= M(2 \rightarrow 3)\vec{r}(2) \\ &= M(2 \rightarrow 3)M(1 \rightarrow 2)\vec{r}(1) \; . \end{aligned} \tag{2.7}$$

By comparing equations (2.6) and (2.7) we obtain:

$$M(1 \rightarrow 3) = M(2 \rightarrow 3)M(1 \rightarrow 2) \; . \tag{2.8}$$

Similarly, transfer maps of any number of subsystems can be multiplied in inverse order to get the transfer map of the whole system [Berz 92]. If the transfer maps are first order then their multiplications comply with matrix algebra. This would be extended to higher order transfer maps represented in the form of a matrix.

2.2.2 Interpretation of Transfer Matrix

If x and x' in equation (2.4) represent the position and inclined angle of a ray, a transfer matrix element has its own physical meaning for a system [Brown 67], [Wollnik 87a].

1. If $(x|x) = 0$ then we get from the first row of equation (2.4):

   $x = (x|x')x'_0$.

   This means that final coordinate x does not depend on initial coordinate x_0. So all particles or rays with the same inclined angle relative to the optic axis are focused to the same point. This system is called parallel-to-point, and this location corresponds to the focal point in ordinary optics.

2. If $(x|x') = 0$ then we get from the first row of the equation (2.4):

   $x = (x|x)x_0$.

This means that final coordinate x does not depend on initial inclined angle x'_0. So all rays starting at the same point with different initial angles are focused to the same point. This system is called point-to-point, and corresponds to the paraxial image condition in ordinary optics.

3. If $(x'|x) = 0$ then we get from the second row of the equation (2.4):

   $x' = (x'|x')x'_0$.

   This means that final inclined angle x' does not depend on initial coordinate x_0. So all rays starting with the same initial angles have the same final angles. This system is called parallel-to-parallel.

4. If $(x'|x') = 0$ then we get from the second row of equation (2.4):

   $x' = (x'|x)x_0$.

   This means that final inclined angle does not depend on initial inclined angle. So all rays starting at the same point with different initial angles have the same final angles. This system is called point-to-parallel.

2.3 Phase Space Transformation

2.3.1 2-dimensional Phase Space Ellipse

A two dimensional beam phase ellipse is described by Twiss parameters [Wollnik 87a] or Courant-Snyder parameters [Courant 58] by a standard equation of an ellipse:

$$\gamma x^2 + 2\alpha x x' + \beta x'^2 = \epsilon \, . \tag{2.9}$$

where

$$\gamma\beta - \alpha^2 = 1 \, . \tag{2.10}$$

Alternatively, in matrix form:

$$\begin{pmatrix} x & x' \end{pmatrix} \begin{pmatrix} \gamma & \alpha \\ \alpha & \beta \end{pmatrix} \begin{pmatrix} x \\ x' \end{pmatrix} = \epsilon \, . \tag{2.11}$$

The area of the ellipse is $\pi\epsilon$, when ϵ is the emittance of the beam.

Let the transfer map from point 1 to point 2 be M. If there are no couplings with other coordinates of different phase plane like (y, y') or $(\Delta t, \Delta w)$, then the transfer map is given by just a two by two matrix:

$$M = \begin{pmatrix} M_{11} & M_{12} \\ M_{21} & M_{22} \end{pmatrix} \, . \tag{2.12}$$

Also:

$$M^{-1} = \begin{pmatrix} M_{22} & -M_{12} \\ -M_{21} & M_{11} \end{pmatrix} (\det M)^{-1} \, , \tag{2.13}$$

where M^{-1} and det M are the inverse matrix and determinant of the matrix M, respectively. Note that det M is equal to one if there is no acceleration in a system [Cotte 38],[Brown 67]. In general, det M is the ratio of the corresponding initial and final momenta [Wollnik 87b], [Douglas 88].

At point 1 in terms of point 2:

$$\begin{pmatrix} x_1 \\ x_1' \end{pmatrix} = M^{-1} \begin{pmatrix} x_2 \\ x_2' \end{pmatrix} \, , \tag{2.14}$$

$$\begin{pmatrix} x_1 & x_1' \end{pmatrix} = \begin{pmatrix} x_2 & x_2' \end{pmatrix} (M^{-1})^{\mathrm{tr}} \, , \tag{2.15}$$

where superscript tr means the transpose of a matrix.

It follows that from equations (2.11), (2.14), and (2.15):

$$\begin{pmatrix} x_2 & x_2' \end{pmatrix} (M^{-1})^{\mathrm{tr}} \begin{pmatrix} \gamma_1 & \alpha_1 \\ \alpha_1 & \beta_1 \end{pmatrix} M^{-1} \begin{pmatrix} x_2 \\ x_2' \end{pmatrix} = \epsilon_1 \, . \tag{2.16}$$

At point 2:

$$\begin{pmatrix} x_2 & x_2' \end{pmatrix} \begin{pmatrix} \gamma_2 & \alpha_2 \\ \alpha_2 & \beta_2 \end{pmatrix} \begin{pmatrix} x_2 \\ x_2' \end{pmatrix} = \epsilon_2 \, . \tag{2.17}$$

Let T be:

$$T = \begin{pmatrix} M_{22} & -M_{21} \\ -M_{12} & M_{11} \end{pmatrix} \begin{pmatrix} \gamma_1 & \alpha_1 \\ \alpha_1 & \beta_1 \end{pmatrix} \begin{pmatrix} M_{22} & -M_{12} \\ -M_{21} & M_{11} \end{pmatrix} \, . \tag{2.18}$$

Then the determinant of T is:

$$\det T = (\det M)^{-2} \, . \tag{2.19}$$

The Twiss parameters should also satisfy equation (2.10) at point 2, this will be discussed in section 2.3.2. Therefore we get the phase space transformation by comparing equations (2.16) and (2.17):

$$\begin{pmatrix} \beta_2 \\ \alpha_2 \\ \gamma_2 \end{pmatrix} = (\det M)^{-1} A \begin{pmatrix} \beta_1 \\ \alpha_1 \\ \gamma_1 \end{pmatrix} \, , \tag{2.20}$$

$$\epsilon_2 = (\det M)\epsilon_1 \, , \tag{2.21}$$

where

$$A = \begin{pmatrix} M_{11}^2 & -2M_{11}M_{12} & M_{12}^2 \\ -M_{11}M_{21} & M_{11}M_{22} + M_{12}M_{21} & -M_{12}M_{22} \\ M_{21}^2 & -2M_{21}M_{22} & M_{22}^2 \end{pmatrix} \, . \tag{2.22}$$

If det M is equal to one, i.e. no change in energy, the equations for the phase space transformation give the standard equations, where the area of phase space or beam

emittance is a constant of motion. For an acceleration system, the determinant of a transfer map is less than one and greater than one for a deceleration system.

2.3.2 N-dimensional Phase Space Ellipsoid for an Axially Symmetric Beam

We now extend the formalism to n-dimensional phase space. If a beam is axially symmetric through a system the equation of an n-dimensional ellipsoid can be written in matrix form as:

$$X(1)^{\mathrm{tr}} T(1) X(1) = \epsilon_1 \, . \tag{2.23}$$

where X(1) is the coordinate vector at the point 1, and T(1) is a n $\times$ n real symmetric matrix corresponding to the σ matrix in the Transport notation [Brown 79]. Also $\pi\epsilon_1$ is the phase space area of the projection on one plane.

The volume of the ellipsoid V_n and area of the projection on one plane A are:

$$V_n = \frac{(\pi\epsilon)^{n/2}}{\Gamma(\frac{n}{2}+1)} \, , \tag{2.24}$$

$$A = \pi\epsilon \, . \tag{2.25}$$

Now let's consider matrix T:

1. $T_{ij} = T_{ji}$ by symmetry.

2. In the two dimensional case (n=2) T_{ij} corresponds to the matrix of Twiss parameters:

$$\begin{pmatrix} T_{11} & T_{12} \\ T_{12} & T_{22} \end{pmatrix} = \begin{pmatrix} \gamma & \alpha \\ \alpha & \beta \end{pmatrix} \, . \tag{2.26}$$

3. Its determinant is equal to one.

We consider an upright n-dimensional phase space ellipsoid:

$$\left(\frac{x_1}{x_{10}}\right)^2 + \left(\frac{x_2}{x_{20}}\right)^2 + \cdots\cdots + \left(\frac{x_{n-1}}{x_{10}}\right)^2 + \left(\frac{x_n}{x_{20}}\right)^2 = 1\,, \tag{2.27}$$

where x_{i0} means the maximum of the x_i coordinate in the phase space ellipsoid. As a result of the axial symmetry x_{10} and x_{20} are the same for any pair of phase space coordinates.

Let ϵ be beam emittance on one projected plane from n-dimensional phase space:

$$\epsilon = x_{10}x_{20}\,. \tag{2.28}$$

We also define a matrix element of T to be a coefficient of an n-dimensional phase space ellipsoid:

$$\begin{aligned} T_{ij} &= \text{coefficient of } \; x_i^{n_i}x_j^{n_j} \\ i,\ j &= 1,\ 2,\ 3,\ \cdots\cdots\ n\,, \\ n_i &+ n_j = n\,. \end{aligned} \tag{2.29}$$

With these definitions equation (2.27) leads to:

$$T_{11}x_1^2 + T_{22}x_2^2 + \cdots\cdots + T_{n-1,n-1}x_{n-1}^2 + T_{nn}x_n^2 = \epsilon\,, \tag{2.30}$$

where

$$\begin{aligned} T_{11} &= \frac{\epsilon}{x_{10}^2} \\ T_{22} &= \frac{\epsilon}{x_{20}^2} \\ &\vdots \\ T_{n-1,n-1} &= \frac{\epsilon}{x_{10}^2} \\ T_{nn} &= \frac{\epsilon}{x_{20}^2}\,. \end{aligned}$$

To find the determinant of the T matrix:

$$\det T = \Pi_{i=1}^{n} T_{ii} = 1 \ . \tag{2.31}$$

This was derived from the special case of an upright n-dimensional ellipsoid. But since we can always find a rotated coordinate system in which the ellipsoid is upright, this should be also true for tilted ellipsoids.

Equation (2.23) is rewritten using the transfer map M from point 1 to point 2:

$$X(2)^{\mathrm{tr}}(M^{-1})^{\mathrm{tr}} T(1) M^{-1} X(2) = \epsilon_1 \ . \tag{2.32}$$

At point 2:

$$X(2)^{\mathrm{tr}} T(2) X(2) = \epsilon_2 \ . \tag{2.33}$$

Let T_2' be:

$$T_2' = (M^{-1})^{\mathrm{tr}} T(1) M^{-1} \ . \tag{2.34}$$

Then it is required, with an appropriate constant C, that:

$$\det\left(C T_2'\right) = 1 \ . \tag{2.35}$$

Using the facts from matrix algebra:

$$\det(AB) = \det(A) \cdot \det(B) \ , \tag{2.36}$$

$$\det A^{-1} = (\det A)^{-1} \ , \tag{2.37}$$

$$\det A^{\mathrm{tr}} = \det A \ , \tag{2.38}$$

we get:

$$C = (\det M)^{2/n} \ . \tag{2.39}$$

Therefore, we get a transformation formula for the n-dimensional phase space ellipsoid:

$$T(2) = (\det M)^{2/n} (M^{-1})^{\mathrm{tr}} T(1) M^{-1} \ , \tag{2.40}$$

$$\epsilon_2 = (\det M)^{2/n} \epsilon_1 \ . \tag{2.41}$$

Note if n=2 we get the same result as in section 2.3.1.

2.3.3 Envelope of Phase Space Ellipsoid

The envelope of the phase space ellipsoid in one projection plane is found by searching for the maximum points of the projected two dimensional phase space ellipse at various axial points through a system. The equation of the phase space ellipse in a projection plane (x, x') is given by:

$$T_{xx}x^2 + 2T_{xx'}xx' + T_{x'x'}x'^2 = \epsilon_{xx'} \; . \tag{2.42}$$

Obviously they satisfy the relation:

$$T_{xx}T_{x'x'} - T_{xx'}^2 = 1 \; . \tag{2.43}$$

We replace T_{ij} with Twiss parameters which describe the shape of a 2-dimensional phase space ellipse in a projection plane (x, x'):

$$T_{xx} = \gamma, \quad T_{xx'} = \alpha, \quad T_{x'x'} = \beta \; . \tag{2.44}$$

Then equation (2.23) is written as:

$$\gamma x^2 + 2\alpha xx' + \beta x'^2 = \epsilon_{xx'} \; \equiv \; \epsilon \; . \tag{2.45}$$

Now we find the maxima of the phase space ellipse on the two coordinates. Define $f(x, x')$ to be:

$$f(x, x') \; \equiv \; \gamma x^2 + 2\alpha xx' + \beta x'^2 - \epsilon = 0 \; . \tag{2.46}$$

Then take the gradient to get:

$$\vec{\nabla} f(x, x') = (2\gamma x + 2\alpha x', 2\alpha x + 2\beta x') \; . \tag{2.47}$$

Since $[\vec{\nabla} f(x, x')]_{x'} = 0$ at the maximum value of x, we get $x' = -\frac{\alpha}{\beta}x$. Inserting this into equation (2.46) we get for maximum x:

$$x_m = \sqrt{\beta\epsilon} \; . \tag{2.48}$$

But if we use equation (2.41) for a beam emittance transformation we get the beam envelope of x in terms of initial beam emittance ϵ_1:

$$x_m = \sqrt{(\det M)^{2/n} \beta \epsilon_1} \,. \tag{2.49}$$

Similarly, we get for maximum x':

$$x'_m = \sqrt{(\det M)^{2/n} \gamma \epsilon_1} \,. \tag{2.50}$$

If the determinant of a transfer map is equal to one we get the standard equations for beam envelopes of x and x', where β and γ describe beam envelope characteristics of a system. But in general the beam envelope characteristics of a system are described by the transfer map and Twiss parameters of a phase space from equations (2.49) and (2.50).

2.3.4 Example of n=4 Case

As an actual example we consider the phase space transformation of the ATLAS Positive Ion Injector which consists of axially symmetric rf resonators and magnetic solenoids. In this case the correlations exist between the phase space coordinates due to rotation of an individual particle under axial magnetic field component of solenoids. For example, in a magnetic solenoid coupling between transverse coordinates exist, but longitudinal coordinates remain decoupled in first order. Therefore the transverse phase space is 4-dimensional in rectangular coordinates.

The equation of the phase space ellipsoid is given by equation (2.23) by:

$$\begin{pmatrix} x & x' & y & y' \end{pmatrix} \begin{pmatrix} T_{xx} & T_{xx'} & 0 & 0 \\ T_{xx'} & T_{x'x'} & 0 & 0 \\ 0 & 0 & T_{xx} & T_{xx'} \\ 0 & 0 & T_{xx'} & T_{x'x'} \end{pmatrix} \begin{pmatrix} x \\ x' \\ y \\ y' \end{pmatrix} = \epsilon \,. \tag{2.51}$$

Because of axial symmetry we can simply replace T_{ij} with the Twiss parameters which describe the 2-dimensional phase space ellipse in the equations (2.44) and (2.45):

Therefore inserting Twiss parameters we get:

$$\begin{pmatrix} x & x' & y & y' \end{pmatrix} \begin{pmatrix} \gamma & \alpha & 0 & 0 \\ \alpha & \beta & 0 & 0 \\ 0 & 0 & \gamma & \alpha \\ 0 & 0 & \alpha & \beta \end{pmatrix} \begin{pmatrix} x \\ x' \\ y \\ y' \end{pmatrix} = \epsilon \,. \tag{2.52}$$

The transfer map under axial symmetry is given by:

$$M = \begin{pmatrix} M_{11} & M_{12} & M_{13} & M_{14} \\ M_{21} & M_{22} & M_{23} & M_{24} \\ -M_{13} & -M_{14} & M_{11} & M_{12} \\ -M_{23} & -M_{24} & M_{21} & M_{22} \end{pmatrix} \tag{2.53}$$

From equation (2.40) for the n-dimensional case we get phase the space transformation for n=4:

$$\begin{pmatrix} \beta_2 \\ \alpha_2 \\ \gamma_2 \end{pmatrix} = T_A \begin{pmatrix} \beta_1 \\ \alpha_1 \\ \gamma_1 \end{pmatrix} (\det M)^{-1/2} \,, \tag{2.54}$$

where

$$T_A = \begin{pmatrix} A_{22}^2 + A_{42}^2 & 2(A_{12}A_{22} + A_{32}A_{42}) & A_{12}^2 + A_{32}^2 \\ A_{21}A_{22} + A_{41}A_{42} & A_{11}A_{22} + A_{12}A_{21} + A_{31}A_{42} + A_{32}A_{41} & A_{11}A_{12} + A_{31}A_{32} \\ A_{21}^2 + A_{41}^2 & 2(A_{11}A_{21} + A_{31}A_{41}) & A_{11}^2 + A_{31}^2 \end{pmatrix} , \tag{2.55}$$

$$A_{ij} = (\det M)^{1/2} (M^{-1})_{ij} \quad (i, j = 1, 2, 3, 4) \,. \tag{2.56}$$

For beam emittance and envelope transformations:

$$\epsilon_2 = \sqrt{\det M}\,\epsilon_1 \,, \tag{2.57}$$

$$x_2 = \sqrt{(\det M)^{1/2}\beta_2\epsilon_1} \,, \tag{2.58}$$

$$x_2' = \sqrt{(\det M)^{1/2}\gamma_2\epsilon_1} \,. \tag{2.59}$$

The beam emittance does not change for magnetic solenoids, but in a system including accelerating structures like rf resonators it changes by a factor of the square root of the determinant of the transfer map of the system.

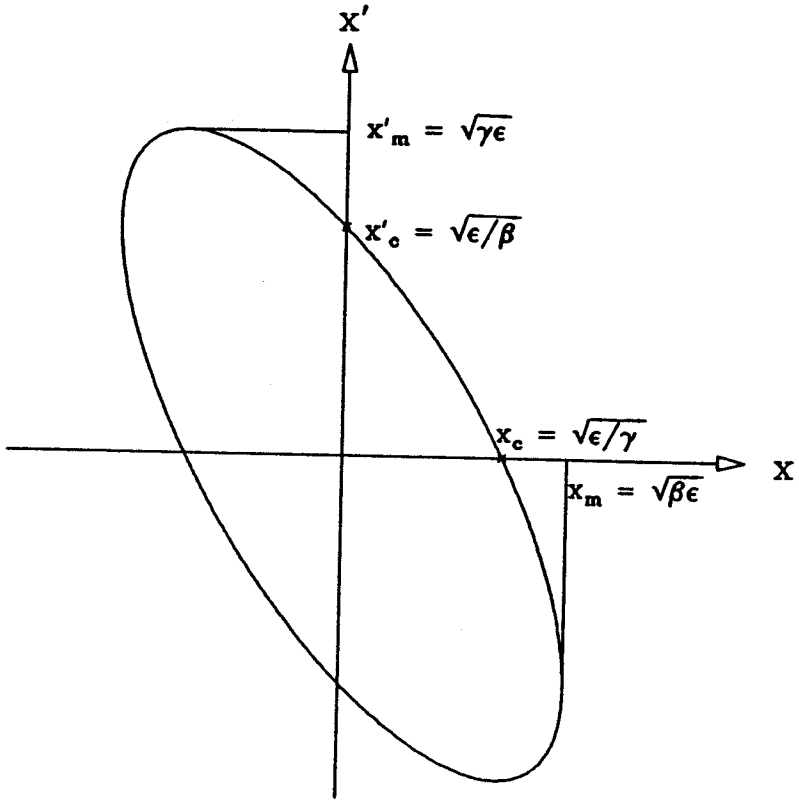

Figure 2.1: A two dimensional beam phase space ellipse. The equation of the ellipse is given by $\gamma x^2 + 2\alpha x x' + \beta x'^2 = \epsilon$. The area of the phase space ellipse is $\pi\epsilon$. The ϵ is called beam emittance.

Chapter 3

The Equations of Motion of Linac Components

3.1 Introduction

The optical elements of the PII linac consist of radio frequency four-gap resonators, superconducting magnetic solenoids, and drift spaces. Because of slow particle beam velocities, less than 0.04c, the equations of motion are not solved by simple approximations as in the high velocity case where rf cavities are treated as thin lenses. Therefore they include nonlinear terms to be solved numerically in the equations of motion.

In this chapter we derive the Taylor series expansion of radial and longitudinal rf electromagnetic fields. We introduce a model solenoidal field with appropriate parameters for the superconducting magnetic solenoids at the PII linac. These higher order fields will be used to describe the nonlinear equations of motion.

Also we derive linear matrix optics both for the transverse and for the longitudinal directions with the following assumptions [Vlasov 68]:

1. The longitudinal component of the transverse focusing field is negligible.

2. The radial velocity component of a particle is negligible relative to the longitu-

dinal component.

3. The longitudinal force of the rf magnetic field is sufficiently small to be replaced by only an rf electric field.

4. The deviation of a particle is small enough to ignore the radial rf electric field component.

Finally we describe the ways that the linear and nonlinear equations of motion are implemented into computer programs.

3.2 Equations of Motion

Since the Positive Ion Injector (PII) consists of only axially symmetric elements the cylindrical coordinate system would best describe related particle motions. However, the equations of motion are written in rectangular coordinates for future possibilities to add nonaxial symmetric elements like quadrupoles.

In rectangular coordinates x and y are deviations in horizontal and vertical directions respectively from the reference trajectory. The distance z along the reference trajectory is used as an independent variable.

The equation of motion of a particle of charge q with rest mass m under a Lorentz force is written by:

$$\frac{d\vec{P}}{dt} = q(\vec{E} + \vec{V} \times \vec{B}) \,, \tag{3.1}$$

where $\vec{E}$ and $\vec{B}$ represent electric and magnetic fields respectively. $\vec{V}$ is the velocity of a particle.

In component form:

$$\frac{d}{dt_s}\left(\frac{mc\beta_s}{\sqrt{1-\beta_s^2}}\right) = qE_z(0)\,, \tag{3.2}$$

$$\frac{d}{dt}\left(\frac{mc\beta_x}{\sqrt{1-\beta^2}}\right) = q(E_x + c\beta_y B_z - c\beta_z B_y)\,,$$

$$\frac{d}{dt}\left(\frac{mc\beta_y}{\sqrt{1-\beta^2}}\right) = q(E_y + c\beta_z B_x - c\beta_x B_z)\,, \tag{3.3}$$

$$\frac{d}{dt}\left(\frac{mc\beta_z}{\sqrt{1-\beta^2}}\right) = q(E_z + c\beta_z B_y c - c\beta_y B_x)\,,$$

where

$$\vec{\beta} \equiv \frac{\vec{V}}{c}\,. \tag{3.4}$$

The subscript s indicates the reference trajectory. Thus the first equation is for a reference particle and the other ones are for a deviated particle from that reference trajectory.

Now we change the independent variable from time to the position of the reference trajectory by using:

$$\frac{d}{dt_s} = c\beta_s\frac{d}{dz}\,,$$

$$\frac{d}{dt} = c\beta_z\frac{d}{dz}\,, \tag{3.5}$$

and

$$\vec{\beta} = \beta_z\frac{d\vec{r}}{dz}\,. \tag{3.6}$$

Also, if we assume $\beta \approx \beta_z$ the equations of motion (3.2) and (3.3) become:

$$\frac{d\beta_s}{dz} = (\frac{q}{mc^2})\frac{(1-\beta_s^2)^{3/2}}{\beta_s}E_z(0)\,, \tag{3.7}$$

$$\begin{aligned}
\frac{d^2x}{dz^2} &= (\frac{q}{mc^2})\frac{\sqrt{1-\beta_z^2}}{\beta_z^2}\left\{E_x + \frac{\beta_z B_z}{c}\frac{dy}{dz} - \frac{\beta_z B_y}{c}\right\} - \frac{1}{\beta_z(1-\beta_z^2)}\frac{d\beta_z}{dz}\frac{dx}{dz}\,, \\
\frac{d^2y}{dz^2} &= (\frac{q}{mc^2})\frac{\sqrt{1-\beta_z^2}}{\beta_z^2}\left\{E_y + \frac{\beta_z B_x}{c} - \frac{\beta_z B_z}{c}\frac{dx}{dz}\right\} - \frac{1}{\beta_z(1-\beta_z^2)}\frac{d\beta_z}{dz}\frac{dy}{dz}\,, \qquad (3.8) \\
\frac{d\beta_z}{dz} &= (\frac{q}{mc^2})\frac{(1-\beta_z^2)^{3/2}}{\beta_z}\left\{E_z + \frac{\beta_x B_y}{c} - \frac{\beta_y B_x}{c}\right\}.
\end{aligned}$$

This set of equations of relativistic form completely describe both the transverse and the longitudinal motions of a particle under acceleration along a reference trajectory.

3.2.1 RF Resonator

The electromagnetic fields for a cylindrically symmetric rf resonator were derived in Appendix A. The equations of motion in an rf resonator are easily found by inserting the fields into equations (3.7) and (3.8):

$$\begin{aligned}
\frac{d\beta_s}{dz} &= (\frac{q}{mc^2})\frac{(1-\beta_s^2)^{3/2}}{\beta_s}E_z(0,z)\cos\phi_s\,, \qquad (3.9) \\
\frac{d^2x}{dz^2} + \frac{1}{\beta_z(1-\beta_z^2)}\frac{d\beta_z}{dz}\frac{dx}{dz} &= (\frac{q}{mc^2})\frac{\sqrt{1-\beta_z^2}}{\beta_z^2}(F_{er1}+F_{br1}+F_{er3}+F_{br3})x\,, \\
\frac{d^2y}{dz^2} + \frac{1}{\beta_z(1-\beta_z^2)}\frac{d\beta_z}{dz}\frac{dy}{dz} &= (\frac{q}{mc^2})\frac{\sqrt{1-\beta_z^2}}{\beta_z^2}(F_{er1}+F_{br1}+F_{er3}+F_{br3})y\,, \qquad (3.10) \\
\frac{d\beta_z}{dz} &= (\frac{q}{mc^2})\frac{(1-\beta_z^2)^{3/2}}{\beta_z}(F_{ez0}+F_{bz1}+F_{ez2}+F_{bz3})\,,
\end{aligned}$$

where

$$\begin{aligned}
F_{er1} &= -\frac{1}{2}\frac{\partial E_z(0,z)}{\partial z}\cos\phi\,, \qquad (3.11) \\
F_{ez0} &= E_z(0,z)\cos\phi\,, \qquad (3.12)
\end{aligned}$$

$$F_{br1} = \frac{\omega}{2c} E_z(0,z)\beta_z \sin\phi \,, \tag{3.13}$$

$$F_{bz1} = -\left(\frac{dx}{dz}x + \frac{dy}{dz}y\right) F_{br1} \,, \tag{3.14}$$

$$F_{er3} = \frac{1}{16}\left\{\frac{\omega^2}{c^2}\frac{\partial E_z(0,z)}{\partial z} + \frac{\partial^3 E_z(0,z)}{\partial z^3}\right\}(x^2+y^2)\cos\phi \,, \tag{3.15}$$

$$F_{ez2} = -\frac{1}{4}\left\{\frac{\omega^2}{c^2}E_z(0,z) + \frac{\partial^2 E_z(0,z)}{\partial z^2}\right\}(x^2+y^2)\cos\phi \,, \tag{3.16}$$

$$F_{br3} = -\frac{1}{16}\frac{\omega}{c}\left\{\frac{\omega^2}{c^2}\frac{\partial E_z(0,z)}{\partial z} + \frac{\partial^2 E_z(0,z)}{\partial z^2}\right\}(x^2+y^2)\beta_z \sin\phi \,, \tag{3.17}$$

$$F_{bz3} = -\left(\frac{dx}{dz}x + \frac{dy}{dz}y\right) F_{br3} \,, \,, \tag{3.18}$$

where

$$\phi = \omega t + \phi_0 = \int \frac{dz}{c\beta_z} + \phi_0 \,, \tag{3.19}$$

$$\phi_s = \omega t_s + \phi_0 = \int \frac{dz}{c\beta_s} + \phi_0 \,. \tag{3.20}$$

3.2.2 Magnetic Solenoid

A magnetic solenoid lens is used as a focusing element for both the horizontal and vertical directions simultaneously. We introduce a solenoidal field which along the optic axis has the form [Dragt 90], [Berz 93]:

$$B_z(0,z) = \frac{B_0}{2}\left\{\tanh(\frac{z}{d}) - \tanh(\frac{z-l}{d})\right\} \,, \tag{3.21}$$

where B_0 is the maximum field strength. The length and half aperture of the solenoid are l, d respectively.

Since energy is conserved in a magnetic field, the terms containing $\frac{d\beta_z}{dz}$ in the equations of motion (3.8) vanish because the expression $\frac{d\beta_z}{dz}$ was an approximation of exact form of $\frac{d\beta}{dz}$, which is zero in a pure magnetic field. Also, the field components of a magnetic solenoid are calculated from the model solenoidal field on axes and equation (B.6) of Appendix B.

Thus from the equations of motion (3.7), (3.8) with calculated solenoid field components, we obtain a set of differential equations of motion of the model solenoid:

$$\frac{d\beta_s}{dz} = 0\,, \tag{3.22}$$

$$\frac{d^2x}{dz^2} = (\frac{q}{mc})\frac{\sqrt{1-\beta_z^2}}{\beta_z}\left\{\frac{dy}{dz}(B_{z0}+B_{bz2}) - x(B_{r1}+B_{r3})\right\}\,,$$

$$\frac{d^2y}{dz^2} = (\frac{q}{mc})\frac{\sqrt{1-\beta_z^2}}{\beta_z}\left\{\frac{dx}{dz}(B_{z0}+B_{bz2}) - y(B_{r1}+B_{r3})\right\}\,, \tag{3.23}$$

$$\frac{d\beta_z}{dz} = (\frac{q}{mc})(1-\beta_z^2)^{3/2}\left\{\frac{dx}{dz}y - \frac{dy}{dz}x\right\}(B_{r1}+B_{r3})\,,$$

where

$$B_{r1} = -\frac{1}{2}\frac{\partial B_z(0,z)}{\partial z}\,, \tag{3.24}$$

$$B_{r3} = \frac{1}{16}\frac{\partial^3 B_z(0,z)}{\partial z^3}(x^2+y^2)\,, \tag{3.25}$$

$$B_{z0} = B_z(0,z)\,, \tag{3.26}$$

$$B_{z2} = -\frac{1}{4}\frac{\partial^2 B_z(0,z)}{\partial z^2}(x^2+y^2)\,, \tag{3.27}$$

$$B_z(0,z) = \frac{B_0}{2}\left\{\tanh(\frac{z}{d}) - \tanh(\frac{z-l}{d})\right\}\,, \tag{3.28}$$

$$\frac{\partial B_z(0,z)}{\partial z} = \frac{B_0}{2d}\left\{\mathrm{sech}^2(\frac{z}{d}) - \mathrm{sech}^2(\frac{z-l}{d})\right\}\,, \tag{3.29}$$

$$\frac{\partial^2 B_z(0,z)}{\partial z^2} = \frac{B_0}{d^2}\left\{-\mathrm{sech}^2(\frac{z}{d})\tanh(\frac{z}{d}) + \mathrm{sech}^2(\frac{z-l}{d})\tanh(\frac{z-l}{d})\right\}, \quad (3.30)$$

$$\frac{\partial^3 B_z(0,z)}{\partial z^3} = \frac{B_0}{d^3}\left\{\mathrm{sech}^2(\frac{z}{d})\left[3\tanh^2(\frac{z}{d})-1\right]\right\}$$

$$- \frac{B_0}{d^3}\left\{\mathrm{sech}^2(\frac{z-l}{d})\left[3\tanh^2(\frac{z-l}{d})-1\right]\right\}. \quad (3.31)$$

3.2.3 Drift Space

Drift space is considered as field free region:

$$\frac{d\beta_s}{dz} = 0, \quad (3.32)$$

$$\frac{d^2x}{dz^2} = 0,$$

$$\frac{d^2y}{dz^2} = 0, \quad (3.33)$$

$$\frac{d\beta_z}{dz} = 0.$$

3.3 Linear Transfer Map

Even though the derived equations of motion are nonlinear, it is useful to consider linear solutions. The beam optics of a system is well described with linear solutions in most cases if nonlinearity is not so strong. The 1st order theory is mostly well defined for phase space distribution and its transformation in accelerator physics.

The transfer map is represented in six phase space coordinates:

$$(\, x,\ x',\ y,\ y',\ \Delta t,\ \Delta w\,), \quad (3.34)$$

where

$$\begin{aligned} x' &= \frac{dx}{dz}\,, \\ y' &= \frac{dy}{dz}\,, \\ \Delta t &= t - t_s\,, \end{aligned} \tag{3.35}$$

$$\Delta w = w - w_s\,. \tag{3.36}$$

i.e. Δt and Δw mean deviations of time of flight and kinetic energy from a reference particle respectively.

3.3.1 Transfer Map of a Drift Space

The differential equations of motion in equations (3.32) and (3.33) are easily solved for a drift space of length ℓ:

Transverse Motion

For transverse motion:

$$\begin{aligned} x &= x_0 + \ell x_0'\,, \\ x' &= x_0'\,, \\ y &= y_0 + \ell y_0'\,, \\ y' &= y_0'\,, \end{aligned} \tag{3.37}$$

where subscript 0 indicates initial values of phase space coordinates.

Longitudinal Motion

For longitudinal motion:

$$\begin{aligned} \beta_s &= \beta_{s0}\,, \\ \beta_z &= \beta_{z0}\,. \end{aligned} \tag{3.38}$$

Obviously there is no deviation in energy for a drift space:

$$\Delta w = \Delta w_0 \, . \tag{3.39}$$

To find the deviation of time of flight we define:

$$\Delta\beta = \beta_z - \beta_s \, . \tag{3.40}$$

Then from equation (3.36):

$$\Delta t = \Delta t_0 + \frac{\ell}{c}(\beta_z - \beta_s) = \frac{\ell}{c}\left\{ -\frac{\Delta\beta}{\beta_s^2} + \frac{(\Delta\beta)^2}{\beta_s^3} + \cdots \right\} \, . \tag{3.41}$$

The relativistic relation:

$$\beta = \sqrt{1 - \left(1 + \frac{w}{mc^2}\right)^{-2}} = \frac{pc}{mc^2 + w} \, , \tag{3.42}$$

where p is the momentum of a particle.

From equation (3.42) for an off axial particle we find:

$$\begin{aligned}
\beta_z &= \left\{ 1 - \left(1 + \frac{w_s + \Delta w}{mc^2}\right)^{-2} \right\}^{1/2} \\
&= \left\{ 1 - \left(\frac{mc^2}{mc^2 + w_s}\right)^2 \left(1 - \frac{2\Delta w}{mc^2 + w_s}\right) \right\}^{1/2} \\
&\approx \left\{ \beta_s^2 + \frac{2(mc^2)^2}{(mc^2 + w_s)^3 \Delta w} \right\}^{1/2} \\
&\approx \beta_s + \frac{\beta_s^2 m^2 c \Delta w}{p_s^3} \, .
\end{aligned} \tag{3.43}$$

Using $\Delta w = \Delta w_0$, from equations (3.40) and (3.43) we obtain:

$$\Delta\beta = \frac{\beta_s^2 m^2 c \Delta w_0}{p_s^3} \,. \tag{3.44}$$

Therefore from equations (3.41) and (3.44) we get for a drift space of length ℓ:

$$\Delta t = \Delta t_0 + \ell \left\{ -\frac{m^2}{p_s^3}\Delta w_0 + \frac{m^4 c \beta_s}{p_s^6}\Delta w_0^2 + \cdots \right\} . \tag{3.45}$$

Note that the drift space is not linear for longitudinal motion unlike transverse motion.

If we combine equations (3.37), (3.39) and (3.45) in matrix form up to 1st order we get the transfer matrix for a drift space of length ℓ:

$$\begin{pmatrix} x \\ x' \\ y \\ y' \\ \Delta t \\ \Delta w \end{pmatrix} = \begin{pmatrix} 1 & \ell & 0 & 0 & 0 & 0 \\ 0 & 1 & 0 & 0 & 0 & 0 \\ 0 & 0 & 1 & \ell & 0 & 0 \\ 0 & 0 & 0 & 1 & 0 & 0 \\ 0 & 0 & 0 & 0 & 1 & -\frac{\ell m^2}{p_s^3} \\ 0 & 0 & 0 & 0 & 0 & 1 \end{pmatrix} \begin{pmatrix} x_0 \\ x_0' \\ y_0 \\ y_0' \\ \Delta t_0 \\ \Delta w_0 \end{pmatrix} . \tag{3.46}$$

3.3.2 Transfer Map of a RF Resonator

Transverse Map

If just 1st order terms of x or y are taken in the differential equations of motion (3.9), (3.10) with the approximation $\beta_z \approx \beta_s$, we find the linear differential equation of motion:

$$\frac{d^2x}{dz^2} + \alpha(z)\frac{dx}{dz} + \kappa(z)x = 0 \,, \tag{3.47}$$

where

$$\alpha(z) = \frac{1}{\beta_s(1-\beta_s^2)}\frac{d\beta_s}{dz}, \tag{3.48}$$

$$\kappa(z) = -\frac{q}{mc^2}\frac{\sqrt{1-\beta_s^2}}{\beta_s^2}\left\{-\frac{1}{2}\frac{\partial E_z(0,z)}{\partial z}\cos\phi_s + \frac{\omega}{2c}E_z(0,z)\beta_s\sin\phi_s\right\}. \tag{3.49}$$

This equation is linear in form. But it is not solved in closed form because $\alpha(z)$ and $\kappa(z)$ are not constant due to acceleration and varying electric field profile respectively along the resonator axes.

If the velocity of a beam is very high, enough to ignore change of velocity along the accelerating gap structure, $\alpha(z)$ is negligible. But in the low velocity case with rapid energy gain such as the PII linac it can not be neglected any more.

Therefore we consider a thin part of an accelerating gap of a resonator where α and κ might be considered as constant. Thus the solutions of the equations of motion in the thin part are easily solved in matrix form. In this way the whole transfer map of a resonator is found by matrix multiplications of the transfer matrices of each thin part.

The solutions of transverse motion for a thin part of a resonator are given by:
(i) if $\alpha^2 - 4\kappa > 0$

$$x = e^{-\alpha z/2}\left\{\left[\cosh(pz/2) + \frac{\alpha}{p}\sinh(pz/2)\right]x_0 + \left[\frac{2}{p}\sinh(pz/2)\right]x_0'\right\},$$

$$x' = -e^{-\alpha z/2}\left\{\left[\frac{2\kappa}{p}\sinh(pz/2)\right]x_0 + \left[\cosh(pz/2) - \frac{\alpha}{p}\sinh(pz/2)\right]x_0'\right\}, \tag{3.50}$$

(ii) if $\alpha^2 - 4\kappa < 0$

$$x = e^{-\alpha z/2}\left\{\left[\cos(pz/2) + \frac{\alpha}{p}\sin(pz/2)\right]x_0 + \left[\frac{2}{p}\sin(pz/2)\right]x_0'\right\},$$

$$x' = -e^{-\alpha z/2}\left\{\left[\frac{2\kappa}{p}\sin(pz/2)\right]x_0 + \left[\cos(pz/2) - \frac{\alpha}{p}\sin(pz/2)\right]x_0'\right\}, \quad (3.51)$$

(iii) if $\alpha^2 - 4\kappa = 0$

$$x = \cosh(\alpha z/2)x_0 + \frac{2}{\alpha}\sinh(\alpha z/2)x_0' ,$$
$$x' = \frac{\alpha}{2}\sinh(\alpha z/2)x_0 + \cosh(\alpha z/2)x_0' , \quad (3.52)$$

where

$$p \equiv |\alpha^2 - 4\kappa| . \quad (3.53)$$

If we combine equations (3.50) - (3.52) in matrix form, we have transfer maps M for a small section of a resonator:

$$\begin{pmatrix} x \\ x' \end{pmatrix} = M \bullet \begin{pmatrix} x_0 \\ x_0' \end{pmatrix} , \quad (3.54)$$

where

(i) if $\alpha^2 - 4\kappa > 0$

$$M = e^{-\alpha z/2}\begin{pmatrix} \cosh(\frac{pz}{2}) + \alpha\sinh(\frac{pz}{2})/p & 2\sinh(\frac{pz}{2})/p \\ -2\kappa\sinh(\frac{pz}{2})/p & \cosh(\frac{pz}{2}) - \alpha\cosh(\frac{pz}{2})/p \end{pmatrix} , \quad (3.55)$$

(ii) if $\alpha^2 - 4\kappa < 0$

$$M = e^{-\alpha z/2}\begin{pmatrix} \cos(\frac{pz}{2}) + \alpha\sin(\frac{pz}{2})/p & 2\sin(\frac{pz}{2})/p \\ -2\kappa\sin(\frac{pz}{2})/p & \cos(\frac{pz}{2}) - \alpha\sin(\frac{pz}{2})/p \end{pmatrix} , \quad (3.56)$$

(iii) if $\alpha^2 - 4\kappa = 0$

$$M = \begin{pmatrix} \cosh(\frac{\alpha z}{2}) & 2\sinh(\frac{\alpha z}{2})/\alpha \\ \alpha\sinh(\frac{\alpha z}{2})/2 & \cosh(\frac{\alpha z}{2}) \end{pmatrix} . \tag{3.57}$$

Note that the determinant of the transfer map is not equal to one in general but $e^{-\alpha z/2}$ because of acceleration.

Since the resonator field is axially symmetric we get the same results for the vertical direction (y, z).

Longitudinal Map

For a longitudinal map it is more convenient to use the energy gain of a charged particle under longitudinal electric field rather than to use the equations of motion derived already.

The longitudinal electric field from equations (A.21) and (A.23) up to 1st order becomes:

$$E_z(r, z, t) = E_z(0, z)\cos(\omega t + \phi_0) . \tag{3.58}$$

Let ϕ be:

$$\phi = \omega t + \phi_0 = \int_0^z \frac{dz}{c\beta_z} + \phi_0 . \tag{3.59}$$

Then the energy gain per unit length of a charged particle is given in differential form by:

$$\frac{dw}{dz} = qE_z(0, z)\cos\phi , \tag{3.60}$$

$$\frac{dw_s}{dz} = qE_z(0, z)\cos\phi_s . \tag{3.61}$$

From the definitions of Δt and Δw we obtain:

$$\frac{d\Delta w}{dz} = qE_z(0,z)(\cos\phi - \cos\phi_s) = -qE_z(0,z)\sin\phi_s\Delta\phi + \cdots , \quad (3.62)$$

$$\frac{d\Delta\phi}{dz} = \omega\left(\frac{1}{c\beta_z} - \frac{1}{c\beta_s}\right) = -\frac{\omega m^2}{p_s^3}\Delta w + \cdots \quad . \quad (3.63)$$

Thus, up to 1st order the above equations become:

$$\frac{d\Delta w}{dz} = -\lambda_1(z)\Delta\phi , \quad (3.64)$$

$$\frac{d\Delta\phi}{dz} = \lambda_2(z)\Delta w , \quad (3.65)$$

where

$$\lambda_1(z) = qE_z(0,z)\sin\phi_s , \quad (3.66)$$

$$\lambda_2(z) = -\frac{\omega m^2}{p_s^3} . \quad (3.67)$$

Now we introduce a new variable:

$$\chi = \int \lambda_2(z)dz . \quad (3.68)$$

Then:

$$\frac{d}{dz} = \lambda_2(z)\frac{d}{d\chi} . \quad (3.69)$$

Thus, equations (3.64) and (3.65) become respectively:

$$\frac{d\Delta w}{d\chi} = -\frac{\lambda_1(z)}{\lambda_2(z)}\Delta\phi , \quad (3.70)$$

$$\frac{d\Delta\phi}{d\chi} = \Delta w . \quad (3.71)$$

By combining (3.70) and (3.71) we obtain a single second order differential equation:

$$\frac{d^2\Delta\phi}{d\chi^2} + \frac{\lambda_1(z)}{\lambda_2(z)}\Delta\phi = 0 \,. \tag{3.72}$$

Let's define:

$$\kappa^2 = \left|\frac{\lambda_1(z)}{\lambda_2(z)}\right| \,. \tag{3.73}$$

By the similar way as in the transverse case if we assume that the change of κ^2 is negligible in a small section of a resonator, we find solutions for a small section:

(i) if $\lambda_1/\lambda_2 > 0$

$$\begin{aligned} \Delta\phi &= \cos(\kappa\chi)\Delta\phi_0 + \Delta w_0 \sin(\kappa\chi)/\kappa \,, \\ \Delta w &= -\kappa \sin(\kappa\chi)\Delta\phi_0 + \Delta w_0 \cos(\kappa\chi) \,. \end{aligned} \tag{3.74}$$

Using equations (3.68), (3.71), and $\Delta\phi = \omega\Delta t$ we obtain:

$$\begin{aligned} \Delta t &= \cos(\kappa\lambda_2 z)\Delta t_0 + \Delta w_0 \sin(\kappa\lambda_2 z)/(\kappa\omega) \,, \\ \Delta w &= -\omega\kappa \sin(\kappa\lambda_2 z)\Delta t_0 + \Delta w_0 \cos(\kappa\lambda_2 z) \,. \end{aligned} \tag{3.75}$$

(ii) if $\lambda_1/\lambda_2 < 0$

$$\begin{aligned} \Delta t &= \cosh(\kappa\lambda_2 z)\Delta t_0 + \Delta w_0 \sinh(\kappa\lambda_2 z)/(\kappa\omega) \,, \\ \Delta w &= \omega\kappa \sinh(\kappa\lambda_2 z)\Delta t_0 + \Delta w_0 \cosh(\kappa\lambda_2 z) \,. \end{aligned} \tag{3.76}$$

(iii) if $\lambda_1/\lambda_2 = 0$

$$\begin{aligned} \Delta t &= \Delta t_0 + \Delta w_0 \lambda_2 z/\omega \,, \\ \Delta w &= \Delta w_0 \,. \end{aligned} \tag{3.77}$$

If we combine equations (3.75) - (3.77) in matrix form, we have transfer maps M for a small section of a resonator:

$$\begin{pmatrix} \Delta t \\ \Delta w \end{pmatrix} = M \bullet \begin{pmatrix} \Delta t_0 \\ \Delta w_0 \end{pmatrix} , \tag{3.78}$$

where

$$M = \begin{pmatrix} \cos(\kappa\lambda_2 z) & \sin(\kappa\lambda_2 z)/(\kappa\omega) \\ -\kappa\omega \sin(\kappa\lambda_2 z) & \cos(\kappa\lambda_2 z) \end{pmatrix} \quad \text{if } \lambda_1/\lambda_2 > 0 \ , \tag{3.79}$$

$$M = \begin{pmatrix} \cosh(\kappa\lambda_2 z) & \sinh(\kappa\lambda_2 z)/(\kappa\omega) \\ \kappa\omega \sinh(\kappa\lambda_2 z) & \cosh(\kappa\lambda_2 z) \end{pmatrix} \quad \text{if } \lambda_1/\lambda_2 < 0 \ , \tag{3.80}$$

$$M = \begin{pmatrix} 1 & \lambda_2 z/\omega \\ 0 & 1 \end{pmatrix} \quad \text{if } \lambda_1/\lambda_2 = 0 \ . \tag{3.81}$$

Note that the transfer map is the same as for drift space if $\kappa = 0$.

3.3.3 Transfer Map of a Magnetic Solenoid

The differential equations of motion of a magnetic solenoid derived in section 3.2.2 are coupled between the x and y coordinates due to rotation even in 1st order. The linear part of equations (3.22), (3.23) gives:

$$\frac{d\beta_s}{dz} = 0 \ , \tag{3.82}$$

$$\frac{d^2x}{dz^2} - \alpha \left\{ \frac{dy}{dz} B_z(0,z) + \frac{1}{2} \frac{\partial B_z(0,z)}{\partial z} y \right\} = 0 \ ,$$

$$\frac{d^2y}{dz^2} - \alpha \left\{ \frac{dx}{dz} B_z(0,z) + \frac{1}{2} \frac{\partial B_z(0,z)}{\partial z} x \right\} = 0 \ , \tag{3.83}$$

$$\frac{d\beta_z}{dz} = 0 \ ,$$

where

$$\alpha = \frac{q\sqrt{1-\beta_z^2}}{mc\beta_z} \approx \frac{q\sqrt{1-\beta_s^2}}{mc\beta_s} \ . \tag{3.84}$$

The differential equations are decoupled in the rotated coordinate system (X, Y, z), which is rotated an angle θ about z axis in the fixed coordinate system (x, y, z) (see Appendix B):

$$\frac{d^2X}{dz^2} - \kappa^2 X = 0 \,,$$

$$\frac{d^2Y}{dz^2} - \kappa^2 Y = 0 \,, \tag{3.85}$$

where

$$\kappa = \frac{qB_z(0,z)}{2mc}\frac{\sqrt{1-\beta_s^2}}{\beta_s} \,. \tag{3.86}$$

Since $\kappa(z)$ is not constant, we also consider a small section of the solenoid to neglect the change of $\kappa(z)$. Then the transfer map M_r in the rotated coordinate system is given by:

$$M_r = \begin{pmatrix} \cos(\kappa z) & \sin(\kappa z)/\kappa & 0 & 0 \\ -\kappa\sin(\kappa z) & \cos(\kappa z) & 0 & 0 \\ 0 & 0 & \cos(\kappa z) & \sin(\kappa z)/\kappa \\ 0 & 0 & -\kappa\sin(\kappa z) & \cos(\kappa z) \end{pmatrix} . \tag{3.87}$$

The transfer map M in the fixed coordinate system is obtained by applying a rotation matrix $R(\theta)$ (see Appendix B) to the transfer map in the rotated coordinate system:

$$\begin{aligned} M &= R(-\theta)M_r \\ &= \begin{pmatrix} C\cdot\cos\theta & S\cdot\cos\theta/\kappa & C\cdot\sin\theta & S\cdot\sin\theta/\kappa \\ -S\kappa\cdot\cos\theta & C\cdot\cos\theta & -S\kappa\cdot\sin\theta & C\cdot\sin\theta \\ -C\cdot\sin\theta & -S\cdot\sin\theta/\kappa & C\cdot\cos\theta & S\cdot\cos\theta/\kappa \\ S\kappa\cdot\sin\theta & -C\cdot\sin\theta & -S\kappa\cdot\cos\theta & C\cdot\cos\theta \end{pmatrix} , \end{aligned} \tag{3.88}$$

where

$$C = \cos(\kappa z) \,, \tag{3.89}$$

$$S = \sin(\kappa z)\,, \tag{3.90}$$

$$\theta = -\int_z \kappa(z)dz\,. \tag{3.91}$$

Therefore in the fixed coordinate system we get the phase space coordinate transformation by the transfer map M:

$$\begin{pmatrix} x \\ x' \\ y \\ y' \end{pmatrix} = M \bullet \begin{pmatrix} x_0 \\ x'_0 \\ y_0 \\ y'_0 \end{pmatrix}\,. \tag{3.92}$$

Since the magnetic solenoid behaves like drift space for longitudinal motion from equations (3.82) and (3.83) we find the same result as the longitudinal map of a drift space.

3.4 Implementation by Computer Programs

The matrix optics and equations of motion under accelerating forces derived in Chapter 2 and Chapter 3 are implemented to computer programs MINJI [Joh 93b] and MINSOL [Joh 93c].

The first order matrix optics program MINJI calculates linear transfer maps point-by-point through a system both for the transverse and for the longitudinal directions . This point-by-point search is necessary because of rapid changes of velocity. Therefore it provides transfer matrices at any point of an element of the system to make it feasible to investigate a beam inside an element.

This matrix optics program provides beam envelopes and Twiss parameters of phase spaces for rotated or unrotated beams. Initial or final phase space matchings are possible with appropriate fitting parameters by using the symplectic nonlinear optimizer in it.

On the other hand the program MINSOL just solves nonlinear differential equations of motion derived in this chapter analytically with off axial fields up to 3rd order.

3.4.1 Numerical Integration

The spatial parts of the axial resonator field profiles including its 1st and 2nd derivatives were calculated using the method of moment [Shepard 85] which nicely fit experimentally measured data using perturbation method [Shepard 93]. To include 3rd order effect of these fields, the 3rd order derivatives were calculated from the 2nd order derivatives. As an integration routine the 4th order Runge-Kutta method with constant step size is used [Press 86].

The more sophisticated integration routine would be used ideally but tests of an integration routine using what we call the forward-backward method shows that using 4th order is enough to give consistent results. The forward-backward method takes the initial conditions of a ray and calculates its final conditions. These final conditions are then used as initial input conditions to try and trace back to the original set of initial conditions.

3.4.2 Model Solenoid

The superconducting magnetic solenoids in the PII linac have the following features [Jaffey 74], [Jaffey 76]: The overall length including coil parts and iron shield is 25 cm and the aperture is 2.5 cm; The maximum central field of the present magnet is 7.6 T with fringe fields dropping rapidly to 10 G at a distance of 1 cm outside the iron shield and 50 mG at a distance of 2.5 cm from the mu-metal shield; Therefore the extension of the solenoidal fields into the resonators is negligible from the present location of the solenoids and resonators in the PII linac.

To describe the solenoidal fields analytically we use the model solenoid of equation (3.21) with appropriate parameters of d, l:

$$B(z) = \frac{B_0}{2}\left\{\tanh(\frac{z}{d}) - \tanh(\frac{z-l}{d}\right\} . \tag{3.93}$$

The solenoid parameters, d, l are adjusted to best describe the real solenoid field.

In adjusting solenoid parameters d is found to be 1.5 cm for the half aperture and l is found to be 10 cm for the body length of solenoid. Figure 3.1 shows the magnetic field profile of the solenoid with the fitted parameters. The effect of fringe fields is calculated both in the raytracing and in matrix optics by considering the length of the fringe field tail and its relative strength to the maximum field strength (see Appendix C).

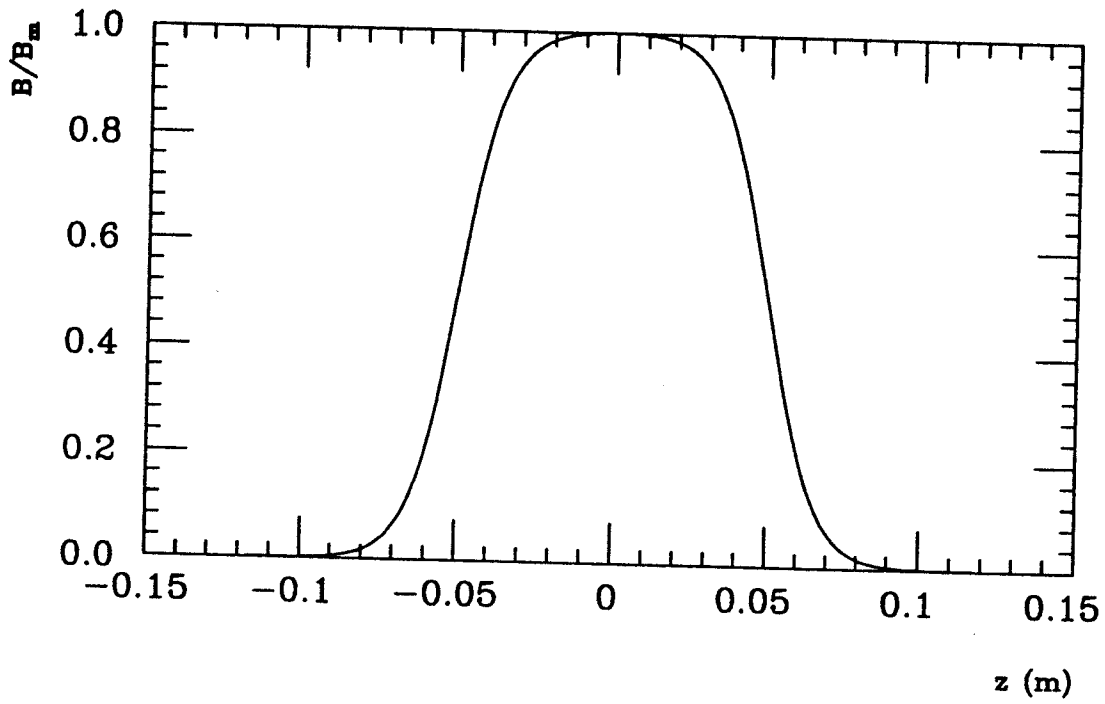

Figure 3.1: The normalized magnetic field profile on axes of the model solenoid with half aperture 1.5 cm and body length 10 cm.

Chapter 4

Application to Resonator Study

4.1 Introduction

The four-gap superconducting resonators have been developed at Argonne for use in the low-beta positive ion injector for the ATLAS linac [Shepard 87],[Shepard 89]. It was previously observed that at low velocities these structures can be focusing in both longitudinal and transverse phase spaces due to an inherent alternating-phase-focusing property [Pardo 87a], [Nolen 93].

Alternating-phase-focusing achieves both transverse and longitudinal focusing by alternating appropriately the signs of the initial rf phases in each resonator. This focusing has been reported in several papers [Good 53],[Chambers 76],[Okamoto 89], [Sagalovsky 92]. But in the PII linac each resonator itself has this property even when operated with a fixed initial rf phase. This might be understood from the relatively fast velocity change within the multiple gap structures to cause effective sign changes of rf phase offset. The strength of transverse focusing seems to be so strong that it might not be necessary to use focusing solenoids at the beginning stage of PII [Nolen 93].

Since these resonators have the potential application to be used for extremely low-beta low q/m beams, it will be useful to understand the focusing properties of them

at low velocities. For this purpose a custom-made first order matrix optics computer program is used.

In this chapter we investigate in detail focusing structures of the I1 and I2 type resonators which are located at the beginning of PII. The limits of injection energy and initial rf phase offset for transverse and longitudinal stabilities are calculated by using the concept of focusing power to see possibility of resonator focusing only.

Throughout this and the following chapters, calculations will be made with $^{238}U^{24+}$ which has a q/m=0.1 and $^{40}Ar^{12+}$ which has a q/m=0.3 because of their relatively low and high charge to mass ratios.

4.2 Focusing Power

The focusing power of a lens is defined as an inverse of the focal length. It can be used to measure the focusing strength of a lens. The focusing power is calculated from a transfer matrix of a lens. In the case of a thin lens which has only focusing action without effecting the position of a ray, the transfer matrix is written in the simple form of:

$$M_t = \begin{pmatrix} 1 & 0 \\ -1/f & 1 \end{pmatrix} . \tag{4.1}$$

In a system of a thin lens M_t followed by a drift space of length f, the resulting transfer matrix becomes:

$$M = \begin{pmatrix} 1 & f \\ 0 & 1 \end{pmatrix} \begin{pmatrix} 1 & 0 \\ -1/f & 1 \end{pmatrix} = \begin{pmatrix} 0 & f \\ -1/f & 1 \end{pmatrix} . \tag{4.2}$$

Since the resulting first column, the first row transfer matrix element, M_{11}, equals zero this corresponds to parallel-to-point system discussed in section 2.2.2 of Chapter

2. All initial parallel rays are focused to a point of distance f. Similarly if the drift space of length f precedes the thin lens M_t, the resulting transfer matrix element of the second column, second row becomes zero. So all initial rays starting at a point of distance f have the same divergences after passing a thin lens. Therefore f is interpreted as the focal length and 1/f as the focusing power of a thin lens and is determined uniquely.

But the above statement is not true for a thick lens which has two principal planes in general. This case is discussed in the following section.

4.2.1 Transverse Case

In a thick lens the focal lengths are defined with respect to two different principal planes P_1 and P_2 in Figure 4.1. Let a transfer matrix of a lens be M_l:

$$M_l = \begin{pmatrix} (x|x) & (x|x') \\ (x'|x) & (x'|x') \end{pmatrix} . \tag{4.3}$$

The focal lengths of a lens can be calculated by two different ways from its transfer matrix M_l. Consider the two systems consisting of a drift length and a lens in Figure 4.1.

The focal length f_1 is calculated from the point-to-parallel system in Figure 4.1. The transfer matrix of a point-to-parallel system is found by applying a lens map to a drift map:

$$\begin{pmatrix} (x|x) & (x|x') \\ (x'|x) & (x'|x') \end{pmatrix} \begin{pmatrix} 1 & f_1 \\ 0 & 1 \end{pmatrix} = \begin{pmatrix} (x|x) & (x|x)f_1 + (x|x') \\ (x'|x) & (x'|x)f_1 + (x'|x') \end{pmatrix} . \tag{4.4}$$

Since the second column, second row element of the resulting transfer matrix should

be zero for point-to-parallel system the drift length f_1 is given by:

$$f_1 = -\frac{(x'|x')}{(x'|x)} . \tag{4.5}$$

The focal length f_2 is calculated from the parallel-to-point system in Figure 4.1. The transfer matrix of the system is found by applying a drift map to a lens map:

$$\begin{pmatrix} 1 & f_2 \\ 0 & 1 \end{pmatrix} \begin{pmatrix} (x|x) & (x|x') \\ (x'|x) & (x'|x') \end{pmatrix} = \begin{pmatrix} (x|x) + f_2(x'|x) & (x'|x')f_2 + (x|x') \\ (x'|x) & (x'|x') \end{pmatrix} . \tag{4.6}$$

Since the first column, first row element of the resulting transfer matrix should be zero for parallel-to-point system the drift length f_2 is given by:

$$f_2 = -\frac{(x|x)}{(x'|x)} . \tag{4.7}$$

It should be mentioned that the drift lengths f_1 and f_2 calculated from the two different systems above are not the real focal lengths of a lens. Because they are calculated from the entrance (f_1) and the exit (f_2) not from the principal planes [Wollnik 87a] of a lens. So they are different by some constants. In the case of a thin lens f_1 and f_2 are real focal lengths and have the same value as each other because $(x|x) = (x'|x') = 1$.

But in any cases the focusing power is proportional to a matrix element $(x'|x)$ of a transfer matrix of a lens:

$$\text{focusing power} \quad \propto \quad -(x'|x) . \tag{4.8}$$

As a matter of fact, to investigate the sign of $(x'|x)$ is a more convenient way to study focusing property of a lens than to investigate the sign of focusing power. For example if a lens is so strong that a focal point exists inside the lens then the matrix elements $(x|x)$ and $(x'|x')$ of the lens become negative. Therefore it would look like

a defocusing lens if we observe the drift lengths that were derived in equations (4.5) and (4.7). But $(x'|x)$ provides correct information about the focusing property if the number of intermediate images does not exceed two. In other word, the negative of $(x'|x)$ means that there is a net focusing action which is proportional to $(x'|x)$ and vice versa, as shown in Figure 4.2.

4.2.2 Longitudinal Case

In the longitudinal phase space the transfer matrix of drift space is not the same as in transverse case. The transfer matrix of drift length ℓ was given in equation (3.46) of Chapter 3:

$$M_d = \begin{pmatrix} 1 & -\ell m^2/p_s^3 \\ 0 & 1 \end{pmatrix}, \tag{4.9}$$

where p_s is a momentum of a reference particle.

Let a longitudinal transfer matrix of a lens be M_l:

$$M_l = \begin{pmatrix} (\Delta t|\Delta t) & (\Delta t|\Delta w) \\ (\Delta w|\Delta t) & (\Delta w|\Delta w) \end{pmatrix} \tag{4.10}$$

By the similar way as the transverse case, the drift length f_l is calculated from the point-to-parallel system in Figure 4.1. The transfer matrix of point-to-parallel system is found by applying a lens map to a drift map in the longitudinal phase space:

$$M_l \bullet \begin{pmatrix} 1 & -f_1 m^2/p_{s1}^3 \\ 0 & 1 \end{pmatrix} = \begin{pmatrix} (\Delta t|\Delta t) & -f_1 m^2(\Delta t|\Delta t)/p_{s1}^3 + (\Delta w|\Delta w) \\ (\Delta w|\Delta t) & -f_1 m^2(\Delta w|\Delta t)/p_{s1}^3 + (\Delta w|\Delta w) \end{pmatrix}. \tag{4.11}$$

The vanishing of the second column, second row element of the resulting transfer

matrix gives:

$$f_1 = \frac{p_{s1}^3}{m^2}\frac{(\Delta w|\Delta w)}{(\Delta w|\Delta t)} \,. \tag{4.12}$$

And similarly for parallel-to-point system, the vanishing of first column, first row element of the resulting transfer matrix gives:

$$f_2 = \frac{p_{s2}^3}{m^2}\frac{(\Delta t|\Delta t)}{(\Delta w|\Delta t)} \,. \tag{4.13}$$

Note that p_{s1} and p_{s2} are momenta of the reference particle at the entrance and exit of a lens respectively.

In both cases the focusing power is proportional to a matrix element $(\Delta w|\Delta t)$ of a longitudinal transfer matrix of a lens:

$$\text{focusing power} \quad \propto \quad \frac{m^2}{p_s^3}(\Delta w|\Delta t) \,. \tag{4.14}$$

By the same argument that was used in the transverse case, a convenient way to examine the longitudinal focusing property would be to investigate the inclined angle in the $(\Delta t, z)$ plane of a ray after passing a lens as shown in Figure 4.2. From equation (3.63) in section 3.3.2 of Chapter 3, with keeping in mind that $\Delta\phi = \omega\Delta t$, the inclined angle in the $(\Delta t, z)$ plane is given by:

$$\frac{d\Delta t}{dz} = -\frac{p_s^3}{m^2}\Delta w \,. \tag{4.15}$$

For a parallel ray with $\Delta t_0 = 1$, $\Delta w_0 = 0$ at the beginning, the final value of Δw is given by:

$$\Delta w = (\Delta w|\Delta t) \,. \tag{4.16}$$

Therefore from the above two equations the inclined angle is proportional to a matrix

element $(\Delta w|\Delta t)$:

$$\frac{d\Delta t}{dz} \quad \propto \quad -\frac{p_s^3}{m^2}(\Delta w|\Delta t)\,. \tag{4.17}$$

Since $\frac{d\Delta t}{dz}$ is negative for focusing action, $(\Delta w|\Delta t)$ is positive for focusing action and negative for defocusing action.

4.3 Focusing Structures of I1 and I2 type Resonators

4.3.1 Transverse Focusing

The radial force on a particle of electric charge q in an axially symmetric accelerating gap was derived in section 3.2.1 of Chapter 3. The radial force upward to first order is given by:

$$F_x = q\left\{-\frac{1}{2}\frac{\partial E_z(0,z)}{\partial z}\cos\phi_s + \frac{\omega}{2c}E_z(0,z)\beta_s\sin\phi_s\right\}x\ , \tag{4.18}$$

where ϕ_s is local rf phase of a central ray.

The 1st and 2nd terms are electric and magnetic forces coming from the rf fields.

Also, the equation of motion was given through equations (3.9), (3.10) of Chapter 3. For the transverse motion:

$$\frac{d^2x}{dz^2} + \alpha(z)\frac{dx}{dz} + \kappa(z)x = 0\ , \tag{4.19}$$

where

$$\alpha(z) = \frac{1}{\beta_s(1-\beta_s^2)}\frac{d\beta_s}{dz}\ , \tag{4.20}$$

$$\kappa(z) = -\frac{1}{mc^2}\frac{\sqrt{1-\beta_s^2}}{\beta_s^2}F_x\ . \tag{4.21}$$

The focusing action in the radial direction at a point z along a resonator axis is determined by:

$$\begin{aligned}\alpha^2 - 4\kappa &> 0 : \text{Focusing}\ ,\\ \alpha^2 - 4\kappa &< 0 : \text{Defocusing}\ .\end{aligned} \tag{4.22}$$

If the change of velocity through a gap is negligible, the focusing action is dominated by the radial force only. So the action at the first half of a gap would be focusing and

defocusing at the second half to give net focusing or defocusing effect depending on the rf phase change [Nolen 92], if the magnetic force term is small. But because of the fast energy gain in I1 and I2 type resonators with low-beta structures the change of velocity can not be negligible. Therefore the focusing action should be determined both by the rate of the velocity change and the magnitude of the radial force. The local focusing action may change even at the half of a gap.

4.3.2 Longitudinal Focusing

First order longitudinal focusing is completely determined by the local axial electric field profile and the local phase of a central ray by equations (3.75)-(3.77) of Chapter 3:

$$\begin{aligned} E_z(0,z)\sin\phi_s &< 0 : \text{Focusing} , \\ E_z(0,z)\sin\phi_s &> 0 : \text{Defocusing} . \end{aligned} \tag{4.23}$$

While a beam passes through a multiple gap structure resonator, the longitudinal focusing action may switch to defocusing action due to a change of the local rf phase. This effectively gives alternating phase focusing effect within a resonator.

4.3.3 Alternating Phase Focusing

Each type of resonator is subdivided into 200 thin resonators for matrix optics calculation. So the focusing power of each cell can be calculated by using transfer matrix of each cell. Since each cell behaves almost like a thin lens the focusing powers give nearly the same values for both point-to-parallel and for parallel-to-point conditions. Also, we can calculate the focusing power of each accelerating gap from its transfer matrix.

The focusing power plots of I1 and I2 type resonators in Figure 4.3 and Figure 4.4

show detailed focusing structures inside the resonators. The negative focusing power means defocusing action at the corresponding cell and vice versa. Because of the energy gain the strength of the transverse focusing power (solid line) decreases through a resonator. In I2 type resonators the overall focusing structure is similar to the I1 type resonators. But the absolute value of the focusing power decreases considerably because of the relatively high velocity after getting energy from the I1 resonator.

One thing to note is that at some parts of each gap both transverse and longitudinal focusing can occur simultaneously. Because the change of velocity is not negligible transverse focusing does not depend only on radial force but also depends on the rate of velocity change through equation (4.22). Therefore this feature does not usually appear in high-beta resonators where focusing is dominated by the radial force only.

Another thing to note is that the overall defocusing action in the longitudinal direction is alternated to focusing action at the second half of each resonator. So the initial rf phase offset is also effectively alternated in order to give an alternating-phase-focusing effect. Table 4.1 shows the focusing powers of each gap, which is calculated from the drift lengths f_1 and f_2 discussed at the beginning of this chapter. Alternating-phase-focusing structures appear clearly between the first half and the second half of each resonator. Also, the net transverse and the longitudinal focusing actions of each gap are opposite to each other like in a high-beta structure resonator.

Table 4.1 shows that each accelerating gap does not behave as a thin lens in a low-beta resonator because of its two different focal lengths. As a result the focusing effect of a resonator might not be calculated from the same way as done in Table 4.1 because of its very strong focusing property. Therefore we use the transfer matrix elements $(x'|x)$ for the transverse direction and $(\Delta w|\Delta t)$ for the longitudinal direction. The net focusing effects of I1 and I2 type resonators would be determined by observing the matrix elements of their respective transfer maps.

4.4 The Limits of RF Phase Offset of Resonators

If alternating-phase-focusing properties of the PII resonators are used without additional focusing elements each resonator itself should achieve both the transverse and the longitudinal focusing for a given initial rf phase offset.

To find the stability region of the initial rf phase offset for a resonator at a given initial velocity the transfer matrix of a resonator is calculated for a reference particle with the custom-made matrix optics program. For a given initial rf phase offset the transfer matrix element $(x'|x)$ should be positive to achieve the net transverse focusing. Also, the transfer matrix elements $(\Delta w|\Delta t)$ should be negative to achieve the net longitudinal focusing.

Figure 4.5 and Figure 4.6 show stability limits of the initial rf phase offset at different initial velocities. The electric field gradients were 4.5 MV/m for type I1 resonator and 3.0 MV/m for type I2 resonator. The dotted points at an initial velocity satisfy both conditions for the transverse and the longitudinal focusing. In this calculation the initial rf phase offset was limited between -40 and 40 degrees because above these limits the energy gains are not efficient.

The positive rf phase offset is mainly forbidden due to the condition of longitudinal stability even though transverse focusing is stronger than in the negative case. Some narrow bands of a negative rf phase offset at a given initial β is mainly due to transverse instability.

For example if we accelerate an $^{40}Ar^{12+}$ beam of initial $\beta = 0.0075$ through an I1 type resonator, the range of the initial rf phase offset should be between -40 and 0 degrees. But it will be between -20 and 0 degrees in the I2 type resonator. In fact it should be noted that the points near zero degrees might not be used as stable points because the stability region is cut at zero degrees, where nonlinearity might

be considerable in the longitudinal direction.

According to the stability plots, the limits of stable rf phase offsets depends upon the initial velocity especially for I2 type resonator. Thus the initial velocities should be chosen appropriately to have a wide range of the incident rf phase angles.

4.5 Parameters on Focusing

In this section we investigate the effect of the injection energy and the initial phase offset on the focusing power of I1 and I2 type resonators.

4.5.1 Injection Energy

The injection energy is usually determined by the transit time factors [Livingood 61], [Hereward 70] of corresponding resonators to optimize energy gain if a transverse focusing element is available. This is reasonable because longitudinal stability is obtained rather independently of the injection energy if the initial rf phase offset is chosen to be negative. But if resonator focusing is to be used for transverse focusing the injection energy should be chosen appropriately. For example, the I1 type resonator does not give transverse focusing at an initial β between 0.007 and 0.009 for a uranium beam according to Figure 4.7.

In this calculation the initial rf phase offsets are fixed to be -10 degrees for I1 type and -15 degrees for I2 type resonators. In the I1 type resonator the transverse focusing power decreases as injection energy increases in the region of $\beta_i > 0.01$ according to Figure 4.7. But if we remember that the accelerating structure of an I1 type resonator for the initial β was 0.0085 in Table 1.1 of Chapter 1, the region of interest would be $\beta_i < 0.01$. In this region the transverse focusing has a maximum or a minimum point of β. The maximum transverse focusing power

appears at $\beta \approx 0.0085$ for $^{40}Ar^{12+}$ and at $\beta \approx 0.006$ for $^{238}U^{24+}$. Note that at these points longitudinal focusing powers are approximately maxima. The structure of the longitudinal case is similar to the transverse case.

In an I2 type resonator which has an accelerating structure of $\beta = 0.015$ the region of interest would be $0.01 < \beta < 0.02$. The characteristics of the overall focusing power is very similar to the I1 type case. Unlike I1 type resonators the transverse and longitudinal focusing power have maximum or minimum points of β with the exception that the extreme points do not coincide approximately.

In conclusion the transverse focusing power in the low-beta range of $\beta < 0.02$ has a broad range from a strong focusing action to a rather weak defocusing action. Therefore the injection energy should be taken appropriately to optimize transverse focusing power. This will be discussed in the following section.

4.5.2 RF Phase Offset

The initial rf phase offset was already limited by transverse and longitudinal stability conditions [Promé 70], [Nozomu 90]. It was restricted to be negative for longitudinal stability. In this calculation for the relation between the focusing power and the rf phase offset the initial beta of $\beta = 0.0085$ for I1 type resonator was used. The final value of beta after passing the I1 resonator is used as an initial beta of I2 type resonator.

Figure 4.9 and Figure 4.10 show how focusing powers depend upon the initial rf phase offset. Note that the longitudinal stability is always satisfied for a negative rf phase offset, but this is not true for the transverse case any more. If we consider the efficiency of energy gain from the transit time factor and the nonlinearity of longitudinal phase space near zero rf phase offset the region of interest would be

between -30 and -10 degrees. In this range the transverse and longitudinal focusing powers are inversely proportional to each other. i.e strong longitudinal focusing means weak transverse focusing or defocusing etc.

Note that in a certain area of interest of initial rf phase offset the transverse stability condition is not satisfied at the given injection energies for a $^{238}U^{24+}$ beam. This implies that the injection energy was not matched well to give transverse focusing. This will be discussed in the following section.

In conclusion the transverse focusing powers increase as the initial rf phase offset goes to zero while longitudinal focusing power decreases both for I1 and I2 type resonators.

4.6 Initial Conditions for Focusing

In this section we investigate the possible initial conditions of injection energy and/or rf phase offset for resonator focusing without a transverse focusing element. Since transverse focusing power is very small for $\beta > 0.02$ in an I2 type resonator, it might be enough to consider I1 and I2 type resonators only for transverse focusing.

First we consider the following rf settings for both I1 and I2 type resonators with different initial betas at the entrance of the PII linac:

I1 type: $E_0 = 4.5$ (MV/m) , $\phi_0 = -10°$

I2 type: $E_0 = 3.0$ (MV/m) , $\phi_0 = -15°$

Figure 4.11 and Figure 4.12 are plots of initial beta β_i vs. final beta β_f for $^{40}Ar^{12+}$ and $^{238}U^{24+}$ beams. The new initial beta at the I2 type resonator will be found from the final beta of I1 type resonator.

First consider an $^{40}Ar^{12+}$ beam. An I1 type resonator has a wide range of initial

betas for focusing according to Figure 4.7. But the new initial beta at I2 resonator between 0.01 and 0.015 can not be used due to transverse defocusing if the I2 resonator is to be used as a focusing lens also. Therefore the range of the initial beta at I1 resonator which gives a final beta between 0.01 and 0.015 should be excluded. Fortunately this condition is satisfied because the final beta for the I1 resonator is always greater than 0.015 for an initial $\beta > 0.005$. Therefore an initial beta of 0.0085 would be a reasonable initial condition for an $^{40}Ar^{12+}$ beam. But the transverse focusing power at the I2 resonator decreases considerably compared with that at an I1 resonator without significant difference in the longitudinal focusing power.

Next, consider a $^{238}U^{24+}$ beam. In this case the I1 resonator has a relatively small range of its initial beta of $\beta < 0.007$. The new initial beta at the I2 resonator should be limited to below 0.012 for transverse focusing. Therefore the range of possible initial betas at I1 resonator would be below 0.0075 from Figure 4.11. For example we take $\beta = 0.0063$ for this calculation. Note that an initial beta of 0.0085 at the I1 resonator is not possible with an rf phase offset of -10 degrees. Because according to Figure 4.9, the rf phase offset should be limited between -8 and 0 degrees but in this range the focusing power is very low and also the I2 resonator does not give transverse focusing in Figure 4.8 and Figure 4.11.

In the case of $^{238}U^{24+}$ we have another possibility to increase focusing power by adding another I1 type resonator after the first I1 resonator. This possibility comes from the relatively broad stability region of the I1 type resonator in Figure 4.6. For example we take $\beta_i = 0.0063$ at the I1 resonator then, after passing through the I1 resonator, the final beta would be $\beta_f = 0.0137$ at the second I1 type resonator. This gives another transverse focusing to increase the net focusing power.

4.7 Conclusions

The I1 and I2 type resonators which have four-gap cylindrically symmetric accelerating structure behave as focusing lenses both for the transverse and the longitudinal directions even without alternating the sign of the rf phase offset to give effective alternating phase focusing.

The stability limit of the rf phase offset for transverse and longitudinal stability might be well optimized in the range between -30 and -10 degrees if the incident velocities are well chosen. Transverse and longitudinal focusing power are inversely proportional to each other in this range.

The maximum limit of injection energy for transverse focusing would be 0.186 (MeV/A) or a beta of 0.02 because the transverse focusing power would be negligible beyond this range. The range of injection energy for stability might be limited to a low beta region less than 26 (keV/A) or $\beta < 0.0075$ for a very heavy ion beam of low charge to mass ratio like $^{238}U^{24+}$. Also, if two I1 type resonators are used, the injection energy for $^{238}U^{24+}$ beam would be lowered up to $\beta = 0.0065$ or even less.

Since the tested beams were q/m=0.1 for $^{238}U^{24+}$ and 0.3 for $^{40}Ar^{12+}$ it is expected that the wide range of heavy ions would be focused with I1 and I2 type resonators only at the beginning stage of accelerations.

Table 4.1: Focusing powers of each accelerating gap of I1 and I2 type resonators for $^{40}Ar^{12+}$ with the rf settings and initial velocities shown in Figure 4.3 (I1) and Figure 4.4 (I2).

Res. Type	Gap	Transverse		Longitudinal	
		$1/f_1(m^{-1})$	$1/f_2(m^{-1})$	$1/f_1(m^{-1})$	$1/f_2(m^{-1})$
I1	1	28.902	16.926	-20.187	-19.276
	2	7.402	6.602	-13.566	-8.044
	3	-1.647	-1.510	5.330	3.299
	4	-4.465	-4.392	11.401	11.144
I2	1	2.662	2.380	-4.214	-3.527
	2	0.775	0.733	-1.457	-1.101
	3	-0.799	-0.765	2.122	1.681
	4	-1.704	-1.685	4.063	3.712

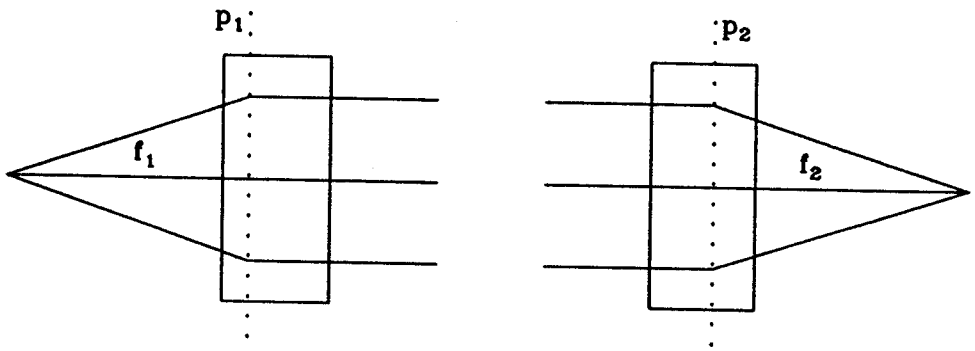

Figure 4.1: The point-to-parallel system(left) and the parallel-to-point system(right). P_1 and P_2 are two different principal planes.

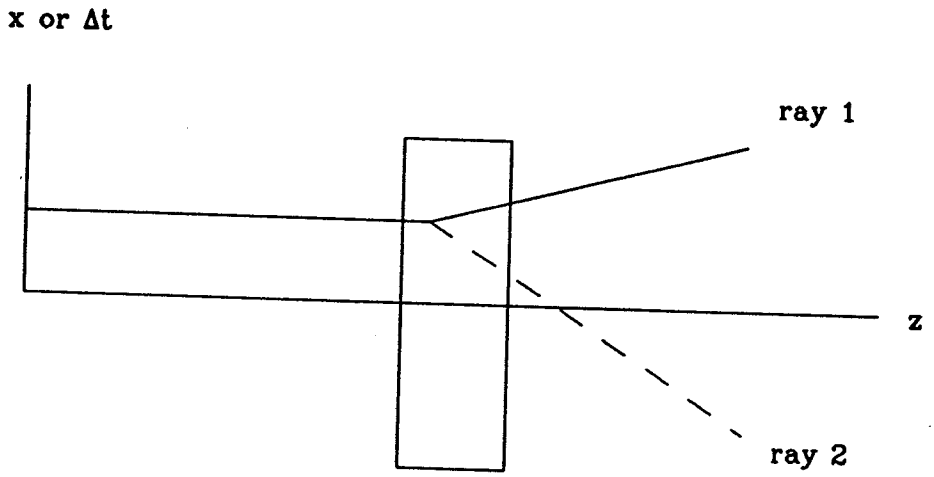

Figure 4.2: The focusing and defocusing actions of a lens. $(x'|x)$ or -$(\Delta w|\Delta t)$ is positive for ray 1 to give net defocusing action and negative for ray 2 to give net focusing action

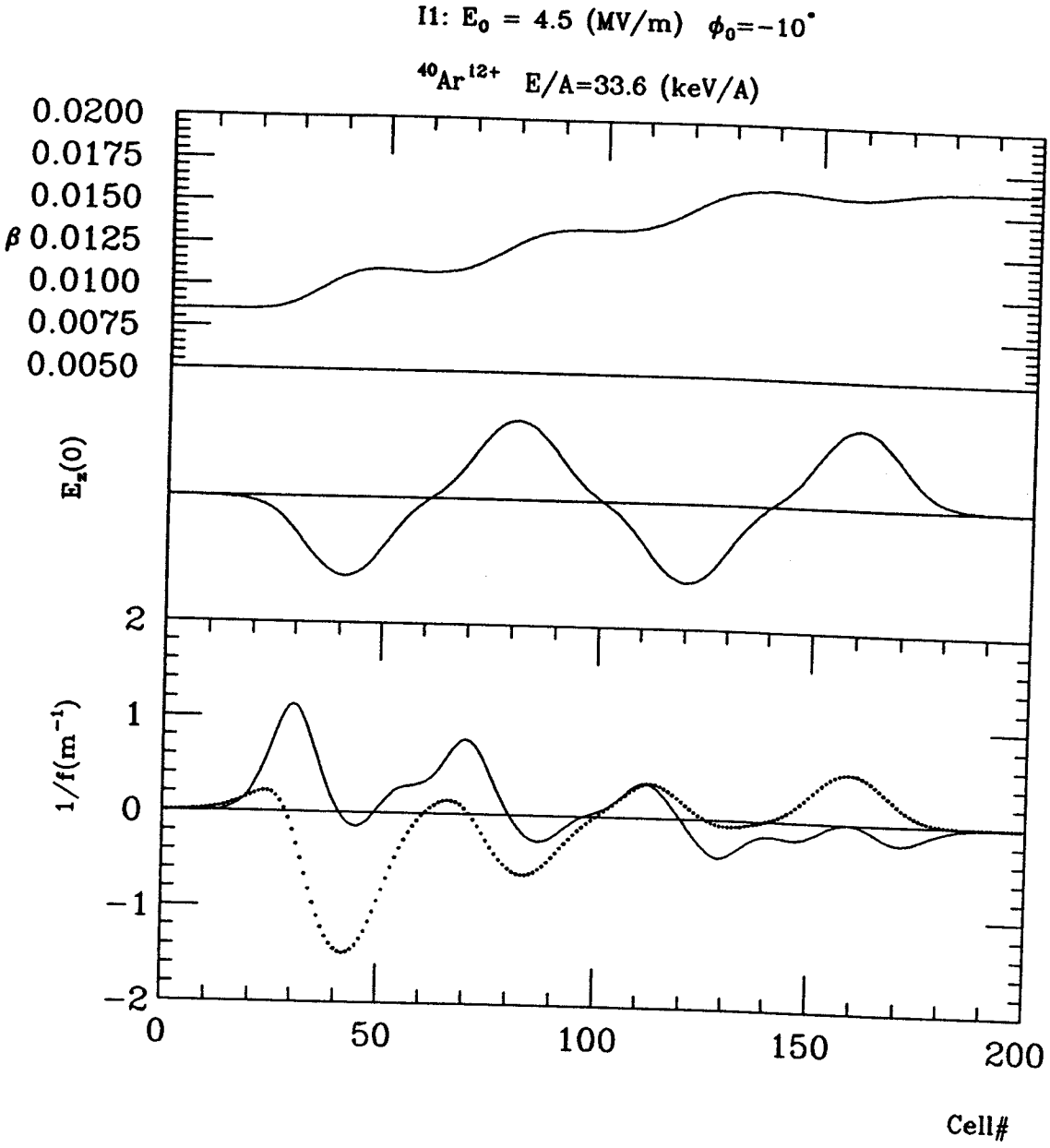

Figure 4.3: The focusing power at each cell of an I1 type resonator for $^{40}Ar^{12+}$ beam with initial value of $\beta = 0.0085$ (bottom). The solid line is for transverse direction and dotted line is for longitudinal direction. The top shows the β profile along the resonator axis. The middle part is an axial electric field profile of the I1 type resonator which has a four gap structure.

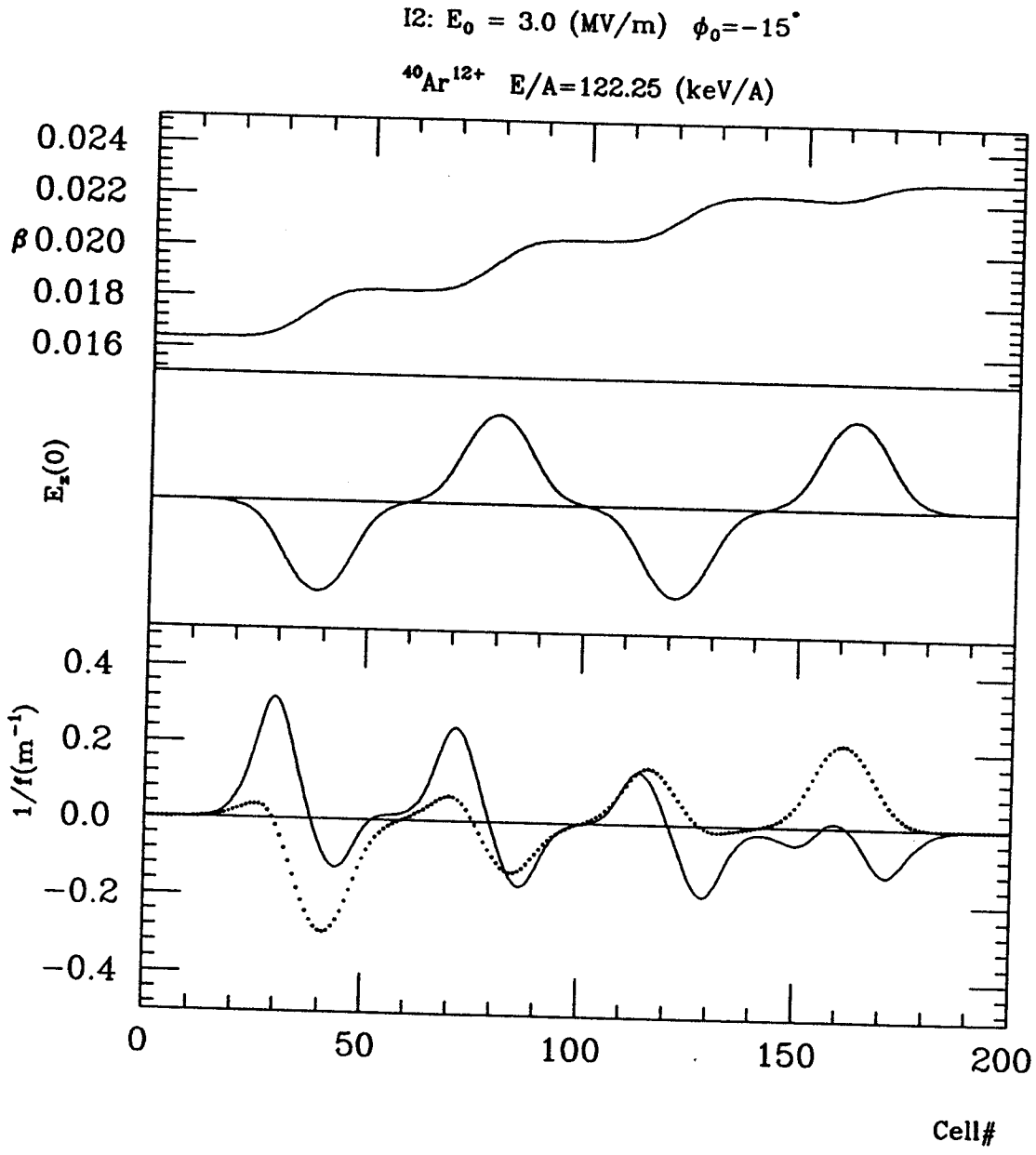

Figure 4.4: The focusing power at each cell of an I2 type resonator for $^{40}Ar^{12+}$ beam with initial value of $\beta = 0.0164$ (bottom). The solid line is for transverse direction and dotted line is for longitudinal direction. The top shows the β profile along the resonator axis. The middle part is an axial electric field profile of the I2 type resonator which has a four gap structure.

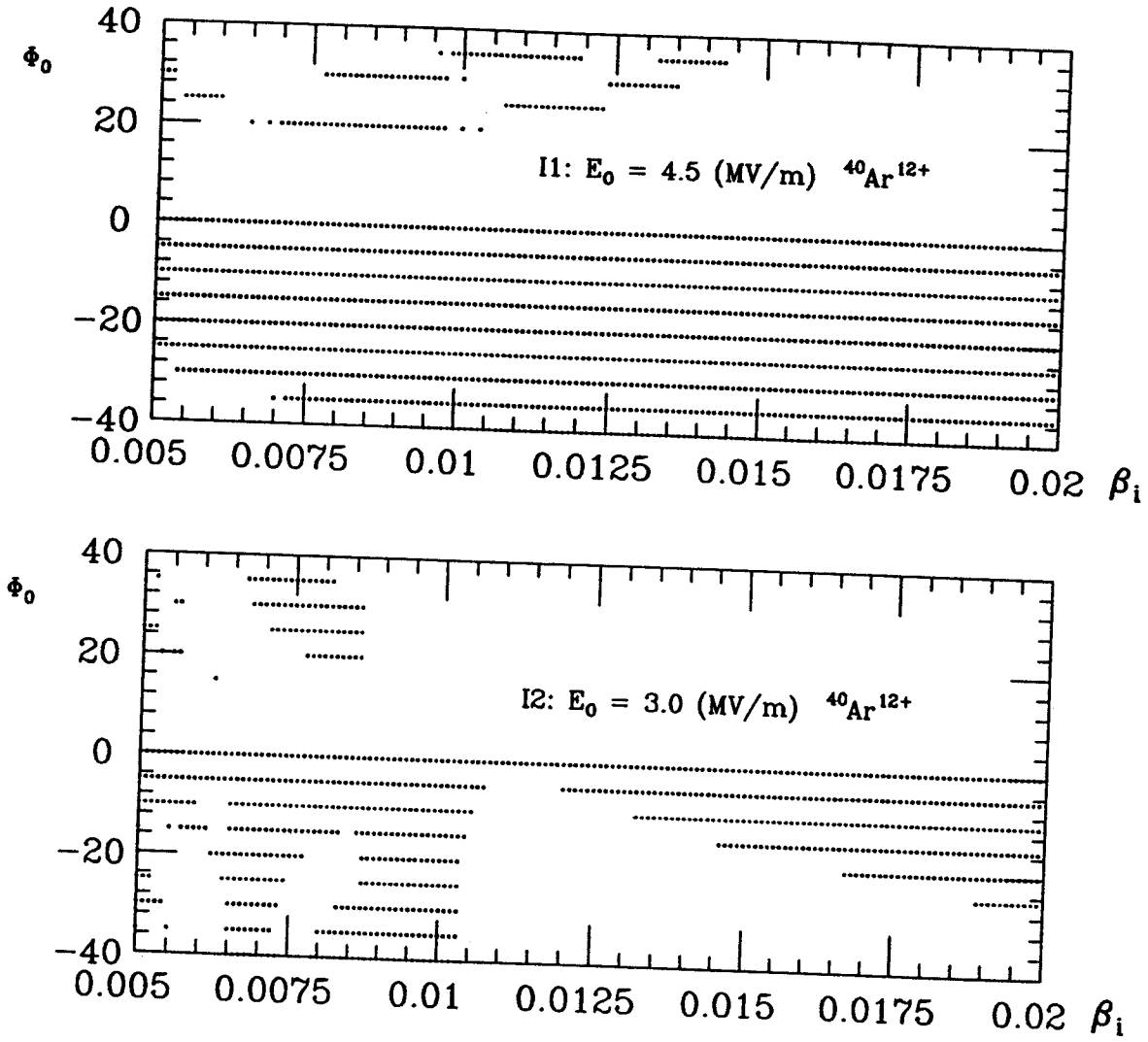

Figure 4.5: The stability region of the rf phase offset of I1 (up) and I2 type (down) resonators as a function of initial β for $^{40}Ar^{12+}$ beam.

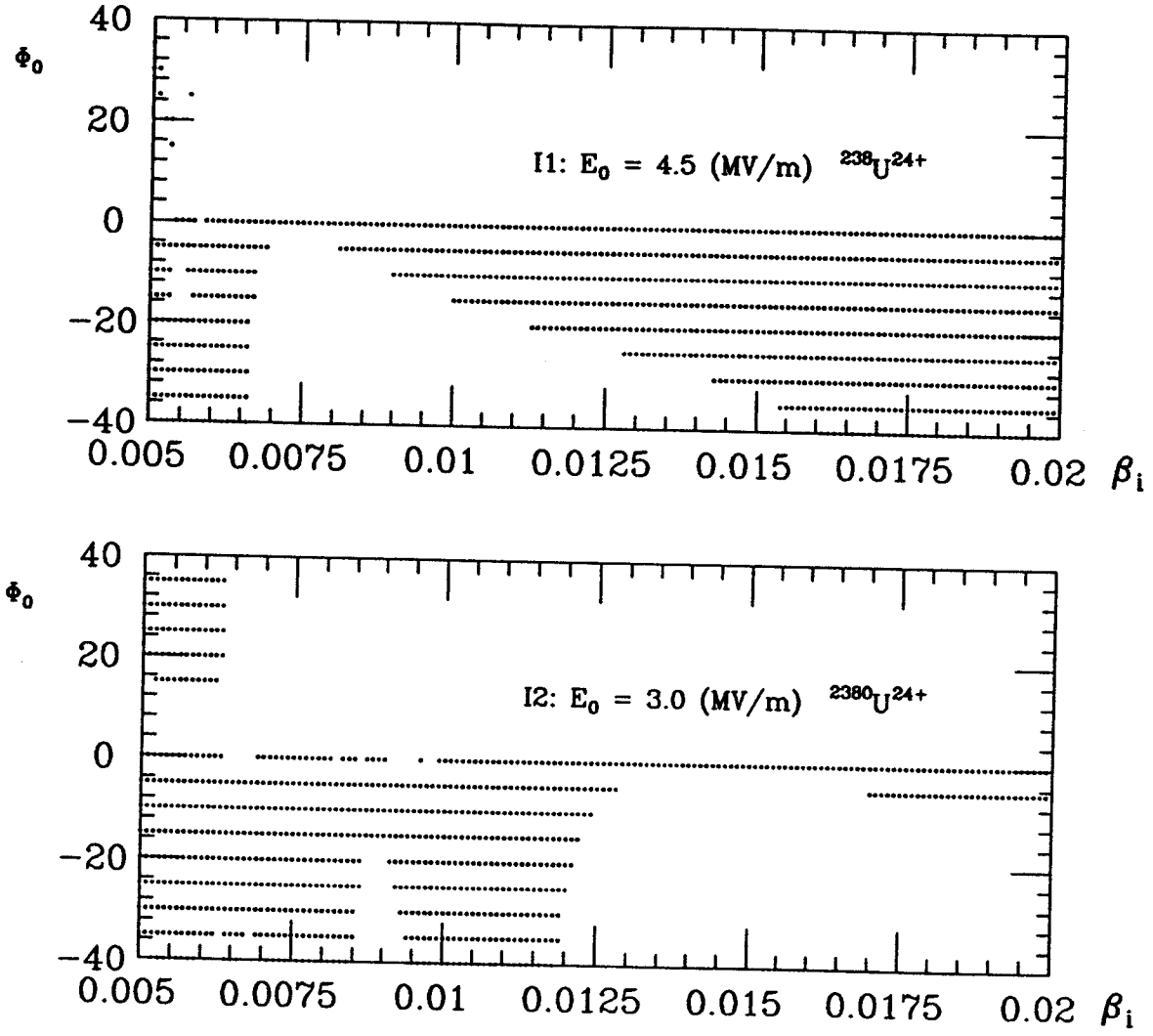

Figure 4.6: The stability region of the rf phase offset of I1 (up) and I2 type (down) resonators as a function of initial β for $^{238}U^{24+}$ beam.

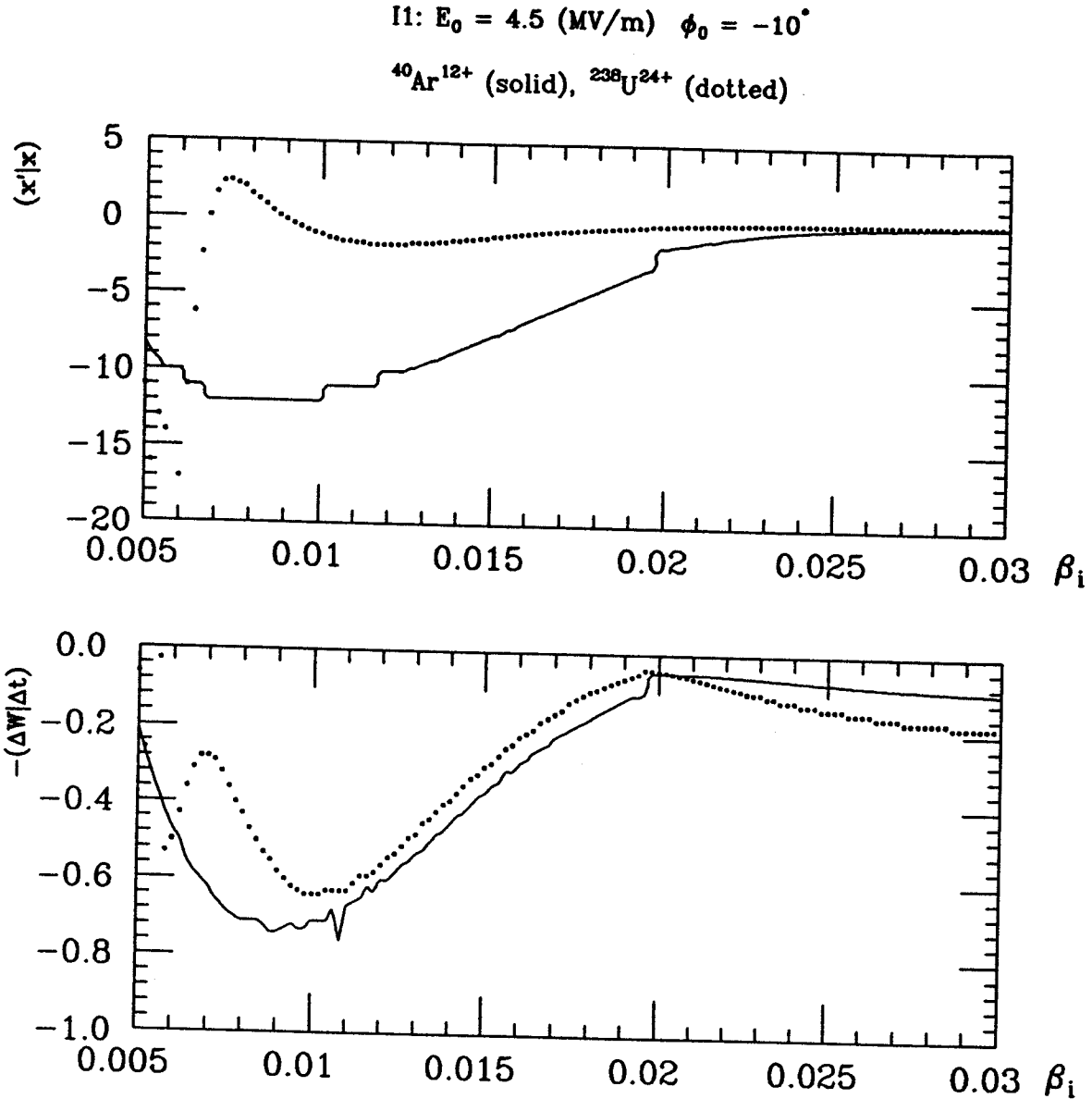

Figure 4.7: The plots of $(x'|x)$ and $-(\Delta w|\Delta t)$ vs. initial beta β_i for an I1 type resonator. The solid line is for $^{40}Ar^{12+}$ and the dotted line is for $^{238}U^{24+}$.

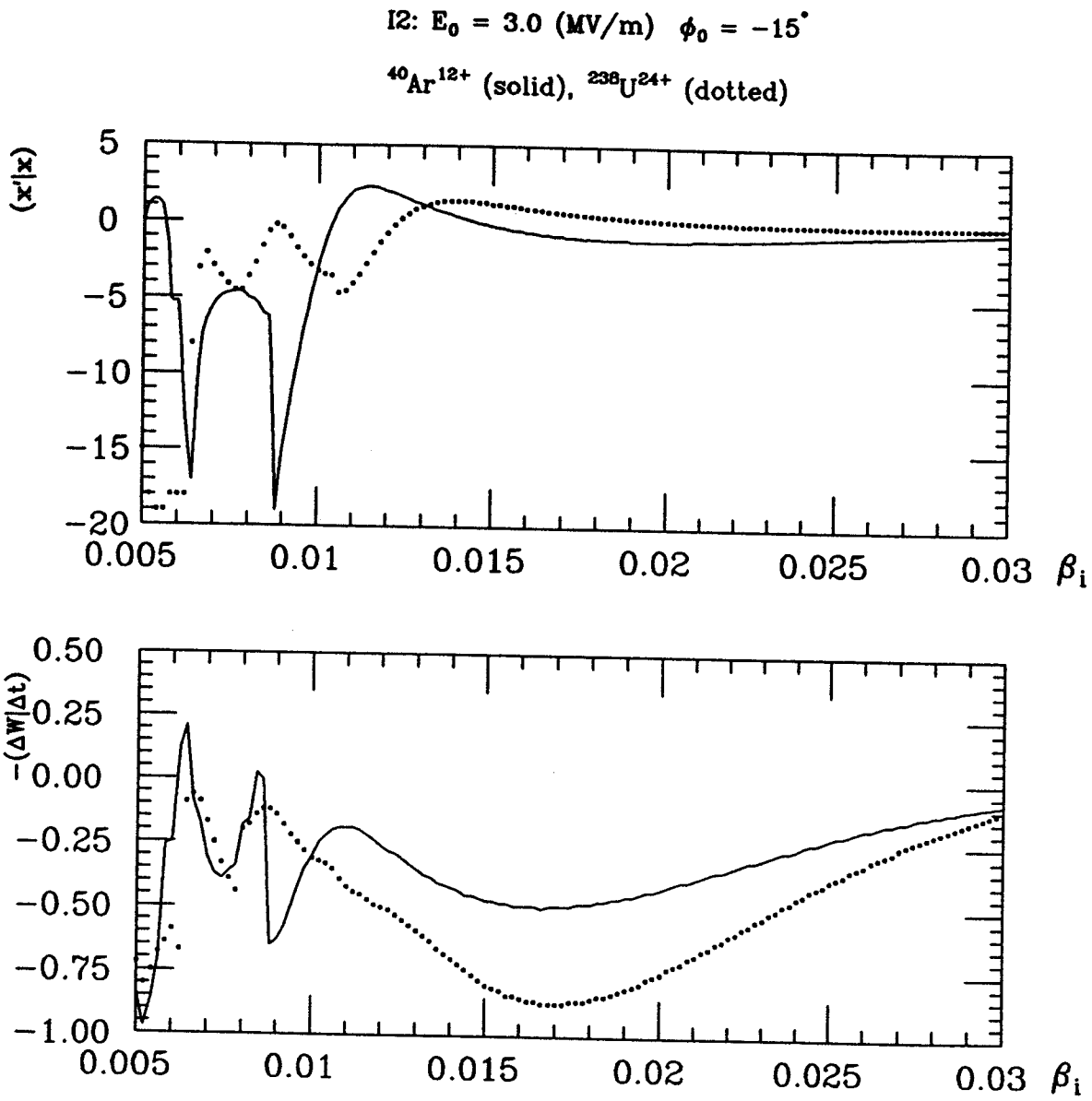

Figure 4.8: The plots of $(x'|x)$ and $-(\Delta w|\Delta t)$ vs. initial beta β_i for an I2 type resonator. The solid line is for $^{40}Ar^{12+}$ and the dotted line is for $^{238}U^{24+}$.

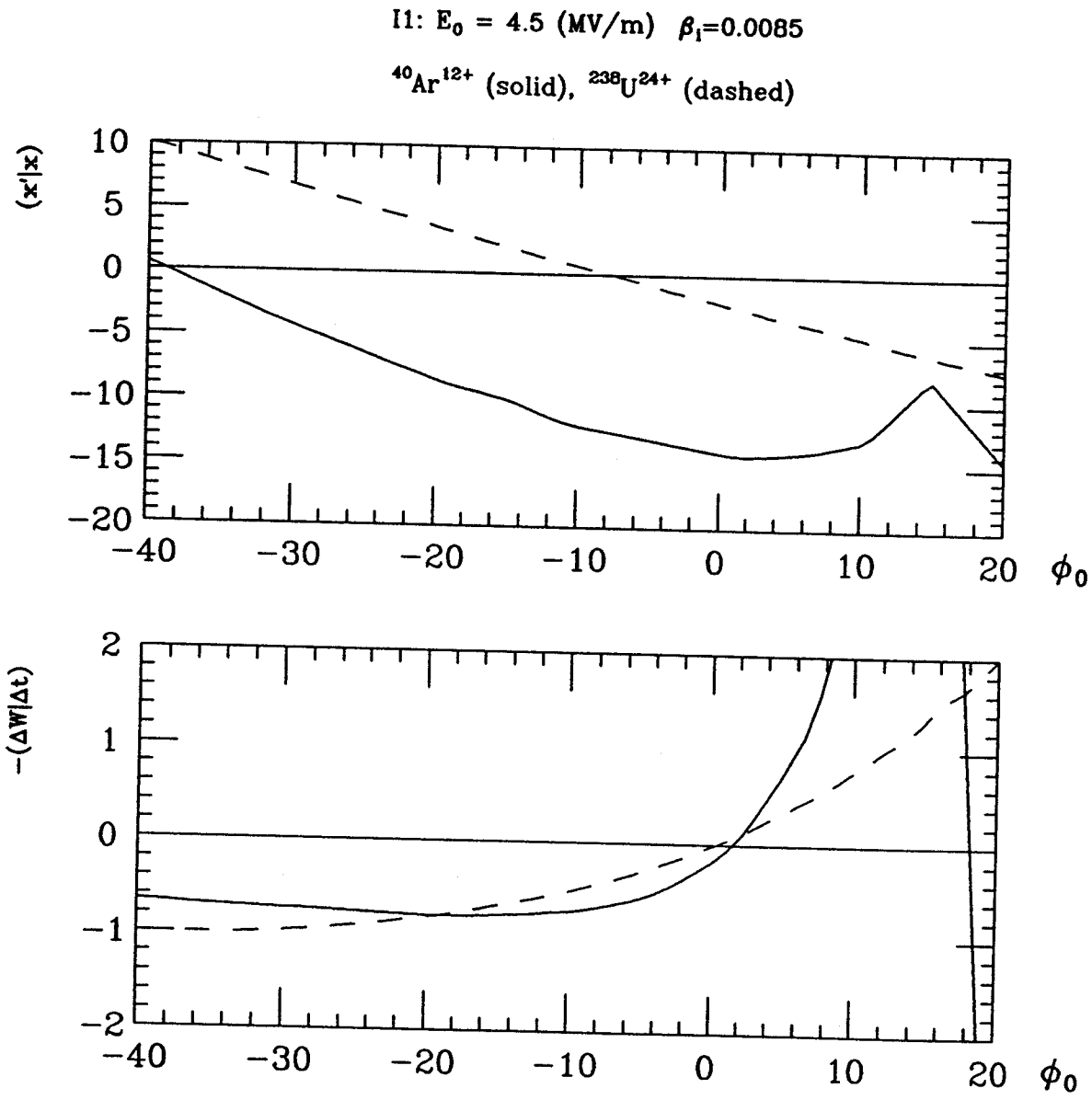

Figure 4.9: The plots of $(x'|x)$ and $-(\Delta w|\Delta t)$ vs. rf phase offset ϕ_0 for an I1 type resonator. The solid line is for $^{40}Ar^{12+}$ and the dashed line is for $^{238}U^{24+}$.

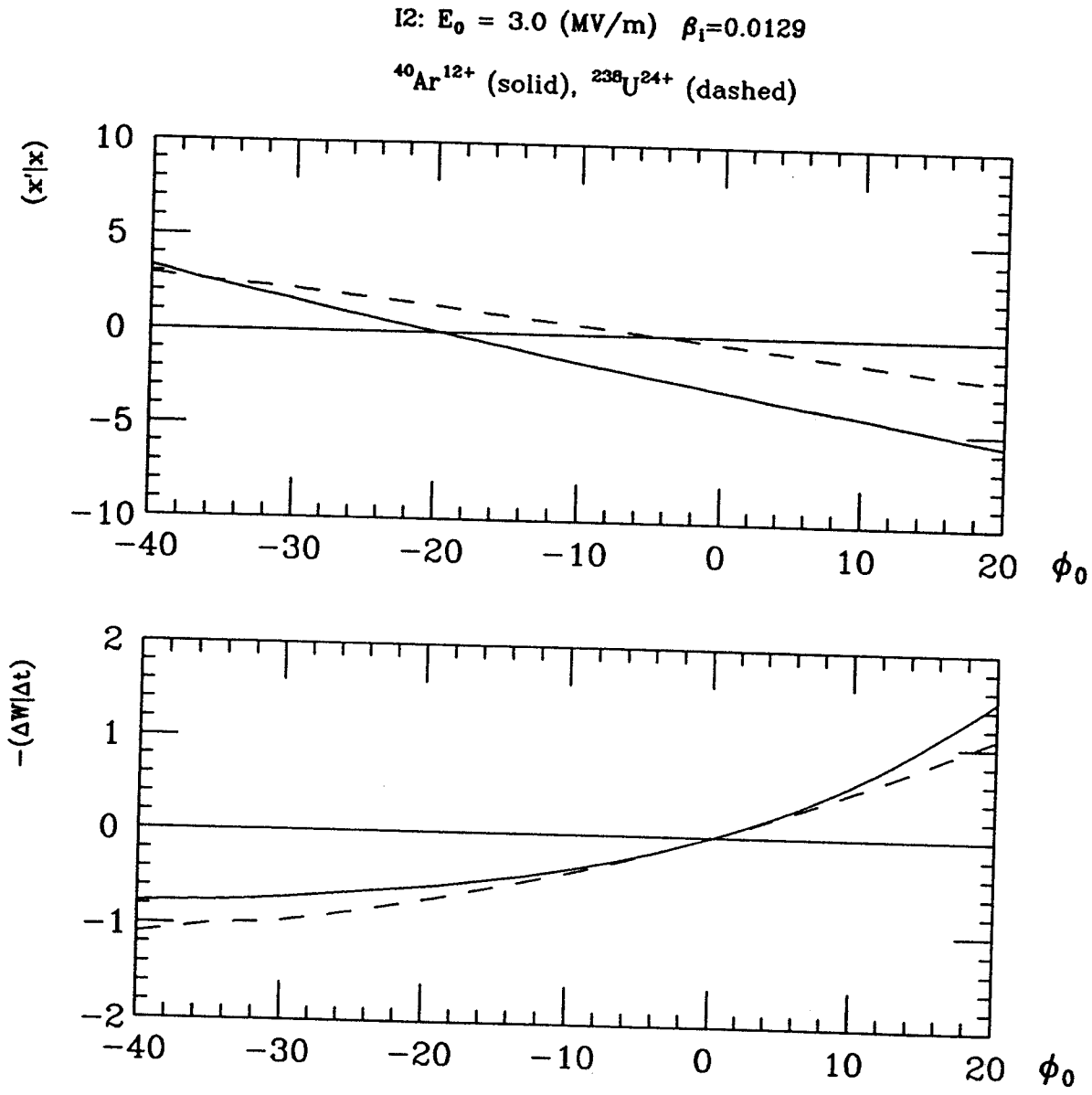

Figure 4.10: The plots of $(x'|x)$ and $-(\Delta w|\Delta t)$ vs. rf phase offset ϕ_0 for an I2 type resonator. The solid line is for $^{40}Ar^{12+}$ with $\beta_i = 0.0164$ and the dashed line is for $^{238}U^{24+}$ with $\beta_i = 0.0164$.

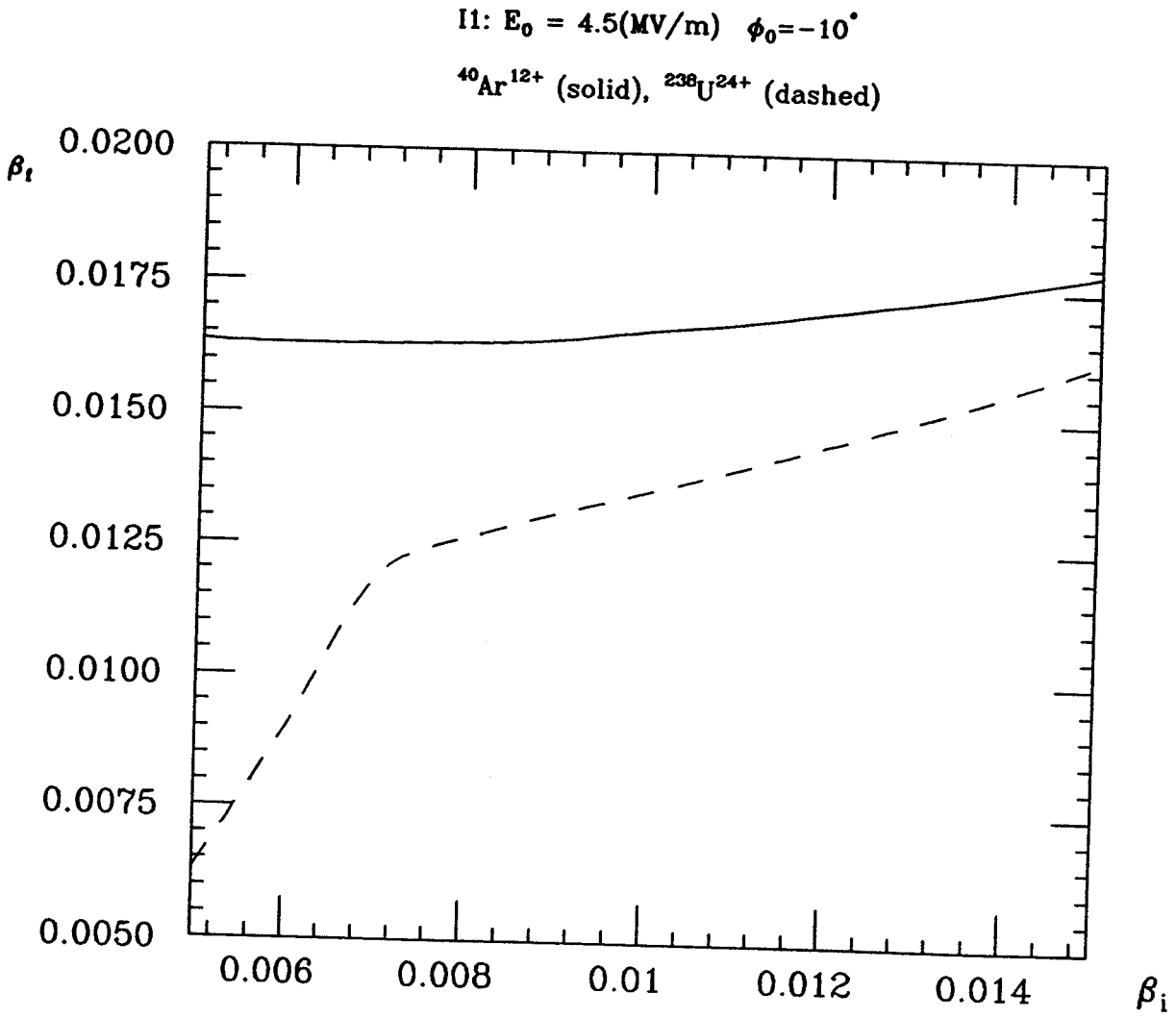

Figure 4.11: The plot for initial beta β_i vs. final beta β_f of an I1 type resonator. The solid line is for $^{40}Ar^{12+}$ and the dashed line for $^{238}U^{24+}$ beam.

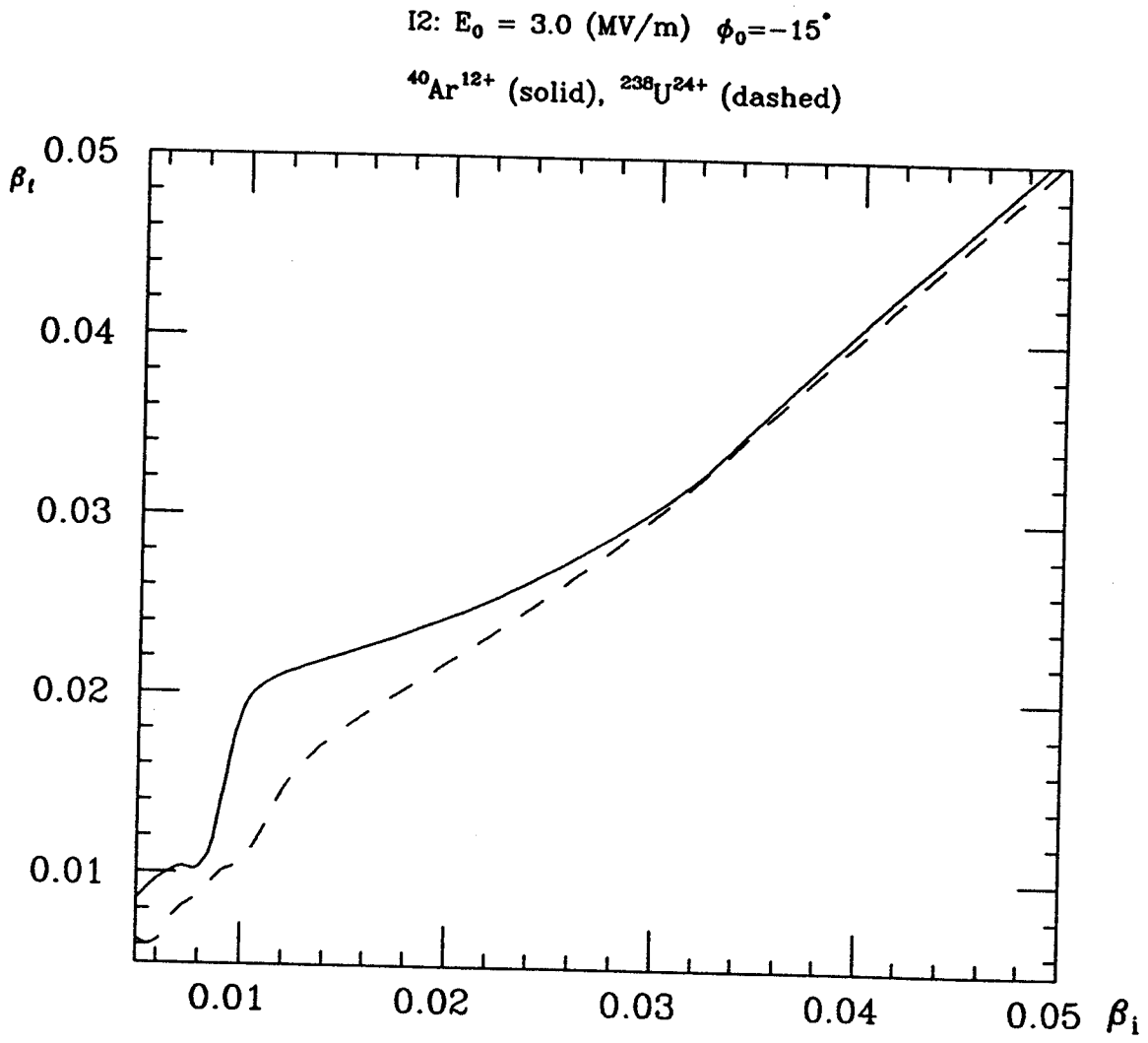

Figure 4.12: The plot for initial beta β_i vs. final beta β_f of I2 type resonator. The solid line is for $^{40}Ar^{12+}$ and dashed line for $^{238}U^{24+}$ beam.

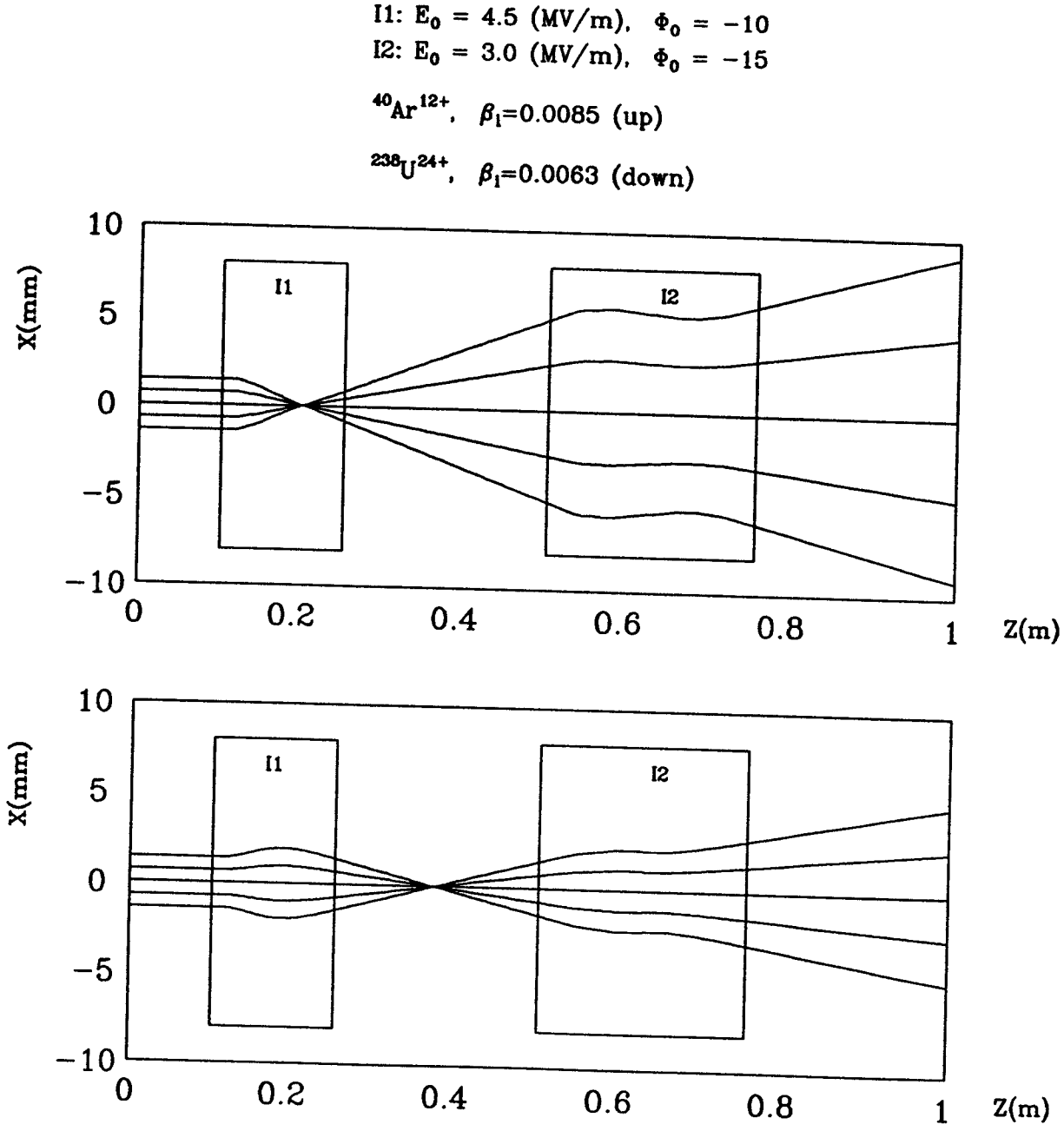

Figure 4.13: The transverse raytracing plots for $^{40}Ar^{12+}$ (up) and $^{238}U^{24+}$ (down) beams with parallel rays at the beginning.

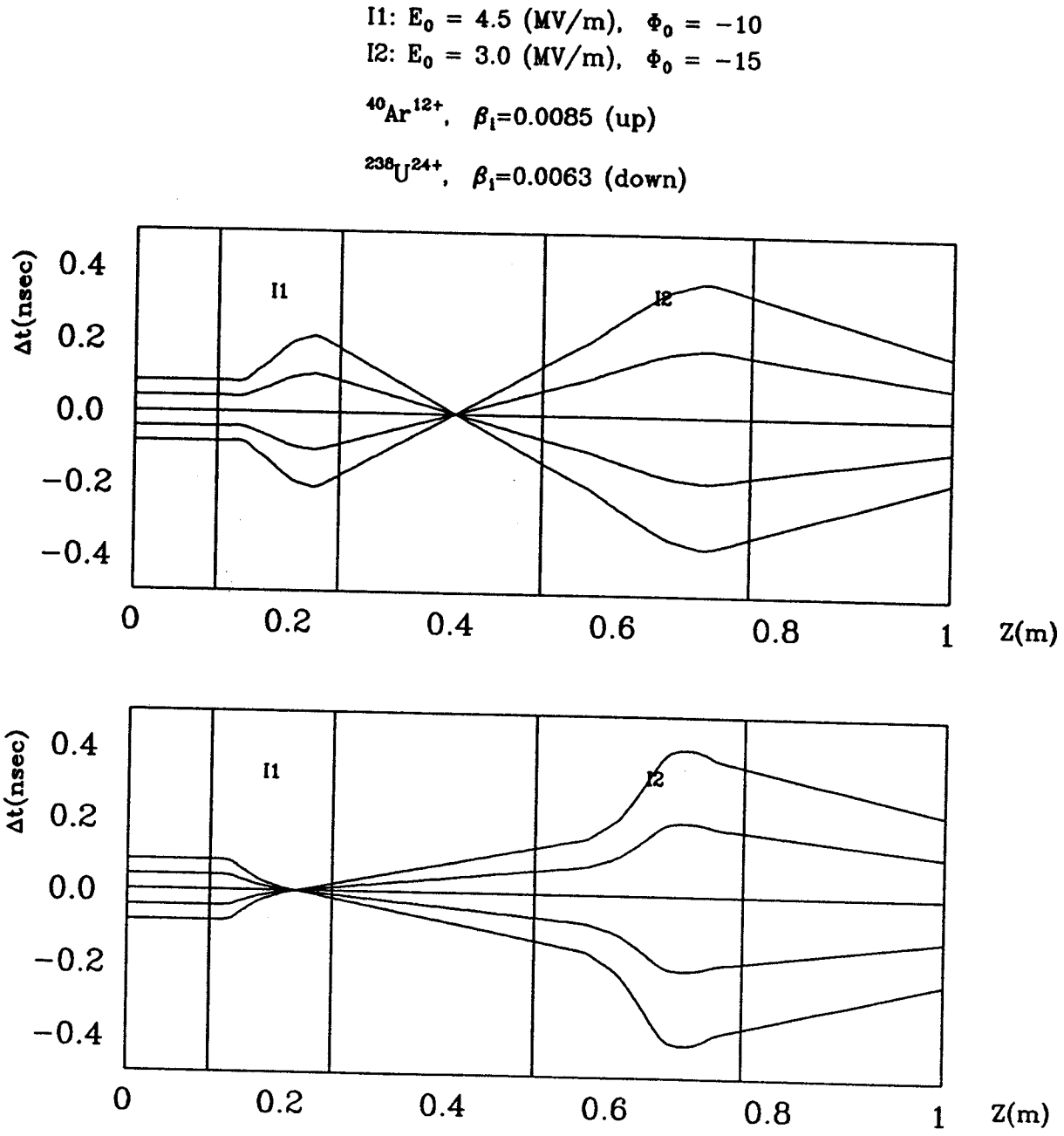

Figure 4.14: The longitudinal raytracing plots for $^{40}Ar^{12+}$ (up) and $^{238}U^{24+}$ (down) beams with parallel rays ($\Delta W = 0$) at the beginning.

Chapter 5

Applications to Acceptance Study

5.1 Introduction

The maximum emittance of a beam that a system can accept is called the acceptance or the admittance of the system; the particles within this acceptance will be transmitted without striking the walls. In accelerators which have a periodic property in motion, the magnitudes of acceptances would be calculated analytically [Chambers 76],[Edwards 87], [Okamoto 89], [Sagalovsky 92]. Even in a linear accelerator we might approximate periodic structure of motion [Bollinger 78] if the length of a system is long enough to assume periodic motions. But this is no longer the case in the Positive Ion Injector which has neither periodic structure nor long system length.

Raytracing calculations by the brute force method have been used as a general way of calculating transverse and longitudinal acceptances [Carne 70]. These calculations start from a square lattice large enough to incorporate the expected acceptance. However, this method is too time consuming to apply to a large system. Also, it does not give quantitative information about the nonlinearity of the system.

In this chapter we introduce a very straight forward way to find the transverse and longitudinal acceptances of a system by using the first order beam envelope

functions calculated from the transfer map. We subdifferentiate the terminology of acceptance into geometrical acceptance and linear acceptance. The geometrical acceptance [Lejeume 80b] is understood as the acceptance of a system calculated from first order phase space transformation theory. This would deviate from the real acceptance if nonlinearity appears. The linear acceptance is understood as the acceptance limit which behaves linearly through a system within given deviations from the higher order distortions of a phase space.

One of the interesting things in beam dynamics might be to quantify the nonlinearity of a beam. It has been reported in several papers [Lysenko 88], [Dragt 91] that some moment invariants for symplectic systems exist. These invariants are formed with some linear combinations of the average of the monomials of the phase space coordinates. The physical meaning of them are not clear at this time [Pusch 93] except for a very simple kind of invariant called generalized rms emittance. But these invariants might be used to quantify the degree of nonlinear motion as Alex J. Dragt pointed out [Dragt 91]. In this chapter we also present a quantitative measure of nonlinearities using the concept of rms emittances and deviations of phase space coordinates between linear and nonlinear transformations.

5.2 Geometrical Acceptance

The geometrical acceptance of a system is defined as the acceptance calculated from linear phase space transformation. This is larger than the useful acceptance if nonlinearities are present.

5.2.1 Transverse Acceptance

The beam envelope at a position in a system with acceleration was derived for an axially symmetric beam in equation (2.49) of Chapter 2. In n-dimensional phase space:

$$x_2 = \sqrt{(\det \mathrm{M})^{2/n}\beta_2\epsilon_1}\ . \tag{5.1}$$

where det M is the determinant of the transfer matrix and β_2, ϵ_1 are the beta-function at the position 2 and the initial beam emittance in one projected plane, respectively.

The beta-function at point 2 is found if the initial Twiss parameters of the phase space and the transfer map are known. Equation (5.1) is still valid for a nonaxially symmetric beam if n=2.

We define:

$$\beta^* = (\det \mathrm{M})^{2/n}\beta\ , \tag{5.2}$$

so that β^* is the effective beta-function.

Then the geometrical transverse acceptance of a system is limited by the apertures of optical elements and effective beta-function:

$$\mathrm{GTacc} = \left(\frac{\mathrm{R}^2(z)}{\beta^*(z)}\right)_{\min}\ . \tag{5.3}$$

where R is the aperture of the optical element. The subscript min indicates the minimum value.

In actual calculations the effective beta-functions are searched through optical elements except drift spaces, to find the transverse acceptance at each element which have different apertures. Then the maximum transverse acceptance will be determined by the smallest one. The transverse acceptance when calculated this way is what we call the geometrical transverse acceptance of a system.

5.2.2 Longitudinal Acceptance

For longitudinal phase space there is no physical aperture which limits acceptances, but to maintain the phase focusing aspect of the resonators phase excursions or time-of-flight deviations must be limited. For example if the rf phase offset is ϕ_0 for the reference particle, then the deviation of rf phase angle should not exceed ϕ_0 for any particle because at zero rf phase nonlinearity would be very important. Hence an estimate of the longitudinal acceptance is obtained by requiring:

$$\Delta t \leq \frac{\phi_0}{\omega} \equiv \mathrm{R_{long}} \,. \tag{5.4}$$

where Δt is the deviation of the time-of-flight and ω is the angular rf frequency of a resonator.

Now $\mathrm{R_{long}}$ is analogous to the radial aperture for the transverse case. With this concept of aperture for the longitudinal case we can also find the longitudinal acceptance of a system. Since there is no coupling between transverse and longitudinal phase spaces in the first order calculation the longitudinal phase space is two-dimensional. Also, longitudinal emittance is constant through the system. One difference in longitudinal acceptance calculations from the transverse case is that the apertures of transverse focusing elements, like solenoids, do not affect the longitudinal acceptance. So we have for an estimate of the longitudinal acceptance:

$$\mathrm{GLacc} = \left(\frac{\mathrm{R_{long}^2}(z)}{\beta(z)} \right)_{\mathrm{min}} \,. \tag{5.5}$$

where $\mathrm{R_{long}}$ was defined above.

The longitudinal acceptance calculated this way is what we call the geometrical longitudinal acceptance of a system. In practice, we find that the longitudinal acceptance defined in this way is a good starting point for determining the linear acceptance which will be discussed soon.

This concept of the aperture for the longitudinal case does not seem to be self-consistent because there is no limitation on the longitudinal acceptance if a system is purely linear. But, if we consider a nonlinear system, for longitudinal acceptances we might find or estimate the stability limits of longitudinal motions without much difficulty. So these limits would be used as the limits of linear deviations of longitudinal motions.

5.2.3 Fitting of Geometrical Acceptance

The geometrical acceptances can be found numerically by fitting the Twiss parameters of the phase spaces with an appropriate optimizer. The transverse or longitudinal acceptance is calculated for an assumed initial set of Twiss parameters. Then the optimizer varies the Twiss parameters until the maximum values of the geometrical acceptances are determined.

5.3 Linear Acceptance

5.3.1 Scaling of Nonlinearity by Linear Transformation

The nonlinearity of a system was not considered in the geometrical acceptance calculations described above. In practice only a fraction of the geometrical acceptance transforms linearly. We define the linear acceptance of a system as an acceptance which is transformed linearly within given deviation limits from the result of linear and nonlinear transformations.

To establish a quantitative measure of the degree of nonlinearity, a new quantity, called the deviation of the particle i, is defined:

$$\text{dev.} \equiv \frac{| x_l^i - x_n^i |}{x_{lm}} . \tag{5.6}$$

where subscript l, n indicate linear and nonlinear transformations of the particle i, respectively, and x_{lm} means the maximum value of the coordinate x in the linear transformations of the geometrical acceptance.

We introduce a method to find linear acceptances by comparing linear and nonlinear transformations. As an example, let us find the transverse linear acceptance with dev. $\leq 1\%$:

1. Find the geometrical acceptance using an optimizer.
2. Find maximum values of position x_m and divergence x'_m from the linear transformation of the initial geometrical acceptance ellipse.
3. Find deviations of the phase space coordinates of individual rays with coordinates chosen on a grid bounded by the geometrical phase space ellipse from linear and nonlinear transformations.
4. Discard all initial rays for which one of the deviations is greater than 1% to get the linear acceptance from the remaining rays.

Note that this deviation method gives the area and the orientation of a phase space ellipse. The degree of nonlinearity is controlled through the choice of the magnitude of the dev. parameter.

5.3.2 Scaling of Nonlinearity by RMS Emittance

It is well known that the normalized emittance [Billen 75], [Lejeume 80a] is conserved even in an accelerating system. But because of distortions of the phase spaces subjected to nonlinear forces the effective area of phase space tends to increase. So to avoid this weakness we consider the transformations of their effective area called root-mean-square (rms) emittance. The concept of rms emittance has been used to

measure the effective area of a distorted phase space ellipse subjected to nonlinear forces [Lapostolle 71], [Lawson 73], [Lejeume 80a].

The rms emittance is defined for a pair of phase space coordinates x and x' by [Lapostolle 71], [Sacherer 71]:

$$\epsilon_{rms} = 4\sqrt{< x^2 >< x'^2 > - < xx' >^2} \,. \tag{5.7}$$

This rms emittance reverts to the emittance of the phase space ellipse if the phase space ellipse is not distorted.

If a system is linear the coordinates will transform by the transfer map M of the system:

$$\begin{aligned} x_2 &= M_{11}x_1 + M_{12}x_1' \,, \\ x_2' &= M_{21}x_1 + M_{22}x_1' \,. \end{aligned} \tag{5.8}$$

Using equations (5.7) and (5.8) we get the rms emittance transformation [Dragt 91]:

$$\epsilon_{rms2} = (\det \mathrm{M}) \cdot \epsilon_{rms1} \,. \tag{5.9}$$

The rms emittance defined above transforms in the same way as the two-dimensional phase space transformation derived in equation (2.21) of Chapter 2. Thus $(\det \mathrm{M})^{-1}\epsilon_{rms}$ is a constant of the motion. We use it to modify the usual definition of normalized rms emittance:

$$\epsilon_{nrms} = (\det \mathrm{M})^{-1} \cdot \epsilon_{rms} \,. \tag{5.10}$$

Equation (5.10) would yield the common definition of the normalized rms emittance for the transverse case if ϵ_{rms} were multiplied by the initial value of the relativistic factor $\beta\gamma$. Because of the invariance of the normalized rms emittance under linear transformations it might be used as a measure of the nonlinearity of a system by comparing its values between linear and nonlinear transformations.

The invariant result of the normalized rms emittance is true only when no first order couplings exist with the other pairs of phase space coordinates. The general invariants theorems for first order couplings have been developed by several authors only for symplectic systems as pointed out in the introduction of this chapter. But in our case the first order couplings do not appear or can be decoupled by rotating the coordinate system.

5.4 Application to an Alternating-Phase-Focusing System

It was shown in Chapter 3 that transverse focusings by multi-gap resonators were possible without additional focusing elements because of their inherent alternating-phase-focusing properties. As a first application we investigate geometrical and linear acceptances of such a system consisting of rf resonators and drift spaces. Since the focusing power of the PII resonators for the transverse direction may be negligible after considerable energy gains we consider just three successive resonators at the beginning of the PII linac which was shown in Figure 1.2 of Chapter 1. This system configuration is also shown schematically in Figure 5.2.

5.4.1 Geometrical Acceptances on Incident Velocities

Figure 5.1 shows geometrical transverse and longitudinal acceptances on incoming velocities. These acceptances were calculated from the first order matrix optics code MINJI [Joh 93b].

For these acceptance calculations $^{40}Ar^{12+}$ (solid) and $^{238}U^{24+}$ (solid+dots) were used. The rf settings for the electric field gradients E_0 and the initial rf phase offset ϕ_0 for the resonators are:

I1: $E_0 = 4.5$ (MV/m), $\phi_0 = -10°$

I2-1: $E_0 = 3.0$ (MV/m), $\phi_0 = -15°$

I2-2: $E_0 = 3.0$ (MV/m), $\phi_0 = -15°$

We assumed that all three resonators had the same half apertures of 8 mm of a type I1 resonator which has the smallest diameter. Also, we assumed that the magnitude of the initial rf phase offset, 10 degrees for a type I1 resonator, would correspond to a radius of longitudinal case.

Figure 5.2, as an example, shows geometrical transverse (upper) and longitudinal (lower) beam envelopes starting with corresponding acceptances calculated from the matrix optic code MINJI. For a $^{238}U^{24+}$ beam with an incident velocity 0.007c, the calculated geometrical acceptances were 140.49 mm·mr for the transverse direction and 51.07 keV·nsec for the longitudinal direction. The deviations of time of flight were used instead of rf phase angles to include drift spaces for longitudinal phase space. The radius of 10 degrees for longitudinal wall corresponds to 0.57 nsec in the deviation of time of flight for each resonator which has an rf frequency 48.5 MHz.

According to Figure 5.1 the incident velocities of ion beams for this alternating-phase-focusing system should be compromised between the transverse and the longitudinal acceptance; the low velocity region would be limited by longitudinal acceptances and the high velocity region would be limited by transverse acceptances depending on the beam qualities from the ECR ion source.

5.4.2 Estimation of the Linear Acceptances

It would be useful to measure the nonlinearities of a system by comparing normalized rms emittances between linear and nonlinear transformations. In these calculations the linear transformations of individual rays were calculated from the first order trans-

fer map and nonlinear transformations were calculated from raytracing calculations. But basically if a higher order nonlinear map is available it would be used for nonlinear transformations to avoid time-consuming raytracing calculations.

Figure 5.3 shows the linear acceptance of $^{238}U^{24+}$ beam at dev. $\leq 1\%$ with incident velocity 0.007c. The large ellipse in the top left plot is the geometrical transverse acceptance which has a phase space area 140.49π mm·mr. This large ellipse transforms under acceleration to have a maximum beam radius of 8 mm and a beam divergence of 10.9 mr with pure linear transformations at the end of the system. To select a linear region from the geometrical acceptance, as an example here with dev. $\leq 1\%$ from the nonlinear transformations, only the initial rays are kept which satisfy certain deviation conditions:

$$| r_{f2} - r_{f1} | < 0.01 \times 8 = 0.08 \ (mm) ,$$

$$| r'_{f2} - r'_{f1} | < 0.01 \times 10.9 = 0.109 \ (mr) .$$

where subscript f1 and f2 means linear and nonlinear transformations of a ray at the end of the system.

The rays inside a small phase space ellipse are the linear region of the geometrical acceptance with deviation 1%. This gives the transverse linear acceptance of 4.01 mm·mr (area 4.01π mm·mr). Since it is not necessary that the linear region be an exact ellipse we will use rms emittance to define the linear phase space.

The two plots in the lower part of Figure 5.3 show the transformations of the linear phase space under linear (left) and nonlinear (right) transformations. The deviations of individual rays with dev.= 1% does not appear clearly in the nonlinear transformations. But some deviations appear with dev.= 5% as shown in Figure 5.5.

We assumed in the nonlinear transformations that longitudinal phase space was zero at the beginning. It is noticeable that there is relatively large growth of the

longitudinal phase space due to coupling between transverse and longitudinal phase spaces as shown in the top right plot.

In the same manner as the transverse case, Figure 5.5 shows longitudinal phase space plots on axis. We assumed in the nonlinear transformations that the transverse phase space was zero at the beginning. In this case the growth of a new transverse phase space does not appear.

5.5 Nonlinearity of a System

We found linear regions of phase space with certain deviation limits between linear and nonlinear transformations. So we might use the relative deviations of the two transformations as a measure of nonlinearity of a system.

In this section we investigate the relationship between the scaling of nonlinearity by linear transformation and by rms emittance discussed in section 5.3.2 of this chapter. We calculate the normalized rms emittance ϵ_{nrms}, which is the rms emittance divided by the determinant of the transfer map, by:

$$\epsilon_{nrms} = (\det \mathrm{M})^{-1} \cdot \epsilon_{rms} \,. \tag{5.11}$$

Since this is invariant under acceleration we define two kinds of nonlinearity by normalized emittances:

$$N_1 \equiv \frac{\epsilon^l_{nrms} - \epsilon^l_{nrms0}}{\epsilon^t_{nrms0} \cdot p_0} \,, \tag{5.12}$$

$$N_2 \equiv \frac{\epsilon^{t,l}_{nrms} - \epsilon^{t,l}_{nrms0}}{\epsilon^{t,l}_{nrms0}} \,. \tag{5.13}$$

where the superscripts l, t indicate longitudinal and transverse phase spaces respectively, and $\epsilon^{t,l}_{nrms0}$ means normalized transverse (t) or longitudinal (l) emittance at the beginning of a system.

Since the area of longitudinal phase space has dimensions of angular momentum we multiply the initial momentum of a beam p_0 by the transverse phase space in equation (5.12) of which area has dimension of mm·mr. Therefore the nonlinearities defined in the above equations are dimensionless.

The first kind of nonlinearity N_1 might be interpreted as the degree of coupling between longitudinal and transverse phase spaces. i.e. the longitudinal emittance growth per unit transverse phase space area in angular momentum units. N_2 might be understood as the relative growth rate of the normalized rms emittance due to nonlinear forces.

The upper part of Figure 5.6 shows linear transverse acceptances on different linear scales (solid). For this calculation we assumed the geometrical transverse acceptance to be 140.49 mm·mr at the beginning without longitudinal phase space. The linear acceptances increase linearly about the linear scalings or deviations, but this will converge to the geometrical acceptance at a certain limit. The growth of longitudinal phase space (dotted) increase linearly and fast.

The lower part of Figure 5.6 was calculated from linear and nonlinear transformations of two dimensional transverse phase space without any deviations of energy and time of flight at the beginning. It shows the relationships between two kinds of nonlinearities N_1, N_2 with respect to the linear scaling. The coupling between transverse and longitudinal phase spaces increases gradually (dotted) while the relative growth of normalized rms emittance tends to decreases (solid). In this plot negative growth rate means compression or the decrease of normalized rms emittance relative to the initial values.

The new creation of the longitudinal phase space does not violate Liouville's theorem [Lichtenberg 69], because in the coupled 2n-dimensional phase space only 2n-

dimensional phase space volume is conserved.

Figure 5.7 shows the same kind of plots as in the transverse case for the longitudinal phase space. The initial geometrical acceptance was 51.07 keV·nsec without transverse acceptance. The relative growth rate of longitudinal phase space increase faster than in the transverse case.

5.6 Application to the PII Linac

In this section we investigate geometrical and linear acceptances of the beginning part of the PII linac with superconducting solenoids as focusing elements. For this calculation we use the model solenoid discussed in Chapter 3.

We also consider just three successive resonators with solenoids between them at the beginning of the PII linac which was shown in Figure 1.2 of Chapter 1. This system configuration is also shown schematically in Figure 5.8.

5.6.1 Incident Velocity on Geometrical Acceptances

If transverse focusing elements like magnetic solenoids are available, the incident velocities need not be limited, at least for transverse focusings. Since longitudinal acceptance increases for higher velocities the optimized velocity for maximum energy gain might be used as an incident velocity. For example 0.0085c will be used instead of 0.0070c as an initial velocity of $^{238}U^{24+}$. This increased initial velocity increases geometrical longitudinal acceptance more than two times relative to lower velocity.

5.6.2 Fitting of Solenoid Strength

The basic concept of the beam optics of the PII linac was to make beam waists at the center of each rf resonator to minimize nonlinearities due to the off axial fields

of the resonators. But since beam waist points depend upon the initial shape of the phase space ellipse it is not easy to find the initial shape of a phase space for the geometrical transverse acceptances and the magnetic field strength of solenoids. But as an approximation for the beam waist condition we use point-to-point conditions between the centers of resonators. This corresponds to the paraxial image conditions in ordinary optics and gives a good approximation for the beam waist if the beam size is not so big. This condition is useful because it does not depend on the initial shape of a phase space but on the transfer map of two corresponding points. The deviations from the waist points might be tuned for beam waists without changing the results of transverse acceptance calculations. The result of fitting the solenoids field strengths using the matrix optics code is shown in Figure 5.8. The beam waist points exist approximately at the centers of each resonator with fitted maximum magnetic field strengths of 4.24 for the 1st, 7.08 for the 2nd , and 7.17 Tesla for the 3rd solenoid.

5.6.3 The Selection of Nonlinear Optical Elements

Figure 5.9 shows the transformations of the linear phase space enclosed by the small ellipse within the large ellipse with dev. $\leq 1\%$. Here the difference between an alternating phase focusing system i.e. transverse focusing by resonators only and a solenoid focusing system is the orientation of linear phase space ellipse. In the solenoid focusing system the orientation of linear phase ellipse is quite different from that of geometrical phase ellipse.

To understand this the effective beta-functions for the two different orientations were plotted in Figure 5.13. Figure 5.13 is the effective beta-function plot through the each element calculated with Twiss parameters from the geometrical acceptance (dotted) and linear acceptances (solid) with dev. $\leq 1\%$. Overall, for the transverse direction, the beam envelope with Twiss parameters from the geometrical acceptance

looks much better than in the linear acceptance case. But the geometrical case is much worse than the linear case for nonlinearities.

Qualitatively, these curves indicate that nonlinearities are minimized by keeping the effective beta-function small in I1 while allowing it to be larger in s1. This might be a very useful concept in identifying the nonlinear elements and to minimize their effects.

5.7 Analysis of the Two Focusing Systems

The one advantage of the solenoid focusing system over the resonator focusing system is that the large transverse acceptance is independent of the incident velocity. So the incident velocity would be adjusted for longitudinal acceptance. On the other hand in the resonator focusing system the incident velocity is limited by both transverse and longitudinal acceptances: the low velocity gives large transverse acceptance but small longitudinal acceptance in general from Figure 5.1.

Here we analyze the two focusing systems with two different incoming velocities: 0.0070c for the resonator focusing system of which the initial velocity was chosen by compromising between transverse and longitudinal acceptances; 0.0085c is used for the solenoid focusing system of which initial velocity is well matched to the PII linac with the uranium beam.

The big difference in the two systems comes from the linear transverse acceptance: The geometrical transverse acceptances of the solenoid focusing system were about two times that of the resonator focusing system both for transverse and longitudinal acceptances. But the linear transverse acceptances of the solenoid focusing system are much more than two times at the same deviations as seen in the upper plots of Figure 5.6 and Figure 5.11.

The explanation might be that most of the nonlinearities against the transverse phase spaces come from the resonators rather than the focusing solenoids. The lower plots of Figure 5.6 and Figure 5.11show quantitatively that the solenoid focusing system is more linear than the resonator focusing system.

But even the growth rate of the longitudinal phase space per linear transverse acceptance (N_1) in the solenoid focusing system is better than in the resonator focusing system, the absolute values of the growth of the longitudinal phase space is much larger than the resonator focusing system because of larger linear transverse acceptances. Therefore the actual linear transverse acceptance will be limited by the absolute values of the growth of the longitudinal phase space.

Figure 5.3 and Figure 5.4 show transformations of the linear transverse acceptance in the resonator focusing system with deviations of 1% and 5% respectively. Figure 5.9 shows the transformation of the linear transverse acceptance in the solenoid focusing system with deviations of 1%. In the 5% deviation of the resonator focusing system the nonlinearity clearly appears in the substructure of the plot with the creation of longitudinal phase space.

On the other hand for the longitudinal linear acceptances on axes in the two systems, there is no significant differences in the nonlinearities from Figure 5.7 and Figure 5.12. This is mainly due to the fact that the growth of the transverse phase space does not appear from the longitudinal acceptances. The geometrical longitudinal acceptance of the solenoid focusing system was about two times that of the resonator focusing system. This ratio does not change so much in the linear acceptances from the upper plots of Figure 5.7 and Figure 5.12.

Figure 5.5 and Figure 5.10 show transformations of the linear longitudinal acceptances on axes in the resonator focusing and the solenoid focusing systems respectively

with deviations of 5%. The new creations of transverse phase space do not appear.

5.8 Conclusions

The scaling of nonlinearity was defined from deviations of linear and nonlinear transformations (dev.). It has complementary relations with the scaling of nonlinearity by N_1, N_2 defined from rms emittances. For example if we require a relative normalized rms deviation of 10 % ($N_2 = 0.1$) at the end of the system for longitudinal phase space we could correlate this scaling by rms emittances with the scaling by the dev. . The $N_2 = 0.1$ corresponds approximately to dev. =0.1 in the lower part of Figure 5.7. So by using dev. =0.1 we can find the corresponding linear acceptance from the geometrical longitudinal acceptance. Therefore this will quantitatively give detailed information about the matching conditions of the initial phase space ellipses that will be linearly transformed.

The calculated longitudinal and transverse acceptances are going to be enough to include acceptances of beams from the ECR ion sources at ATLAS [Bollinger 92] even for the heaviest beam like uranium with very low velocities less than 0.008c. But nonlinearities in the resonator focusing system were relatively large compared with solenoid focusing system due to the strong nonlinearities of the resonators.

One thing to note is the relatively fast increasing of longitudinal phase space coming from the phase space coupling, so longitudinal beam dynamics would be more important than transverse ones to consider nonlinearities of this kind of phase-alternating-focusing system with very low ion velocities.

In the calculations we did not consider the couplings of transverse and longitudinal phase coordinates at the beginning. If higher order transfer maps are known for a given system it might be done easily and fast to study the nonlinearity of a system

starting from real coupled phase spaces between the transverse and the longitudinal directions without time-consuming raytracing type calculations.

Table 5.1: Focusing structures of the resonator focusing system for $^{40}Ar^{12+}$ beam with incident velocity 0.0085c.

Res. Type	Gap	Transverse		Longitudinal	
		$1/f_1(m^{-1})$	$1/f_2(m^{-1})$	$1/f_1(m^{-1})$	$1/f_2(m^{-1})$
I1	1	28.902	16.926	-20.187	-19.276
	2	7.402	6.602	-13.566	-8.044
	3	-1.647	-1.510	5.330	3.299
	4	-4.465	-4.392	11.401	11.144
I2-1	1	2.662	2.380	-4.214	-3.527
	2	0.775	0.733	-1.457	-1.101
	3	-0.799	-0.765	2.122	1.681
	4	-1.704	-1.685	4.063	3.712
I2-2	1	1.959	1.881	-3.171	-3.286
	2	0.824	0.800	-1.681	-1.403
	3	-0.659	-0.642	1.617	1.375
	4	-1.202	-1.210	2.603	2.655

Table 5.2: Focusing structures of the resonator focusing system for $^{238}U^{24+}$ beam with incident velocity 0.0070c.

Res. Type	Gap	Transverse		Longitudinal	
		$1/f_1(m^{-1})$	$1/f_2(m^{-1})$	$1/f_1(m^{-1})$	$1/f_2(m^{-1})$
I1	1	-5.994	-5.562	23.073	13.219
	2	1.373	1.218	-2.471	-1.831
	3	1.506	1.389	-2.841	-2.172
	4	-0.044	-0.041	0.449	0.353
I2-1	1	-2.911	-2.988	8.847	7.112
	2	-0.361	-0.340	0.912	0.782
	3	1.428	1.369	-2.776	-2.463
	4	1.999	1.948	-3.780	-3.588
I2-2	1	-0.722	-0.704	1.703	1.452
	2	-0.261	-0.252	0.620	0.546
	3	-0.185	-0.179	0.455	0.404
	4	-0.309	-0.301	0.753	0.672

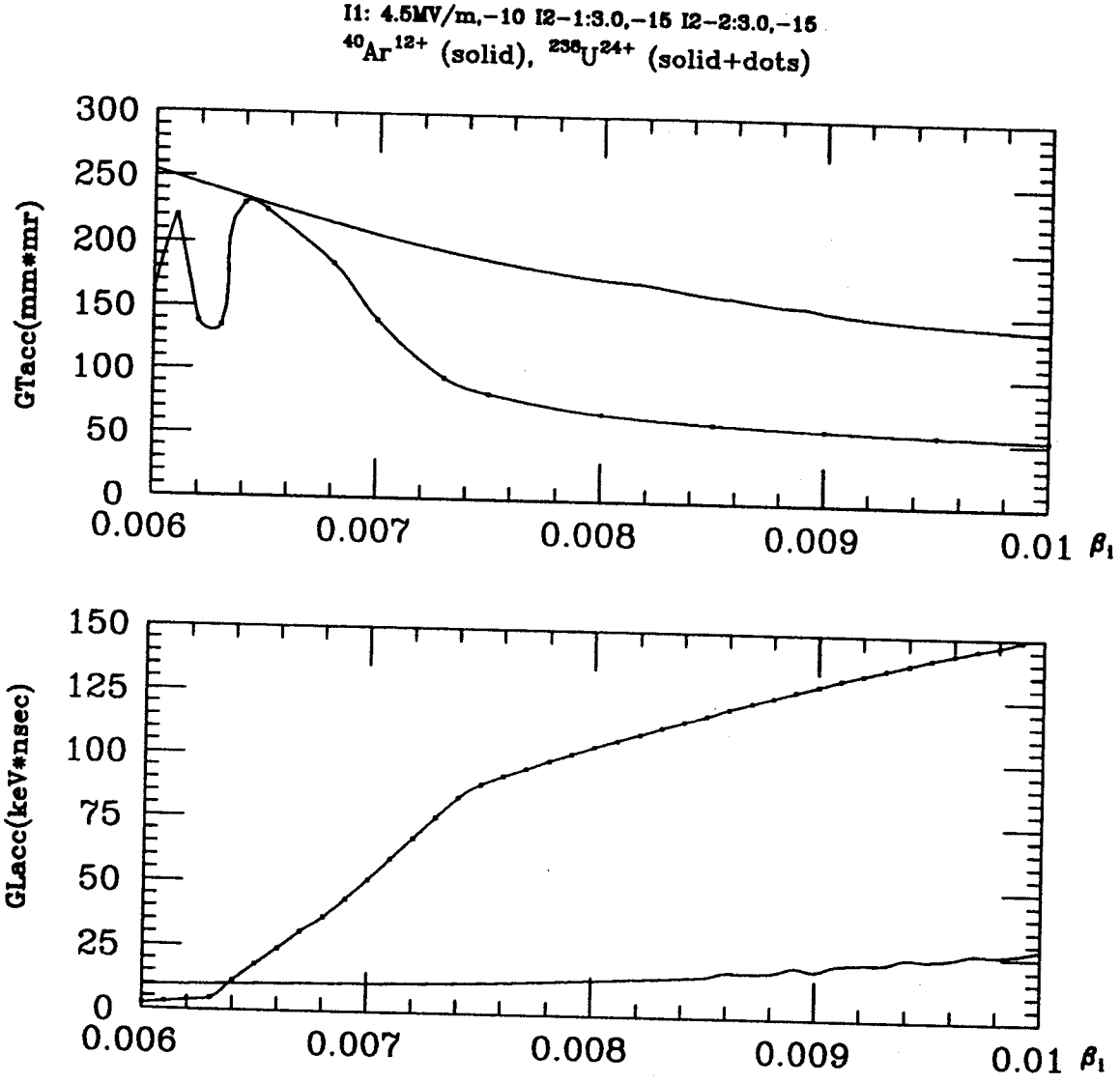

Figure 5.1: The geometrical transverse (upper) and longitudinal (lower) acceptances as a functions of incident velocities.

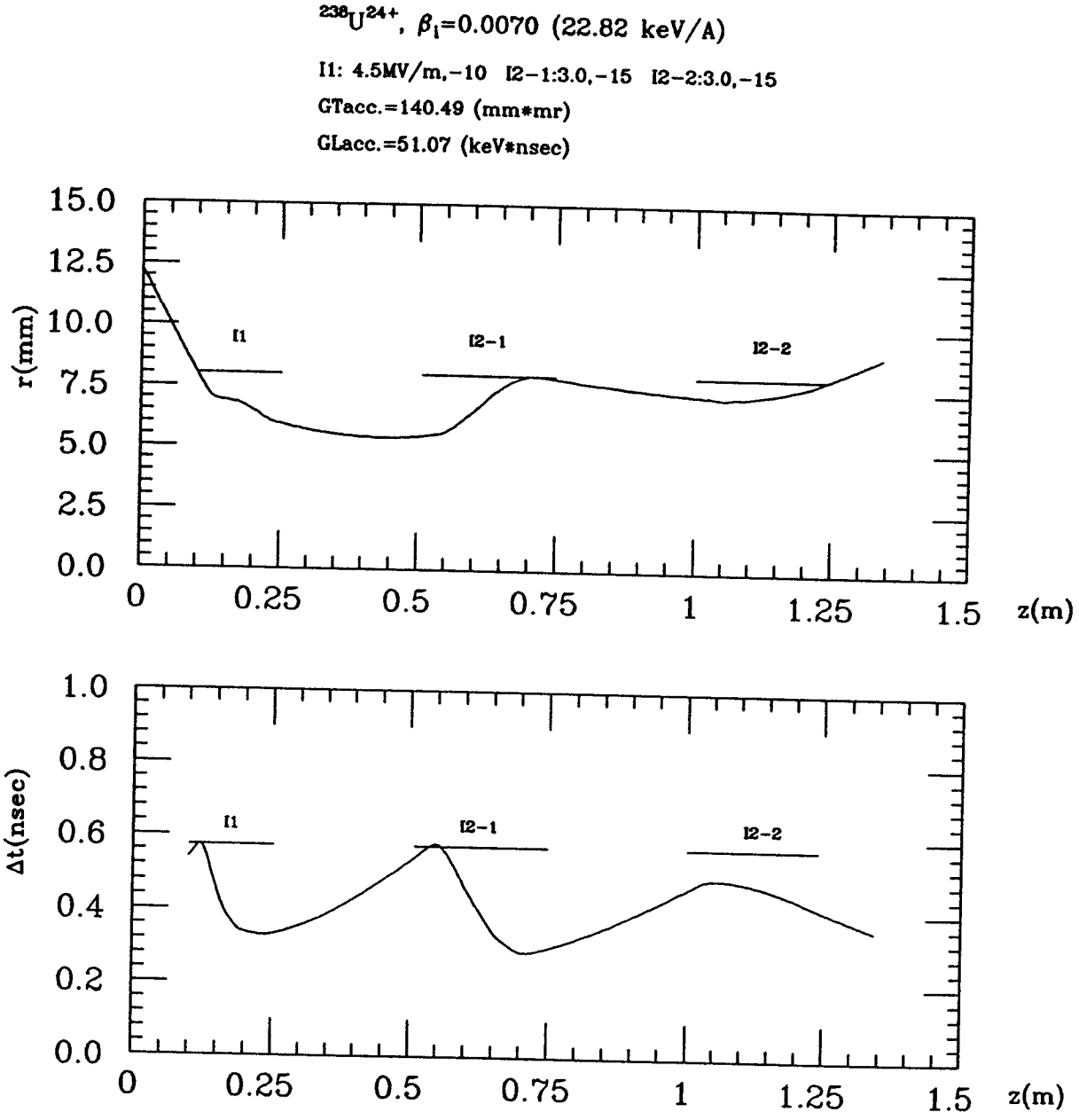

Figure 5.2: The beam envelopes of beam radius (upper) and deviation of time of flight (lower) starting from maximum emittance.

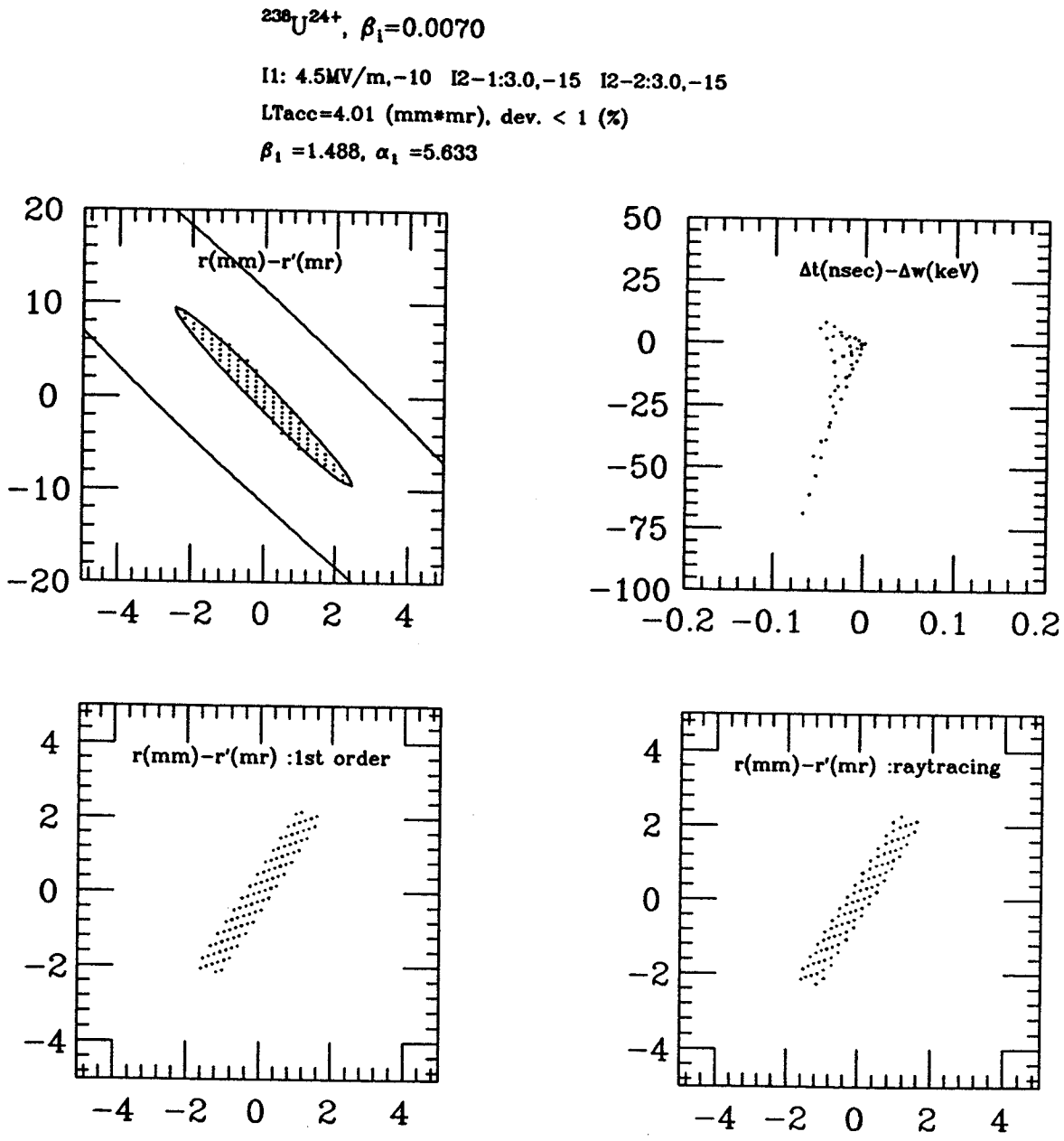

Figure 5.3: The phase space transformations of the transverse linear acceptance for a $^{238}U^{24+}$ beam with an incident velocity of 0.007c and with a deviation of 1%.

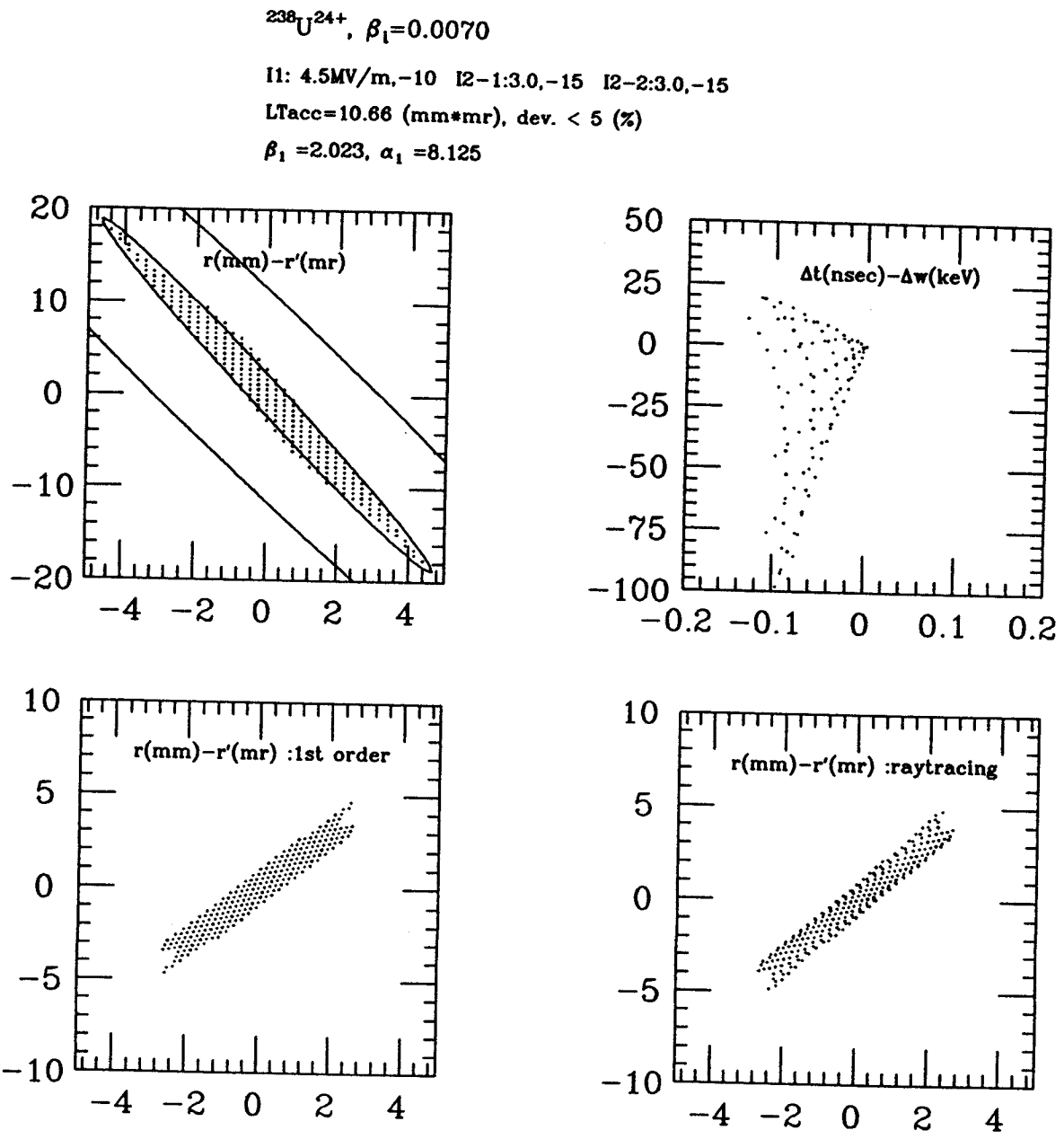

Figure 5.4: The phase space transformations of the transverse linear acceptance for a $^{238}U^{24+}$ beam with an incident velocity 0.007c with a deviation of 5%.

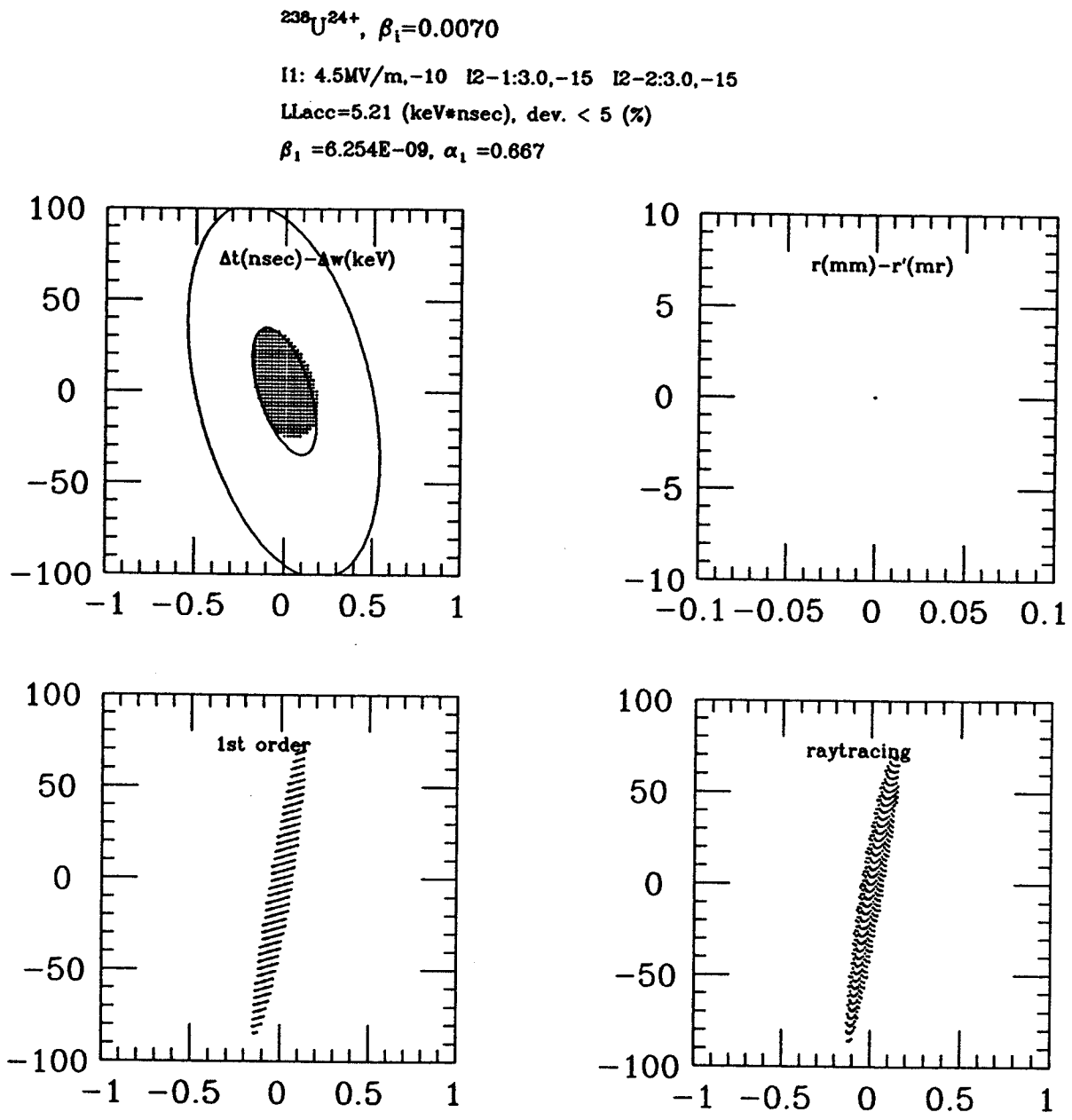

Figure 5.5: The phase space transformations of the longitudinal linear acceptance for a $^{238}U^{24+}$ beam with an incident velocity 0.007c.

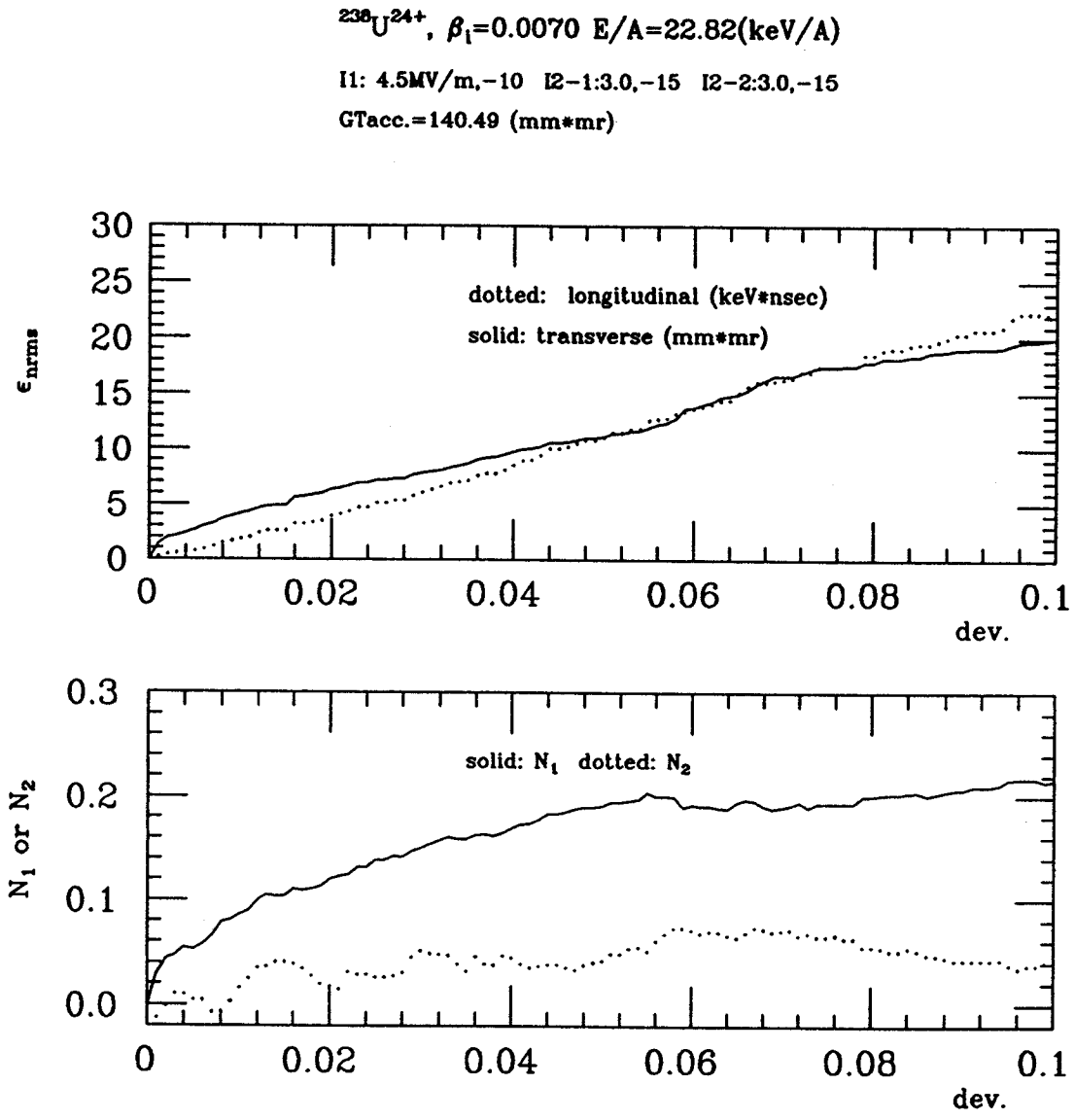

Figure 5.6: The relationship between scalings of nonlinearity by linear transformation and by rms emittance for a $^{238}U^{24+}$ beam with an incident velocity 0.007c. The initial geometrical transverse acceptance was 140.49 mm · mr without longitudinal phase space.

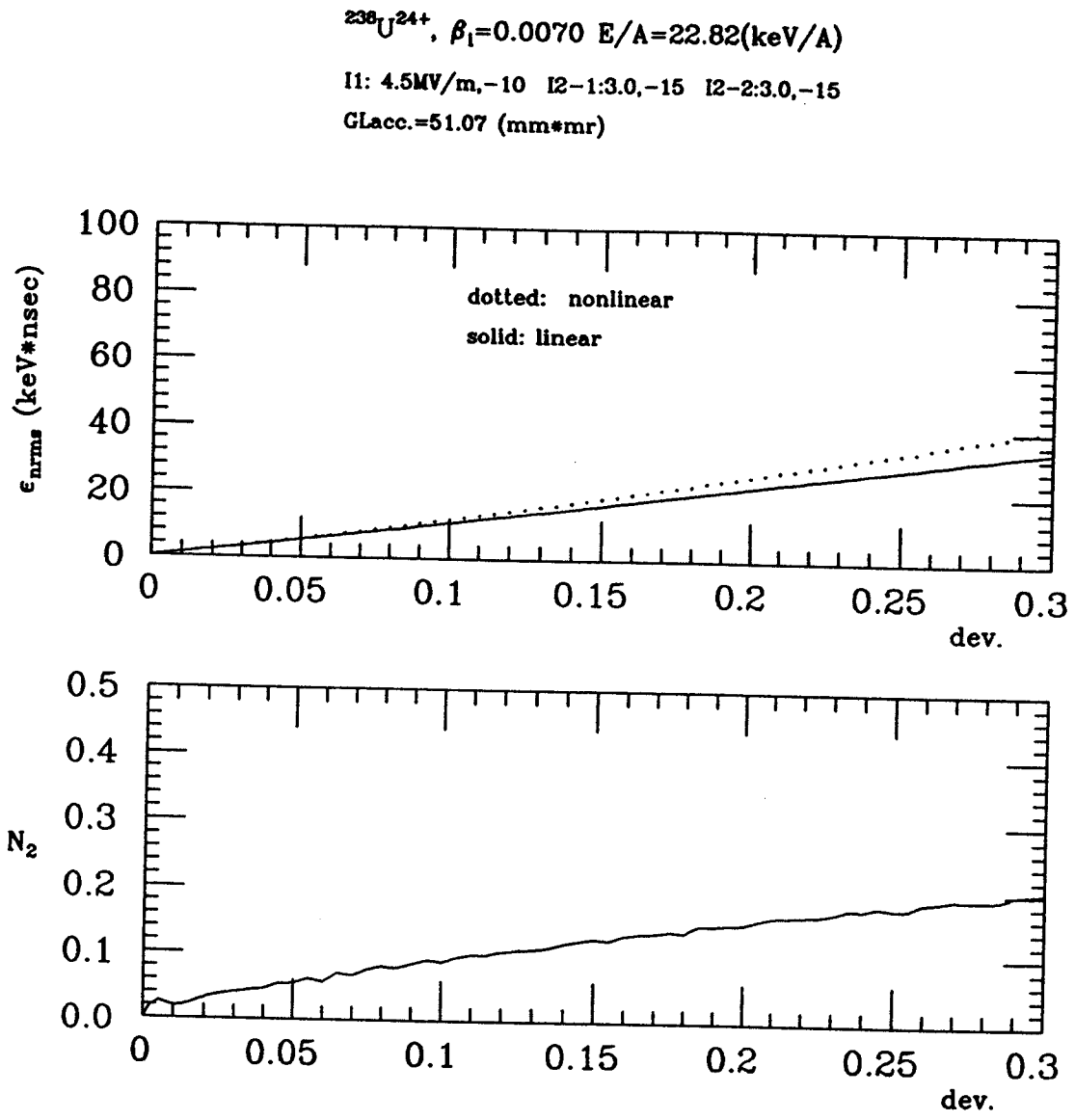

Figure 5.7: The relationship between scalings of nonlinearity by linear transformation and by rms emittance for a $^{238}U^{24+}$ beam with an incident velocity 0.007c. The initial geometrical longitudinal acceptance was 51.07 keV · nsec without transverse phase space.

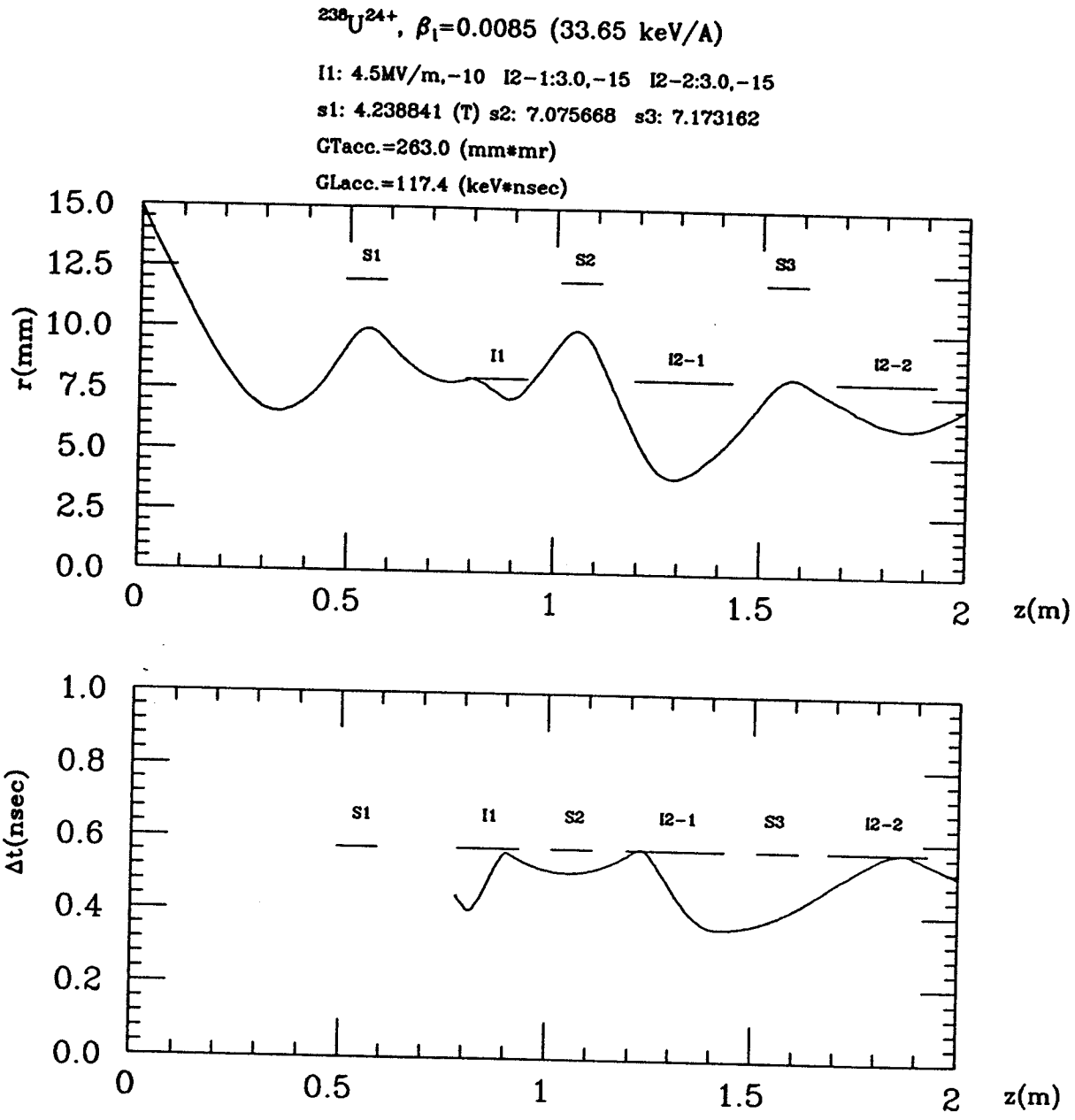

Figure 5.8: The beam envelopes of beam radius (upper) and deviation of time of flight (lower) starting with a maximum emittance in the system using solenoids for the transverse focusing. The incident velocity of the $^{238}U^{24+}$ beam was 0.0085c.

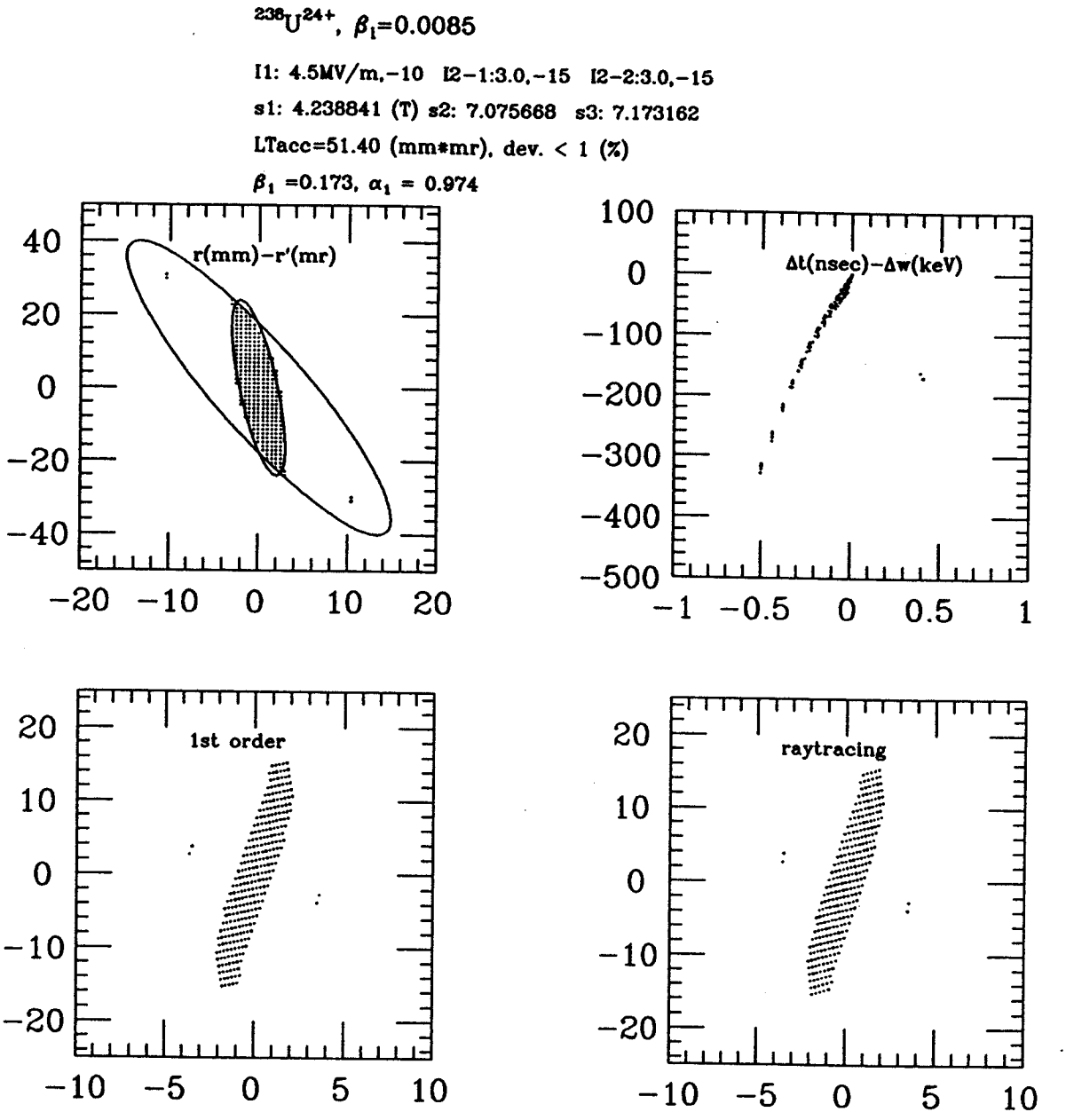

Figure 5.9: The phase space transformations of the transverse linear acceptance in the system using solenoids for the transverse focusing. The incident velocity of the $^{238}U^{24+}$ beam was 0.0085c.

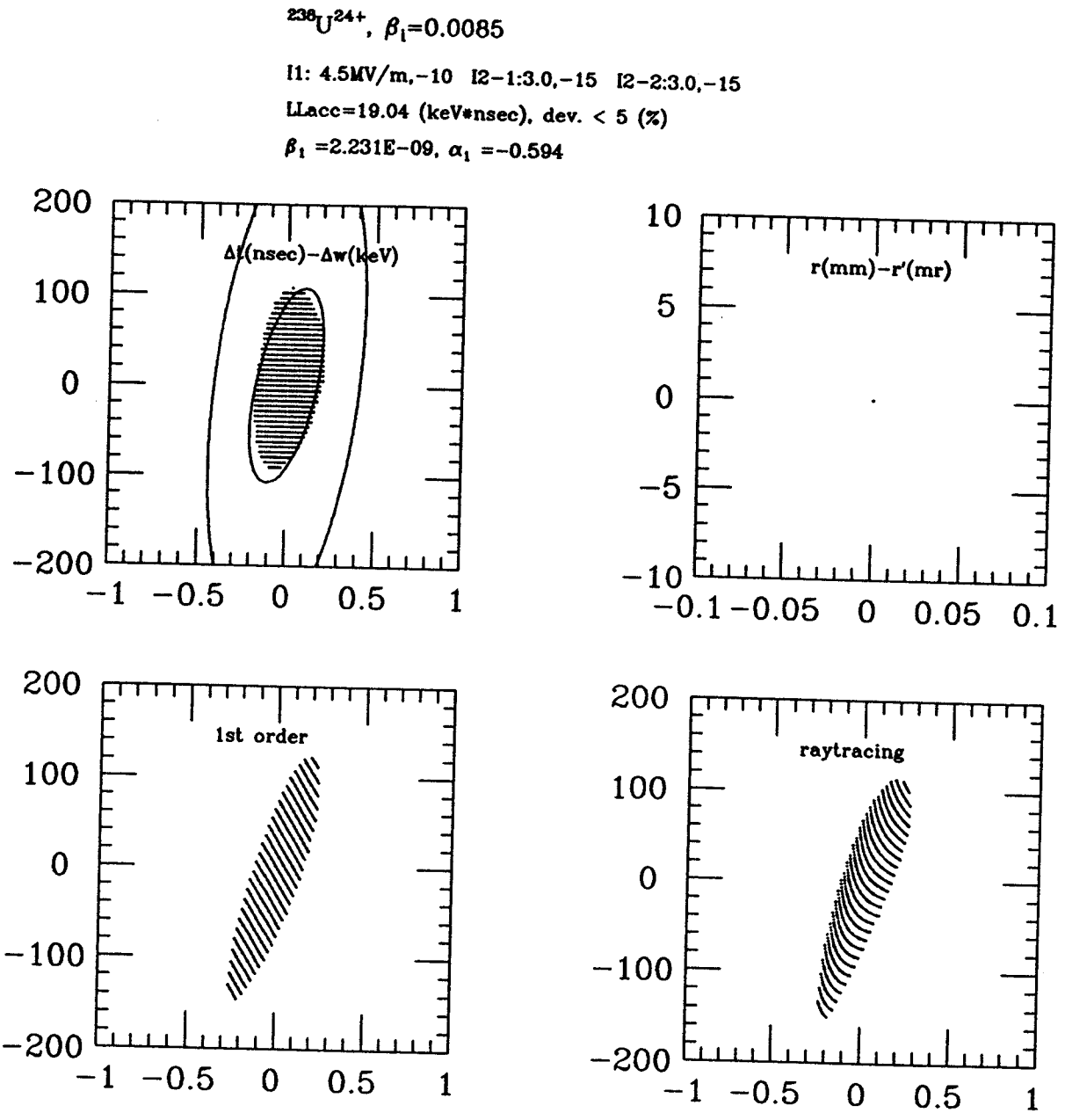

Figure 5.10: The phase space transformations of the longitudinal linear acceptance in the system using solenoids for the transverse focusing. The incident velocity of the $^{238}U^{24+}$ beam was 0.0085c.

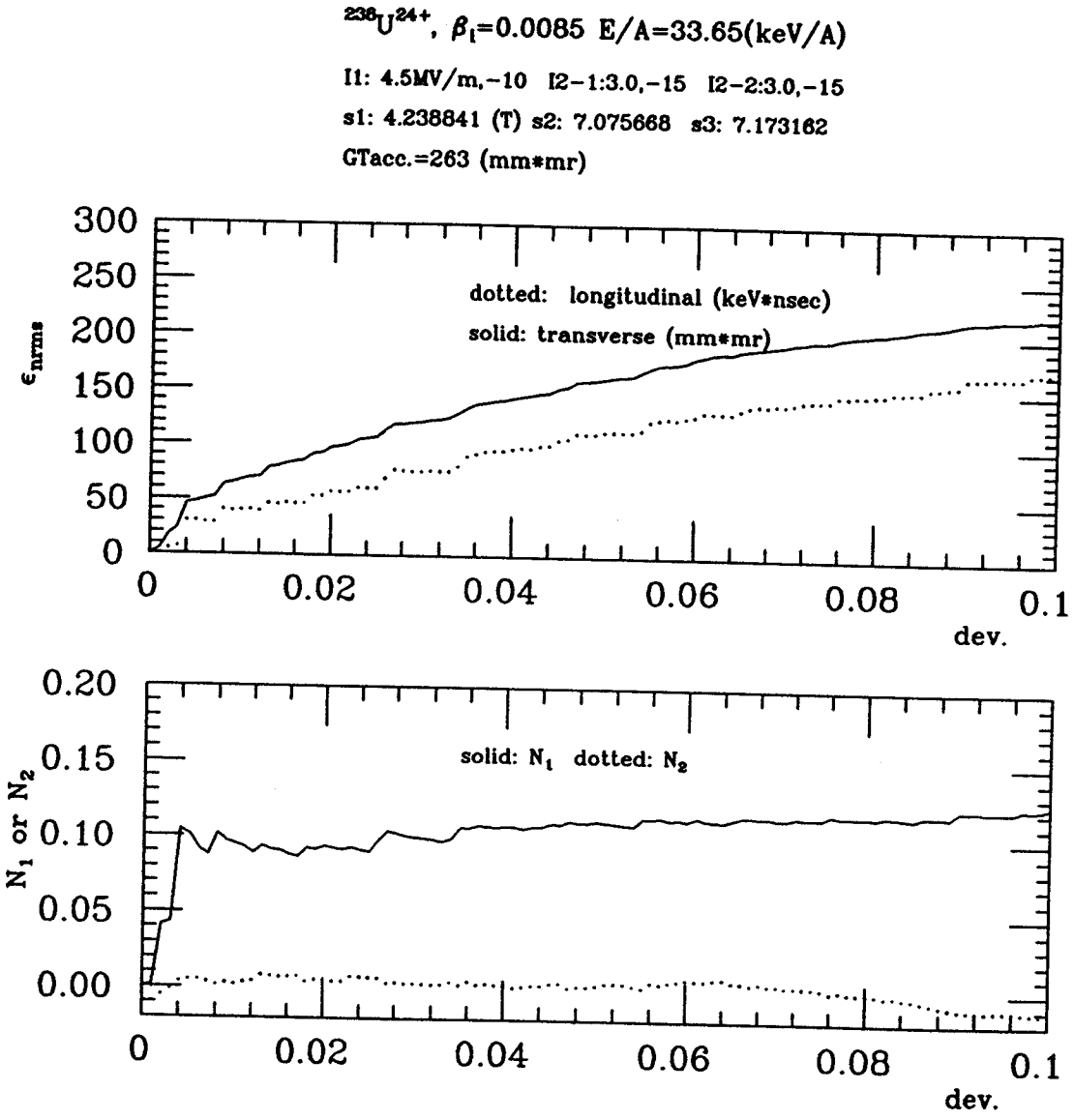

Figure 5.11: the relationship between scalings of nonlinearity by linear transformation and by rms emittance for a $^{238}U^{24+}$ beam with an incident velocity 0.0085c in the system using solenoids for transverse focusing. The initial geometrical transverse acceptance was 263 mm·mr without longitudinal phase space.

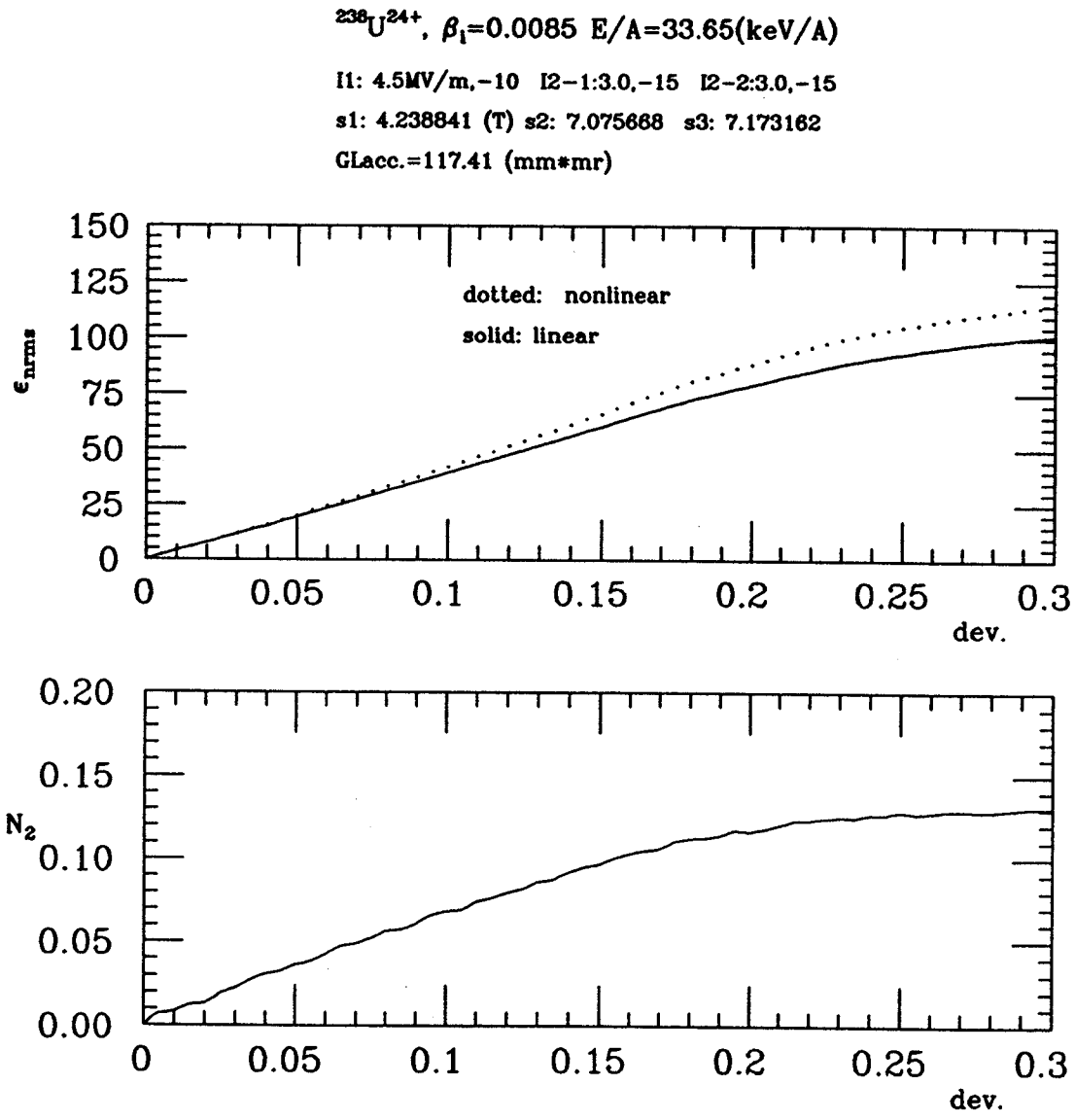

Figure 5.12: The relationship between scalings of nonlinearity by linear transformation and by rms emittance for a $^{238}U^{24+}$ beam with an incident velocity 0.0085c in the system using solenoids for transverse focusing. The initial geometrical longitudinal acceptance was 117.4 keV·nsec without transverse phase space.

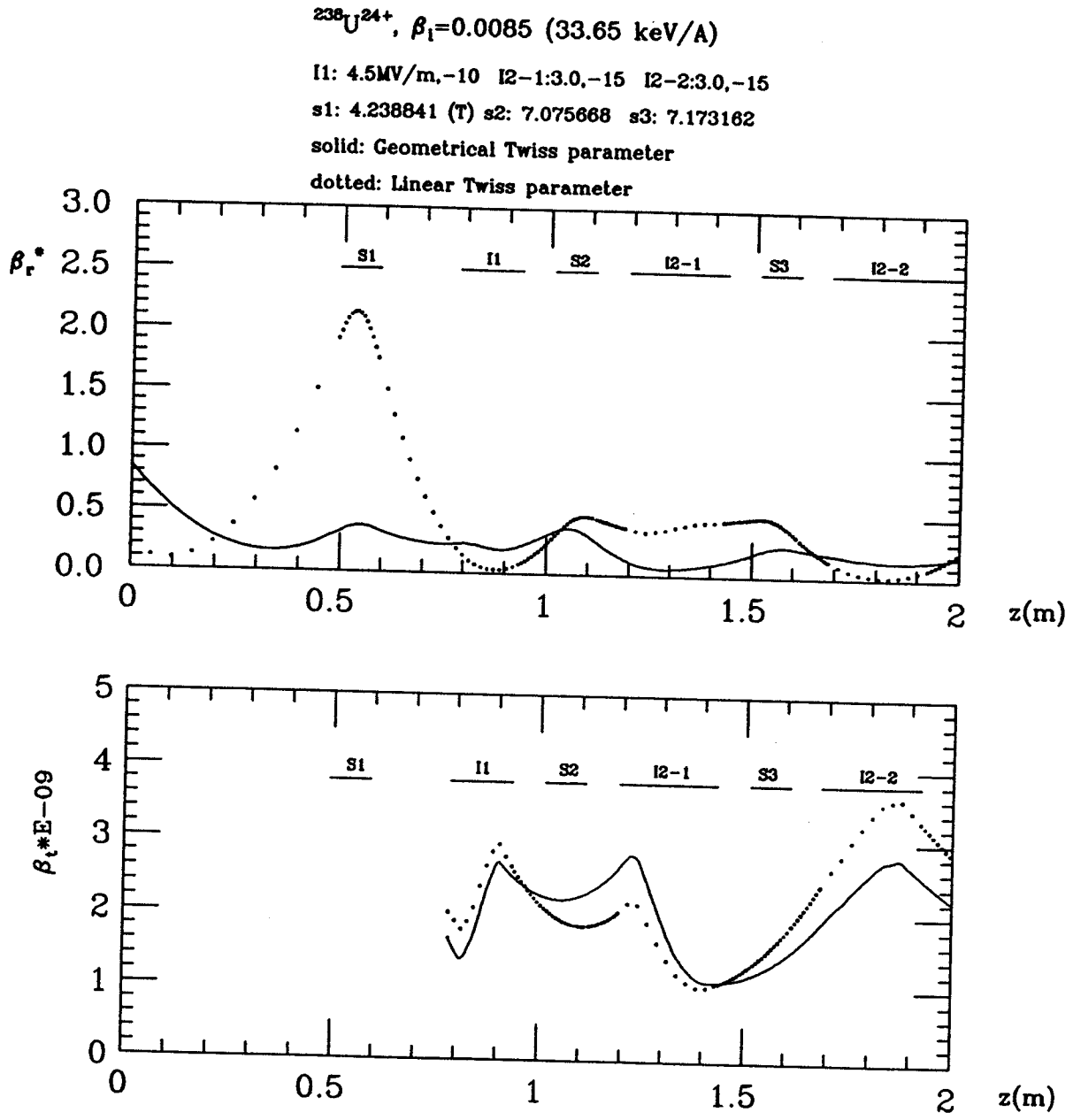

Figure 5.13: The effective beta-functions of the transverse (upper) and the longitudinal (lower) phase spaces for $^{238}U^{24+}$ beam with an incident velocity 0.0085c in the system using solenoids for the transverse focusing. The dotted lines are for Twiss parameters from the geometrical acceptances and the solid line is for Twiss parameters from the linear acceptances.

Chapter 6

Summary and Discussions

First order matrix optics has been applied to the system which includes very-low-beta heavy ion radio frequency resonators. In spite of its rather time consuming point-by-point calculations through each resonator to find its transfer matrix, it has been shown that the transfer map found can be used to investigate the focusing structures of multiple-gap resonators quantitatively. The calculations of focusing powers by using the transfer maps clearly showed the alternating-phase focusing properties of I1 and I2 type resonators of the PII linac. We expect that 1st order matrix optics will be used to design multiple-gap resonators for very low-beta rf resonators in the various sides. For an example, the distances between accelerating gaps might be optimized for required transverse and longitudinal focusing powers with appropriate optimization routines. Also the electric field gradients or incident velocities might be optimized for needed optical properties of each resonator.

The 1st order matrix theory has been extended independently to the phase space transformations under acceleration. By searching beam envelope functions it was possible to find the so called "geometrical acceptances". This, when used with non-linear calculations such as ideally higher order matrix optics programs or raytracing calculations, was used in finding "linear acceptances" with matched phase spaces.

The model solenoid [Berz 93] has been introduced through the calculations instead of existing superconducting solenoids with appropriate physical parameters to fit the real field profiles. The transverse optics of the model solenoids do not seem to be sources of significant nonlinearities even for relatively large size beam envelopes. We expect that this model solenoid will well approximate real solenoidal fields in computer calculations for the whole system of the PII linac with a little more investigation about transverse optics of the model and real solenoids. By using these model solenoids it will be possible to investigate in detail the nonlinear effect of the solenoids for the transverse direction. The nonlinear effect of the solenoids was not included in the code LINRAY [Pardo 89], which has been used for the ATLAS linac, because it has only linear radial focusing terms for resonators and solenoids.

The possibilities to use resonator focusings at the beginning part of the PII linac have been investigated. The stability limits of rf phase offsets and ranges of incident velocities for I1 and I2 type resonators to achieve transverse and longitudinal focusings simultaneously during the accelerations were calculated for two different beams of $^{40}Ar^{12+}$ and $^{238}U^{24+}$. It has been found that there is an intermediate velocity range in which transverse resonator focusing does not occur for $^{238}U^{24+}$: for this beam both lower and higher velocities do display transverse focusing.

The possibilities of using resonator focusing partially at the PII linac for very low velocity heavy ions might be contingent upon transverse beam emittances from the ECR source. There are no differences in longitudinal beam qualities between resonator focusing systems and focusing systems using transverse focusing elements like solenoids. The absolute values of transverse (geometrical) acceptances calculated in Chapter 5 might be enough to accept beam emittances from the ECR source. But, as expected, it turned out qualitatively that the resonators were major sources of nonlinearities which reduced linear acceptances significantly. As a result the resonator

focusing scheme is inferior to the existing system using superconducting solenoids as transverse focusing elements in terms of overall linear acceptance.

The other aspect to note is that lowering incident velocity to increase the transverse acceptances in the resonator focusing system causes decreasing of the longitudinal acceptances. Thus the initial velocity should be determined by a compromise between the transverse and the longitudinal emittances from the ion source.

We have also proposed a new method to match phase space ellipses by comparing linear and nonlinear transformations of individual particles. The consistency of this method was checked with the growth of rms emittances which measure the order or disorder of phase space distributions. We expect that this kind of analysis would be useful also in other beam transport systems.

Finally we would like to point out the effect of the higher order coupling of phase space coordinates in the rf resonators. The longitudinal phase space is newly created even if its initial area was zero because of coupling of the transverse coordinates due to nonlinear radial forces. This coupling effect also arises from the interactions between transverse and longitudinal coordinates. As a consequences of phase space couplings the new created or distorted longitudinal phase space distributions are asymmetric both in time and energy. Therefore this asymmetric distribution of longitudinal phase space should be considered in beam dynamic calculations to redefine the central ray or synchronous particle of a bunch at the end of each resonator. But this would not be a simple procedure because the asymmetric distribution of phase spaces is not be known until initial phase spaces are given. This effect is corrected automatically in actual tuning of the accelerating system by measuring the center of the energy and the rf phase angle for each resonator. This is one advantage of an accelerator which consists of a series of independently phased rf resonators.

Appendix A

Electromagnetic Fields in an RF Resonator

We derive the time dependent electromagnetic fields of a rf resonator which has axial symmetry, when the axial electric field on the resonator axis is known.

We assume that the rf resonator electric field components are written in cylindrical coordinates, (r, θ, z) by:

$$\begin{aligned} E_r(r,z,t) &= E_r(r,z)\cos(\omega t + \phi_0)\,, \\ E_\theta(r,z,t) &= 0\,, \\ E_z(r,z,t) &= E_z(r,z)\cos(\omega t + \phi_0)\,. \end{aligned} \tag{A.1}$$

where ω is angular frequency of rf field and ϕ_0 is initial rf phase angle.

We assume that the spatial part of the longitudinal rf field is expanded by Taylor series in terms of r:

$$E_z(r,z) = \sum_{k=0}^{\infty} \frac{1}{k!} \frac{\partial^k E_z(0,z)}{\partial r^k} r^k\,. \tag{A.2}$$

We first apply Gauss' law to the infinitely thin cylindrical pill box of radius r shown in Figure A.1. If there is no source of electric charge Gauss' law of $\mathrm{div}\vec{E} = 0$ leads to:

$$\int_0^r \{E_z(r', z+\Delta z) - E_z(r', z)\}\, 2\pi r' dr' + 2\pi r E_r(r,z)\Delta z = 0\,, \tag{A.3}$$

or

$$E_r(r,z) = -\frac{1}{r}\int_0^r \frac{\partial E_z(r',z)}{\partial z} r' dr' \ . \tag{A.4}$$

From equations (A.2) and (A.4) we find a radial component of rf electric field:

$$E_r(r,z) = \sum_{k=0}^{\infty} \frac{1}{k!(k+2)} \frac{\partial^{k+1} E_z(0,z)}{\partial z \partial r^k} r^{k+1} \ ,$$

$$E_r(r,z,t) = E_r(r,z)\cos(\omega t + \phi_0) \ . \tag{A.5}$$

Since the electric field is axially symmetric Faraday's law of $\mathrm{curl}\vec{E} = -\frac{\partial \vec{B}}{\partial t}$ becomes:

$$\frac{\partial E_z(r,z,t)}{\partial r} = \frac{\partial E_r(r,z,t)}{\partial z} + \frac{\partial B_\theta}{\partial t} \ , \tag{A.6}$$

in other words magnetic field has only one component in $\hat{\theta}$ direction.

Also Ampere's law of $\mathrm{curl}\vec{B} = \frac{1}{c^2}\frac{\partial \vec{E}}{\partial t}$ gives:

$$-\frac{\partial B_\theta}{\partial z} = \frac{\omega}{c^2} E_r(r,z)\sin(\omega t + \phi_0) \ , \tag{A.7}$$

where c is the speed of light in vacuum.

Thus from equations (A.5) and (A.7) we obtain rf magnetic field:

$$B_\theta(r,z) = \sum_{k=0}^{\infty} \frac{1}{k!(k+2)} \frac{\partial^k E_z(0,z)}{\partial r^k} r^{k+1} \ ,$$

$$B_\theta(r,z,t) = -(\frac{\omega}{c^2}) B_\theta(r,z)\sin(\omega t + \phi_0) \ . \tag{A.8}$$

From equations (A.5), (A.6), and (A.8) we get the rf longitudinal field:

$$E_z(r,z) = E_z(0,z) - \sum_{k=0}^{\infty} \frac{1}{k!(k+2)^2} \left\{ \frac{\partial^{k+2} E_z(0,z)}{\partial z^2 \partial r^k} + \frac{\omega^2}{c^2} \frac{\partial^k E_z(0,z)}{\partial r^k} \right\} r^{k+2} , \tag{A.9}$$

$$E_z(r,z,t) = E_z(r,z)\cos(\omega t + \phi_0) .$$

The partial derivative $\frac{\partial^n E_z(0,z)}{\partial r^n}$ in the above equation can be found iteratively in terms of the longitudinal component of rf electric field and its partial derivatives on axis:

$$\frac{\partial E_z(0,z)}{\partial r} = 0 ,$$

$$\frac{\partial^2 E_z(0,z)}{\partial r^2} = -\frac{2!}{2^2} \left[\frac{\partial^2 E_z(0,z)}{\partial z^2} + \frac{\omega^2}{c^2} E_z(0,z) \right] ,$$

$$\frac{\partial^3 E_z(0,z)}{\partial r^3} = 0 ,$$

$$\frac{\partial^4 E_z(0,z)}{\partial r^4} = \frac{4!}{2^2 \cdot 4^2} \left[\frac{\partial^2}{\partial z^2} \left(\frac{\partial^2 E_z(0,z)}{\partial r^2} \right) + \frac{\omega^2}{c^2} \frac{\partial^2 E_z(0,z)}{\partial r^2} \right]$$

$$= \frac{4!}{2^2 \cdot 4^2} \left[\frac{\partial^4 E_z(0,z)}{\partial z^4} + \frac{\omega^2}{c^2} \left(2\frac{\partial^2 E_z(0,z)}{\partial z^2} + \frac{\omega^2}{c^2} E_z(0,z) \right) \right] ,$$

$$\frac{\partial^5 E_z(0,z)}{\partial r^5} = 0 ,$$

$$\frac{\partial^6 E_z(0,z)}{\partial r^6} = \frac{6!}{2^2 \cdot 4^2 \cdot 6^2} \left[\frac{\partial^2}{\partial z^2} \left(\frac{\partial^4 E_z(0,z)}{\partial r^4} \right) + \frac{\omega^2}{c^2} \frac{\partial^4 E_z(0,z)}{\partial r^4} \right]$$

$$= \frac{6!}{2^2 \cdot 4^2 \cdot 6^2} \left[\frac{\partial^6 E_z(0,z)}{\partial z^6} + 3\left(\frac{\omega^2}{c^2} \right) \frac{\partial^4 E_z(0,z)}{\partial z^4} \right]$$

$$+ \quad \frac{6!}{2^2 \cdot 4^2 \cdot 6^2} \left[\frac{\omega^2}{c^2} \left(3 \frac{\omega^2}{c^2} \frac{\partial^2 E_z(0,z)}{\partial z^2} + \frac{\omega^4}{c^4} E_z(0,z) \right) \right]$$

$$\vdots \qquad\qquad\qquad\qquad \vdots$$

In the general expression:

$$\frac{\partial^{(2n+1)} E_z(0,z)}{\partial r^{(2n+1)}} = 0 \,,$$

$$\frac{\partial^{2(n+1)} E_z(0,z)}{\partial r^{2(n+1)}} = C'_{zn} \frac{\partial^{2(n+1)} E_z(0,z)}{\partial z^{2(n+1)}} + C'_{zn} \left(\frac{\omega^2}{c^2} \right)^{n+1} E_z(0,z)$$

$$+ \sum_{k=0}^{n-1>0} \left[C'_{zn}(n+1) \left(\frac{\omega^2}{c^2} \right)^{n-k} \frac{\partial^{2(k+1)} E_z(0,z)}{\partial z^{2(k+1)}} \right] , \qquad \text{(A.10)}$$

where

$$C'_{zn} = (-1)^{n+1} \frac{[2(n+1)]!}{2^2 \cdot 4^2 \cdot 6^2 \cdots [2(n+1)]^2} \,, \qquad \text{(A.11)}$$

$$(n = 0,\ 1,\ 2,\ 3,\ \cdots) \,.$$

Thus from equations (A.9) and (A.10) we obtain:

$$E_z(r,z) = \sum_{n=0}^{\infty} C_{zn} \left[\frac{\partial^{2n} E_z(0,z)}{\partial z^{2n}} \left(\frac{\omega^2}{c^2} \right)^n E_z(0,z) \right] r^{2n} +$$

$$\sum_{n=2}^{\infty} \sum_{k=0}^{n-2} \left[C_{zn}(n+1) \left(\frac{\omega^2}{c^2} \right)^{n-k-1} \frac{\partial^{2(k+1)} E_z(0,z)}{\partial z^{2(k+1)}} \right] r^{2n} \,, \qquad \text{(A.12)}$$

$$E_z(r,z,t) = E_z(r,z) \cos(\omega t + \phi_0) \,.$$

where

$$C_{zn} = (-1)^n \frac{1}{[2 \cdot 4 \cdot 6 \cdot \cdots \cdot (2n)]^2} = (-1)^n \frac{1}{2^{2n}(n!)^2} . \qquad \text{(A.13)}$$

From equations (A.5) and (A.13):

$$E_r(r,z) = \sum_{n=0}^{\infty} C_{rn} \left[\frac{\partial^{2n+1} E_z(0,z)}{\partial z^{2n+1}} \left(\frac{\omega^2}{c^2} \right)^n \frac{\partial E_z(0,z)}{\partial z} \right] r^{2n+1} +$$

$$\sum_{n=2}^{\infty} \sum_{k=0}^{n-2} \left[C_{rn}(n+1) \left(\frac{\omega^2}{c^2} \right)^{n-k-1} \frac{\partial^{2(k+1)+1} E_z(0,z)}{\partial z^{2(k+1)+1}} \right] r^{2n+1} ,$$

$$E_r(r,z,t) = E_r(r,z) \cos(\omega t + \phi_0) , \qquad \text{(A.14)}$$

where

$$C_{rn} = (-1)^{n+1} \frac{1}{2^{2n+1}(n+1)(n!)^2} . \qquad \text{(A.15)}$$

Also from equations (A.8) and (A.13) :

$$B_\theta(r,z) = \sum_{n=0}^{\infty} C_{rn} \left[\frac{\partial^{2n} E_z(0,z)}{\partial z^{2n}} \left(\frac{\omega^2}{c^2} \right)^n \frac{\partial E_z(0,z)}{\partial z} \right] r^{2n} +$$

$$\sum_{n=2}^{\infty} C_{rn} \sum_{k=0}^{n-2} \left[(n+1) \left(\frac{\omega^2}{c^2} \right)^{n-k-1} \frac{\partial^{2(k+1)} E_z(0,z)}{\partial z^{2(k+1)}} \right] r^{2n+1} , \qquad \text{(A.16)}$$

$$B_\theta(r,z,t) = -(\frac{\omega}{c^2}) B_\theta(r,z) \sin(\omega t + \phi_0) .$$

Note that the terms related to ω are the result of a time dependent rf electric field.

Summary

The time dependent electric and magnetic fields have been derived for a cylindrically symmetric system in general form when the rf electric field on axis is known. If we take just terms up to 3rd order in equations (A.13) - (A.15) we get:

$$\begin{aligned} E_r(r,z,t) &= E_r(r,z)\cos(\omega t+\phi_0)\,, \\ E_\theta(r,z,t) &= 0\,, \\ E_z(r,z,t) &= E_z(r,z)\cos(\omega t+\phi_0)\,, \qquad \text{(A.17)} \\ B_r(r,z,t) &= 0\,, \\ B_\theta(r,z,t) &= -\frac{\omega}{c^2}B_\theta(r,z)\sin(\omega t+\phi_0)\,, \\ B_z(r,z,t) &= 0\,, \qquad \text{(A.18)} \end{aligned}$$

where

$$\begin{aligned} E_r(r,z) &= -\frac{1}{2}\frac{\partial E_z(0,z)}{\partial z}r+\frac{1}{16}\left\{\frac{\omega^2}{c^2}\frac{\partial E_z(0,z)}{\partial z}+\frac{\partial^3 E_z(0,z)}{\partial z^3}\right\}r^3\,, \\ E_z(r,z) &= E_z(0,z)-\frac{1}{4}\left\{\frac{\omega^2}{c^2}E_z(0,z)+\frac{\partial^2 E_z(0,z)}{\partial z^2}\right\}r^2\,, \qquad \text{(A.19)} \\ B_\theta(r,z) &= \frac{1}{2}E_z(0,z)r-\frac{1}{16}\left\{\frac{\omega^2}{c^2}E_z(0,z)+\frac{\partial^3 E_z(0,z)}{\partial z^3}\right\}r^3\,. \qquad \text{(A.20)} \end{aligned}$$

In rectangular coordinates:

$$\begin{aligned} E_x(r,z,t) &= E_x(r,z)\cos(\omega t+\phi_0)\,, \\ E_y(r,z,t) &= E_y(r,z)\cos(\omega t+\phi_0)\,, \\ E_z(r,z,t) &= E_z(r,z)\cos(\omega t+\phi_0)\,, \qquad \text{(A.21)} \\ B_x(r,z,t) &= -\frac{\omega}{c^2}B_\theta(r,z)\sin(\omega t+\phi_0)\,, \end{aligned}$$

$$
\begin{aligned}
B_y(r,z,t) &= -\frac{\omega}{c^2} B_\theta(r,z)\sin(\omega t+\phi_0)\,, \\
B_z(r,z,t) &= 0\,, \qquad\qquad (A.22)
\end{aligned}
$$

where

$$
\begin{aligned}
E_x(r,z) &= -\frac{1}{2}\frac{\partial E_z(0,z)}{\partial z}x + \frac{1}{16}\left\{\frac{\omega^2}{c^2}\frac{\partial E_z(0,z)}{\partial z} + \frac{\partial^3 E_z(0,z)}{\partial z^3}\right\}(x^2+y^2)x\,, \\
E_y(r,z) &= -\frac{1}{2}\frac{\partial E_z(0,z)}{\partial z}y + \frac{1}{16}\left\{\frac{\omega^2}{c^2}\frac{\partial E_z(0,z)}{\partial z} + \frac{\partial^3 E_z(0,z)}{\partial z^3}\right\}(x^2+y^2)y\,, \\
E_z(r,z) &= E_z(0,z) - \frac{1}{4}\left\{\frac{\omega^2}{c^2}E_z(0,z) + \frac{\partial^2 E_z(0,z)}{\partial z^2}\right\}(x^2+y^2)\,, \qquad (A.23) \\
B_x(r,z) &= \frac{1}{2}E_z(0,z)x - \frac{1}{16}\left\{\frac{\omega^2}{c^2}E_z(0,z) + \frac{\partial^3 E_z(0,z)}{\partial z^3}\right\}(x^2+y^2)x\,, \\
B_y(r,z) &= \frac{1}{2}E_z(0,z)y - \frac{1}{16}\left\{\frac{\omega^2}{c^2}E_z(0,z) + \frac{\partial^3 E_z(0,z)}{\partial z^3}\right\}(x^2+y^2)y\,. \qquad (A.24)
\end{aligned}
$$

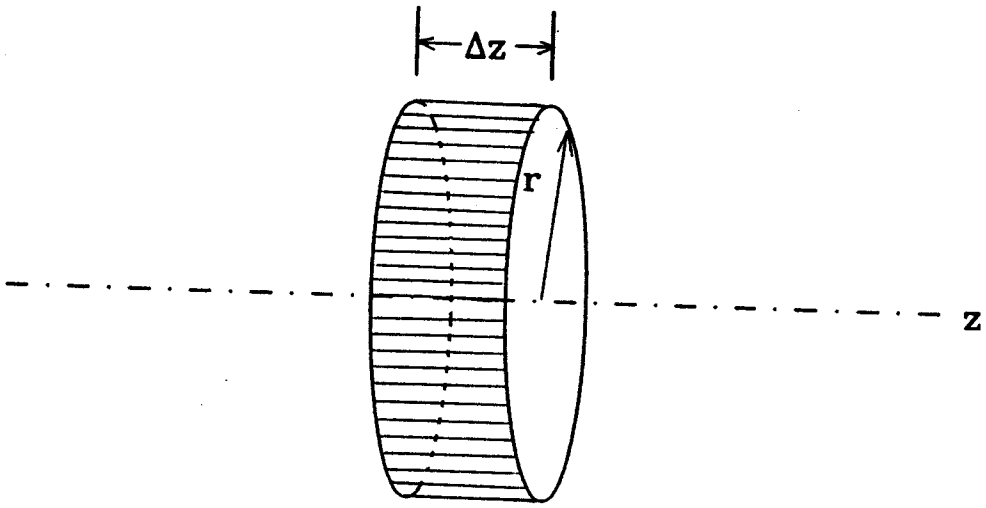

Figure A.1: Cylindrical pill box.

Appendix B

The System in a Cylindrically Symmetric Magnetic Field

B.1 Magnetic Field in Magnetic Solenoid

We expand the off axial field of a static magnetic solenoid which has axial symmetry, when the axial magnetic field on axis is known.

The relation between the magnetic field $\vec{B}$ and magnetic vector potential $\vec{A}$ is given by:

$$\vec{B} = \text{curl } \vec{A} \,. \tag{B.1}$$

In component form:

$$\begin{aligned} B_r &= \left\{ \frac{\partial A_z}{\partial \theta} - \frac{\partial (r A_\theta)}{\partial z} \right\} \frac{1}{r} \,, \\ B_\theta &= \frac{\partial A_r}{\partial z} - \frac{\partial A_z}{\partial r} \,, \\ B_z &= \left\{ \frac{(\partial (r A_\theta)}{\partial r} - \frac{\partial A_r}{\partial \theta} \right\} \frac{1}{r} \,. \end{aligned} \tag{B.2}$$

Since the vector potential is dependent on only the angle θ in an axially symmetric

system equation (B.2) becomes:

$$\begin{aligned} B_r &= -\frac{\partial(rA_\theta)}{\partial z}\frac{1}{r}\,, \\ B_\theta &= 0\,, \\ B_z &= \frac{\partial A_r}{\partial \theta}\frac{1}{r}\,. \end{aligned} \tag{B.3}$$

It is well known that the rotationally symmetric magnetic vector potential can be expanded by the following power series [Forest 84], [Jiye 86]:

$$A_\theta = A(z,r) = \sum_{k=0}^{\infty}(-1)^k \frac{1}{k!(k+1)!}\left(\frac{r}{2}\right)^{2k+1}\frac{\partial^{2k}B_z(0,z)}{\partial z^{2k}}, \tag{B.4}$$

$$(\ k\ =\ 0,\ 1,\ 2,\ \cdots\ )\,.$$

Thus from equations (B.3) and (B.4) we find the magnetic field expansion in terms of the magnetic field on axes and its derivatives. Up to the 3rd order of r:

$$\begin{aligned} B_r(r,z) &= -\frac{1}{2}\frac{\partial B_z(0,z)}{\partial z}r + \frac{1}{16}\frac{\partial^3 B_z(0,z)}{\partial z^3}r^3\,, \\ B_\theta(r,z) &= 0\,, \\ B_z(r,z) &= B_z(0,z) - \frac{1}{4}\frac{\partial^2 B_z(0,z)}{\partial z^2}r^2\,. \end{aligned} \tag{B.5}$$

In rectangular coordinates:

$$B_x(r,z) = -\frac{1}{2}\frac{\partial B_z(0,z)}{\partial z}y + \frac{1}{16}\frac{\partial^3 B_z(0,z)}{\partial z^3}(x^2+y^2)y\,,$$

$$B_y(r,z) = -\frac{1}{2}\frac{\partial B_z(0,z)}{\partial z}x + \frac{1}{16}\frac{\partial^3 B_z(0,z)}{\partial z^3}(x^2+y^2)x\,, \tag{B.6}$$

$$B_z(r,z) = B_z(0,z) - \frac{1}{4}\frac{\partial^2 B_z(0,z)}{\partial z^2}(x^2+y^2)\,.$$

B.2 Angular momentum conservation

The Lagrangian function of a particle of electric charge q and rest mass m in static magnetic field [Jackson 75] is given by in cylindrical coordinates:

$$\begin{aligned} L &= -mc^2\sqrt{1-\frac{V^2}{c^2}} + q\vec{V}\cdot\vec{A} \\ &= -mc^2\sqrt{1-\left(\dot{r}^2+r^2\dot{\theta}^2+\dot{z}^2\right)^{-1}} + qr\dot{\theta}A_\theta\,, \end{aligned} \tag{B.7}$$

where $\vec{V}$ is velocity of a particle.

From the Lagrangian function the equations of motion are given by:

$$\frac{d}{dt}\left(\frac{\partial L}{\partial \dot{q}_j}\right) = \frac{\partial L}{\partial q_j}\,, \quad (j = r,\theta,z)\,. \tag{B.8}$$

Since θ is cyclic in the Lagrangian function, from equation (B.8) the canonical momentum P_θ is a constant of the motion [Goldstein 59]:

$$P_\theta = \frac{\partial L}{\partial \dot{\theta}} = \frac{mr^2\dot{\theta}}{\sqrt{1-\frac{v^2}{c^2}}} + qrA_\theta\,. \tag{B.9}$$

i.e. angular momentum is conserved in static magnetic field.

B.3 Rotation of a Particle in Magnetic Field

The rotation angle of a particle under a magnetic field can be found from equation (B.9):

$$\dot{\theta} = \frac{d\theta}{dz}\dot{z} = -\frac{q}{m}\sqrt{1-\beta^2}\frac{A_\theta}{r} . \tag{B.10}$$

Thus integrating the above equation with respect to the axial distance we obtain:

$$\theta(z) = -(\frac{q}{m})\sqrt{1-\beta^2}\int \frac{A_\theta}{r}\left\{(c\beta)^2 - \dot{r}^2 - (r\dot{\theta}^2)\right\}^{-1/2} dz . \tag{B.11}$$

If we neglect $\dot{r}^2$ and $(r\dot{\theta})^2$ terms in the bracket and take the first term of A_θ in equation (B.4), then we get the rotation angle along the optic axis:

$$\theta(z) = -\left(\frac{q}{m}\right)\frac{\sqrt{1-\beta^2}}{2c\beta}\int_z B_z(0,z)dz . \tag{B.12}$$

B.4 Decoupling of Equations of Motion

The linear differential equations of motion for a magnetic solenoid in section 3.3.3 of Chapter 3 are coupled in rectangular coordinates. For the x-direction:

$$\frac{d^2x}{dz^2} - \alpha\left\{\frac{dy}{dz}B_z(0,z) + \frac{1}{2}\frac{\partial B_z(0,z)}{\partial z}y\right\} = 0 , \tag{B.13}$$

where

$$\alpha \equiv \frac{q\sqrt{1-\beta_s^2}}{mc\beta_s} . \tag{B.14}$$

To decouple equation(B.13) we introduce a rotated coordinate system (X, Y, z), which is rotated by an angle $\theta(z)$ with respect to the fixed coordinate system (x, y, z) by:

$$\begin{aligned} X &= x\cos\theta + y\sin\theta , \\ Y &= -x\sin\theta + y\cos\theta . \end{aligned} \tag{B.15}$$

Thus from equations (B.13) and (B.15) we find:

$$\begin{aligned} &\left\{\frac{d^2X}{dz^2}\cos\theta - \frac{d^2Y}{dz^2}\sin\theta\right\} - \left\{\frac{dX}{dz}\sin\theta + \frac{dY}{dz}\cos\theta\right\}\frac{d\theta}{dz} - \\ &\left\{\frac{dX}{dz}\sin\theta + X\frac{d\theta}{dz}\cos\theta + \frac{dY}{dz}\cos\theta - Y\frac{d\theta}{dz}\sin\theta\right\}\bullet \\ &\left\{\alpha B_z(0,z) + \frac{d\theta}{dz}\right\} - \left\{\frac{1}{2}\alpha\frac{\partial B_z(0,z)}{\partial z} + \frac{d^2\theta}{dz^2}\right\} y = 0 . \end{aligned} \tag{B.16}$$

Also from equation (B.12):

$$\begin{aligned} \frac{d\theta}{dz} &= -\frac{\alpha}{2}B_z(0,z) , \\ \frac{d^2\theta}{dz^2} &= -\frac{\alpha}{2}\frac{\partial B_z(0,z)}{\partial z} . \end{aligned} \tag{B.17}$$

Therefore from equations (B.16) and (B.17) we obtain:

$$\left\{\frac{d^2X}{dz^2} + \left(\frac{\alpha B_z(0,z)}{2}\right)^2 X\right\}\cos\theta - \left\{\frac{d^2Y}{dz^2} + \left(\frac{\alpha B_z(0,z)}{2}\right)^2 Y\right\}\sin\theta = 0 . \tag{B.18}$$

Since $cos\theta$ and $\sin\theta$ are independent each other it follows that:

$$\frac{d^2X}{dz^2} + \left(\frac{\alpha B_z(0,z)}{2}\right)^2 X = 0$$

$$\frac{d^2Y}{dz^2} + \left(\frac{\alpha B_z(0,z)}{2}\right)^2 Y = 0\,. \qquad \text{(B.19)}$$

In other words equation (B.13) is decoupled in rotated coordinates system. The equation of motion in the $y-$ direction is also decoupled by the same way.

B.5 Rotation of Transfer Map

Since the motions under magnetic field are coupled in a fixed coordinate system the first order transfer map of such a magnetic element is found in the rotated coordinates system to decouple the motions. To find the transfer map at the fixed system the transfer map is rotated inversely relative to the rotated coordinates system.

In this section we find the rotation matrix to get a transfer map in the rotated coordinate system by an angle θ counterclockwise about the z-axis. (x, y, z), (X, Y, z) are the fixed and the rotated coordinate systems respectively.

The position vector in the rotated system is related to the fixed system by:

$$X = \cos\theta x - \sin\theta y\,,$$

$$Y = \cos\theta x + \sin\theta y\,. \qquad \text{(B.20)}$$

The corresponding momentum vector (x', y') transforms by the same way as the position vector (x, y):

$$X' = \cos\theta x' - \sin\theta y'\,,$$

$$Y' = \cos\theta x' + \sin\theta y' \,. \tag{B.21}$$

Therefore from the above two equations we get a rotation map $R(\theta)$:

$$R(\theta) = \begin{pmatrix} \cos\theta & 0 & -\sin\theta & 0 \\ 0 & \cos\theta & 0 & -\sin\theta \\ \sin\theta & 0 & \cos\theta & 0 \\ 0 & \sin\theta & 0 & \cos\theta \end{pmatrix} . \tag{B.22}$$

If we apply the rotation matrix to a transfer map in a fixed coordinate system, we find the transfer map in the rotated coordinate system.

Appendix C

Calculation of Fringe Field

C.1 Length of Fringe Field Tail

The limit of the solenoidal field can be calculated directly from the model axial field equation rewritten by:

$$B(z) = \frac{B_0}{2}\left\{\tanh(\frac{z+l/2}{d}) - \tanh(\frac{z-l/2}{d})\right\} . \qquad \text{(C.1)}$$

The maximum strength of field is:

$$B_m = B_0 \tanh(\frac{l}{2d}) . \qquad \text{(C.2)}$$

In terms of an exponential function equation (C.1) becomes:

$$\frac{2B(z)}{B_0} = \frac{z^2-1}{z^2+1} - \frac{z^2-a^2}{z^2+a^2} , \qquad \text{(C.3)}$$

where

$$z = e^{z/d}, \quad a = e^{l/d} . \qquad \text{(C.4)}$$

Let R be the ratio of the maximum field strength B_m to the field strength at the distance of $z = z^\star$:

$$R = \frac{B_{z^\star}}{B_m} . \tag{C.5}$$

Then from equations (C.2) and (C.3) we obtain:

$$z^{\star^4} + \left\{ a^2(1 - \frac{2}{R\tilde{B}}) + 1 \right\} z^{\star^2} + a^2(1 - \frac{2}{R\tilde{B}}) = 0 , \tag{C.6}$$

where

$$\tilde{B} = \tanh(\frac{l}{2d}) . \tag{C.7}$$

Equation (C.6) is easily solved to get the half width of the full range of the solenoidal fields at a specific ratio R:

$$z^\star = \frac{d}{2} \ln \left\{ a^2(\frac{2}{R\tilde{B}} - 1) \right\} . \tag{C.8}$$

C.2 Transfer Map of a Solenoid

Since a solenoidal field has a long tail the total transfer map of a solenoid includes a pretty long drift space besides its physical length. So it would be convenient to filter the drift space out to have a transfer map independent of the length of the fringe field tails.

Let M be the total transfer map of a solenoid. The map is then decomposed into a map of a right tail field M_r, a map of a body field M_b, and a map of a left tail of a solenoidal field M_l:

$$M = M_r M_b M_l . \tag{C.9}$$

We also decompose the transfer map of a tail field into a map of the drift space corresponding to the length of the tail and a map of the fringe field including only a field effect of a tail:

$$M_l = M_{fl} M(d) \ ,$$
$$M_r = M(d) M_{fr} \ , \tag{C.10}$$

where $M(d)$ is a drift map of length d.

Thus from equation (C.10) we find the fringe field maps:

$$M_{fl} = M_l M(-d) \ ,$$
$$M_{fr} = M(-d) M_r \ , \tag{C.11}$$

in other words, fringe fields map are obtained by multiplying the negative drift map to the map of the fringe field tails.

Also from equations (C.9) and (C.11) we obtain the transfer of a solenoid independent of the drift spaces of tails:

$$M_s = M_{fr} M_b M_{fl} \ . \tag{C.12}$$

Bibliography

[Ben-Zvi 79] I. Ben-Zvi and Z. Segalov, *Particle Accelerators*, Vol. 10, (1979) 31.

[Ben-Zvi 88] I. Ben-Zvi, *Particle Accelerators* ,Vol. 23, (1988) 265.

[Berz 92] Martin Berz, NSCL, Michigan State University, *Linear Beam Theory*, Lecture note for "Introduction to Accelerator Physics (PHY987)", (1992).

[Berz 93] Martin Berz, NSCL, Michigan State University, *COSY INFINITY* (Version 6), an arbitrary order general purpose optics code, (1993).

[Billen 75] J.H. Billen, *Rev. Sci. Instrum.*, Vol.46, No. 1, (1975) 33.

[Bollinger 78] L. M. Bollinger et al., Argonne National Laboratory, *A Proposal for a Precision Heavy Ion Linac Accelerator*, (1978).

[Bollinger 92] L. M. Bollinger et al., *First Operational Experience with the Positive-Ion Injector of ATLAS*, ANL internal report (PHY-7050-HI-92).

[Bollinger 93] L.M. Bollinger et al., *Nuclear Physics*, A553, (1993) 859c-862c.

[Brown 67] K.L. Brown, *SLAC-75*, (1967).

[Brown 73] K.L. Brown, D.C. Carey, Ch. Iselin and F. Rothacker, *TRANSPORT*, a computer program for designing charged particle beam transport systems, SLAC 91(1973 rev.), NAL 91, and CERN 80-04, (1973).

[Brown 79] K.L. Brown, *TRANSPORT*, the ion optical program, Technical Report 91, SLAC-91, (1979).

[Brown 81] K.L. Brown, *NIM* 187 , (1981) 51-65.

[Carne 70] A. Carne, B. Schnizer, P. Lapostolle, M. Promé, Numerical Methods. Acceleration by a Gap, in *Linear Accelerators*, P.M. Lapostolle and A.L. Septier, ed., Amsterdam, North Holland, (1970) 747.

[Chambers 76] E. E. Chambers and I. Ben-Zvi, *Particle Accelerators*, Vol. 7, (1976) 137.

[Cotte 38] M. Cotte, *Ann. Phys.*, (Paris) 10, (1938) 333.

[Courant 58] E.D. Courant and H.S. Snyder, *Ann. Phys.*, 3, (1958) 1-48.

[Douglas 88] D.R. Douglas, J. Kewisch, and R.C. York, *Proceedings of the 1988 Linear Accelerator Conference*, Williamsberg, Virginia, (1988) 328.

[Dragt 90] Alex J. Dragt, *NIM*, A298, (1990) 441.

[Dragt 91] Alex J. Dragt and Filippo Neri, Govindan Rangarajan, *Physical Review A*, Vol.45, Number 4 (1991) 2572.

[Edwards 87] D.A. Edwards and M.J. Syphers, *AIP Conference Proceedings 184*, Vol. 1, (1989) Ch. 1 and Ch. 4.

[Forest 84] Étienne Forest, Ph.D. Thesis, (1984) 262.

[Goldstein 59] H. Goldstein, *Classical Mechanics*, Addison-Wesley, Reading, Mass., (1959) 54.

[Good 53] M.L. Good, *Phys Rev.*, 92, (1953) 538A.

[Hereward 70] H.G. Hereward, The General Theory of Linear Accelerators, in *Linear Accelerators*, P.M. Lapostolle and A.L. Septier, ed., Amsterdam, North Holland, (1970) 19.

[Jackson 75] J.D. Jackson, *Classical Electrodynamics*, (2nd edition), John Wiley & Sons, Inc., (1975) 574.

[Jaffey 74] A.H. Jaffey and T.K. Khoe, *NIM*, 121, (1974) 413.

[Jaffey 76] A.H. Jaffey, R. Benaroya, and T.K. Khoe, *Proceeding of 1976 Proton Linear Accelerator Conference*, (1976) 102.

[Jiye 86] Xiemen Jiye, *Aberration Theory in Electron and Ion Optics*, Academic Press, Inc., (1986) 14.

[Joh 93a] K. Joh and J.A. Nolen, *Proceedings of the 1993 IEEE Particle Accelerator Conference*, Washington, D.C., (1993) to be published.

[Joh 93b] K. Joh, ATLAS, Physics Div., Argonne National Lab, *MINJI*, first order matrix optics code (1993), unpublished.

[Joh 93c] K. Joh, ATLAS, Physics Div., Argonne National Lab, *MINSOL*, ray-tracing code for PII linac (1993), unpublished.

[Lapostolle 71] P.M. Lapostolle, *IEEE Trans. Nucl. Sci.*, NS-18, No. 3, (1971) 1101.

[Lawson 73] J.D. Lawson, and P.M. Lapostolle, R.L. Gluckstern, *Particle Accelerators*, Vo. 5, (1973) 61.

[Lejeume 80a] C. Lejeume and J. Aubert, in Emittance and Brightness: Definitions and Measurements, Advances in Electronics and Electron Physics, suppl. 13A, *Applied Charged Particle Optics*, ed. A.L. Septier, ed., Academic Press, (1980) 159.

[Lejeume 80b] The "Geometrical Acceptance" was used to mean acceptance within which every particle is transmitted without striking the walls. C. Lejeume and J. Aubert, in Emittance and Brightness: Definitions and Measurements, Advances in Electronics and Electron Physics, suppl. 13A, *Applied Charged Particle Optics*, ed. A.L. Septier, ed., Academic Press, (1980) 159.

[Lichtenberg 69] Alan J. Lichtenberg, *Phase-space dynamics of particles*, New York Wiley, (1969).

[Livingood 61] John J. Livingood, *Principles of Cyclic Particle Accelerators*, D. Van Nostrand Company, Inc., New York, (1961) 123.

[Lu 87] J.-Q. Lu, I. Ben-Zvi, and John G. Cramer, *NIM*,A262, (1987) 200.

[Lysenko 88] Walter P. Lysenko, Mark S. Overley, *AIP Conference Proceedings*, 177 (1988) 323.

[Nolen 92] Jerry A. Nolen, Jr., *Encyclopedia of Applied Physics*, Vol.3, VCH Publishers, Inc., (1992) 273-291.

[Nolen 93] J.A. Nolen, K. Joh, *Proceedings of the 1993 IEEE Particle Accelerator Conference*, Washington, D.C., (1993) to be published.

[Nozomu 90] UEDA Nozomu, INS-T-500 [Accelerator-12], Technical Report, Tokyo, Japan, (1990) Appendix A.

[Okamoto 89] Hiromi Okamoto, *NIM*, A284, (1989) 233.

[Pardo 87a] R.C. Pardo, K.W. Shepard, and M. Karls, *Proceedings of 1987 IEEE Particle Accelerator Conference*, Washington, D.C., (1987) 1228.

[Pardo 87b] R.C. Pardo, L.M. Bollinger and K.W. Shepard, *NIM*, B24/25, (1987) 746.

[Pardo 89] R.C. Pardo, K.W. Shepard, and M. Karls, *LINRAY*, raytracing program for the ATLAS linac.

[Pardo 92] R.C. Pardo et al., *1992 Linear Accelerator Conference Proceedings*, Ottawa, Ontario, Canada, (1992) 61.

[Press 86] William H. Press, Brian P. Flannery, Saul A. Teukolsky, William T. Vetterling, *Numerical Recipes*, Cambridge University Press, (1986) 550.

[Promé 70] M. Promé, Numerical Methods. Focusing, in *Linear Accelerators*, P.M. Lapostolle and A.L. Septier, ed., Amsterdam, North Holland, (1970) 785.

[Pusch 93] Private communication.

[Sacherer 71] F.J. Sacherer, *IEEE Trans. Nucl. Sci.*, NS-18, No. 3, (1971) 1105.

[Sagalovsky 92] L. Sagalovsky and J. R. Delayen, *1992 Linear Accelerator Conference Proceedings*, Ottawa, Ontario, Canada, (1992) 763.

[Servranckx 85] R.V. Servranckx, K.L. Brown, L. Schachinger, D. Douglas, *User's Guide to the Program DIMAD*, SLAC Report 285 UC-28, (May 1985).

[Shepard 85] K. W. Shepard, *IEEE Transactions on Nuclear Science*, Vol. NS-32, No. 5, (1985) 3574.

[Shepard 87] K. W. Shepard, *Proceedings of the 1987 IEEE Particle Accelerator Conference*, Washington, D.C., (1987) 1812.

[Shepard 89] K. W. Shepard, P. K. Markovich, G. P. Zinkann, B. Clifft, R. Benaroya, *Proceedings of the 1989 IEEE Particle Accelerator Conference*, Chicago, Illinois, (1989) 974.

[Shepard 93] K.W. Shepard, private communication.

[Vlasov 68] A. D. Vlasov, *Theory of Linear Accelerators*, Israel Program for Scientific Translations, Jerusalem, (1968).

[Wollnik 87a] Herman Wollnik, *Optics of Charged Particles*, Academic Press, Inc., Sandiego, California, (1987) 14-17.

[Wollnik 87b] Herman Wollnik, *Optics of Charged Particles*, Academic Press, Inc., Sandiego, California, (1987) 232.